

**MAGNETIC NANOPORE COMPOSITE BEADS FOR
SIMULTANEOUS REMOVAL OF ORGANIC AND
INORGANIC POLLUTANTS IN HIGHLY ACIDIC
WATER**



Dissertation submitted to the Department of Chemistry, University of Zimbabwe
in partial fulfilment of the requirements for the degree of
Master of Science in Chemistry

By

Isheunesu Phiri, *BSc (UZ)*

Supervised By Dr P. Mushonga and Dr J. Kugara

© 2016

Declaration

I declare that this research is my own, unaided work. It is being submitted for the Master of Science Degree in Chemistry at the University of Zimbabwe, Harare. It has not been submitted before for any degree or examination at any other University.

.....

Signature of candidate

Abstract

A novel magnetic nanocomposite bead was synthesised for the simultaneous removal of cationic, anionic and organic pollutants removal in highly acidic water. Copper, chromium (III), phosphate and toluene were used as representative cationic, anionic and organic pollutants respectively. A 3:4:1 aspect ratio (alginate: nanocomposite: xanthan gum) was used for the beads. The magnetic nanocomposite was characterised using, FT-IR, SEM – EDX and XRD. The beads showed greater removal percentage for phosphate at (97.8 %), followed by copper and chromium at 81.8 % and 81.1 % respectively and toluene also at 81.8 %. Isothermal study showed that both the Freundlich and Langmuir isotherm models were the governing equations for sorption with a more perfect fit for the Freundlich isotherm. Pseudo-second-order model was the governing equation for sorption. This sorbent showed great potential to be used for simultaneous removal of cationic, anionic and organic pollutants removal in water.

Key words: zeolites, layered double hydroxides, alginate, activated charcoal, nanocomposite.

Acknowledgements

I would like to acknowledge my supervisor Dr P. Mushonga for his tireless efforts, encouragement and total belief in me. May God richly bless you and your family. I would like to also thank Dr J. Kugara who was also my supervisor and also for making sure we had what we needed. With special mention of Mr Dotito, Mr Nyatanga, Mr Penyaitu for helping me with the analytical instruments, Mrs Siyaduba and Mrs Mugobera from SIRDC for their help with the FT IR. Mr Tendaupenyu, such a humble man, he made sure we had the chemicals we needed. I would like also to acknowledge Mr S Msamadya, my research partner with whom I spent sleepless nights in the lab trying to get things done. I would also like to thank my parents for their moral support and encouragement, am blessed to have you as my parents, I would wish no other. My heartfelt thank you to my sister Sibongile for your selfless acts in making sure I had the tuition fees, words fail me to express how thankful I am. And to the greatest friend and love of my life Ashleigh, my wife, always there for me. Making me believe that I can and your unceasing support, I am thankful. Above all I would like to thank my Lord and Saviour, Jesus, such a dear friend to me.

Table of Contents

Declaration	i
Abstract	ii
Acknowledgements	iii
List of figures	vii
List of tables	xvii
List of abbreviations and symbols	xviii
1.0 Introduction.....	1
1.1 Justification	2
2.0 Literature Review.....	4
2.1 Composite beads	13
2.1.1 Carbon containing composites	13
2.1.2 Alginate containing composites	27
2.1.3 Other nanocomposites.....	36
3.0 Methodology	41
3.1 Materials	41
3.2 Synthesis of Zeolite.....	41
3.2.1 Synthesis of zeolites from bentonite clay	41
3.2.2 Synthesis of zeolites from local clay	42
3.2.3 Synthesis of zeolites from silica and Al ₂ O ₃	42
3.3 Synthesis of magnetic nanoparticles (MNPs), Fe ₃ O ₄	42
3.4 Synthesis of Aluminium – Zinc Layered Double Hydroxides (LDH).....	43
3.5 Coating mixture of zeolite, MNPs, activated charcoal with Zn/Al Layered Double Hydroxide (LDH).....	43

3.6 Synthesis alginate beads impregnated with the magnetic nano composite.....	44
3.7 Preparation of the stock solutions for adsorption	44
3.7.1 The 100 ppm solution	45
3.7.2 The 200 ppm solution	45
3.7.3 The 400 ppm solution	45
3.8 Batch adsorption studies	46
3.8.1 Batch adsorption methods for phosphate	46
3.9 Preparation of reagents	46
3.9.1 Reducing solution preparation	46
3.9.2 Standard solutions preparation.....	46
3.10 Batch adsorption for Chromium (III).....	47
3.11 Preparation of reagents	47
3.11.1 Preparation of Standard solution.....	47
3.11.2 Preparation of samples	48
3.12 Batch Adsorption of copper	48
3.13 Preparation of reagents	48
3.13.1 Preparation of Standard solution.....	48
3.14 Batch Adsorption of Toluene.....	49
3.15 Preparation of reagents	49
3.15.1 Preparation of Standard solution.....	49
4.0 Results and discussion	50
4.1 Characterization of zeolites.....	50
4.2 Characterization magnetic nanoparticles	55

4.3 Characterization of LDHs	59
4.4 Characterization of magnetic nanocomposite	62
4.5 Adsorption studies of phosphate	64
4.6 Adsorption studies of chromium.....	79
4.7 Adsorption studies of copper	93
4.8 Adsorption studies of toluene	106
5.0 Discussions	119
5.1 Equilibrium study.....	120
5.2 Isotherm study.....	123
5.3 Thermodynamics studies	125
6.1 Conclusions.....	127
6.2 Recommendations.....	128
References.....	129

List of figures

- Fig. 2.1** Sodalite cage (a). Sod-cages connected through a double T4-ring (D4R) and a simple T8-ring (S8R) formed in zeolite A (b). Sod-cages connected through a simple T4-ring (S4R) in sodalite (c)
- Fig. 2.2** SEM of zeolite (A), (a) and zeolite/Fe₃O₄ -NCs (B), (b)
- Fig. 2.3** SEM images(a) Nitrogen adsorption–desorption isotherms and (b) pore size distributions for coconut shell carbons
- Fig. 2.4** Schematic diagram of Layered Double Hydroxides
- Fig. 2.5** SEM image of LDH
- Fig. 2.6** Calcium alginate
- Fig. 2.7** SEM images of dry protonated calcium alginate beads: external surface (A and B); cross-section (C and D).
- Fig. 2.8** SEM of porous zirconium alginate beads and its cross section before adsorption (a–d) and after adsorption (e–h).
- Fig. 2.9** Xanthan gum showing the penta saccharide repeats units
- Fig. 2.10** Adsorption of zinc fitted with Langmuir isotherm on AG–AC beads, GAC, zeolite, alginate complex.
- Fig. 2.11** Adsorption of toluene fitted with Langmuir isotherm on AG–AC beads, GAC, zeolite, alginate complex beads.

- Fig. 2.12** Adsorption of zinc and toluene on alginate complex beads fitted with kinetic adsorption model (Eq. (2)).
- Fig. 2.13** (a) Before and, (b) after composite adsorbent adsorption
- Fig. 2.14** SEM images of PAC (a) and PAC-Feo/Ag (b).
- Fig. 2.15** Effect of pH (a) and contact time (b) on adsorption Cr(VI) onto PAC-Feo/Ag (200 rpm agitation speed, 0.3 g/l adsorbent 4 mg/L initial Cr(VI) concentration and $20 \pm 1^\circ\text{C}$).
- Fig. 2.16** Effect of adsorbent dosage (a) and initial Cr(VI) concentration (b) on removal efficiency and adsorption capacity of Cr using PAC-Feo /Ag (pH = 3.0 ± 0.1 , contact time = 60 min and $20 \pm 1^\circ\text{C}$).
- Fig. 2.17** The Langmuir (a), Freundlich (b) isotherm models and pseudo first-order (c) and pseudo second-order (d) kinetic models for the adsorption of Cr(VI) on PAC-Feo/Ag.
- Fig. 2.18** M^{2+} removal on the PPy and the Ppy-RGO composite from a mixed solution of metal ions at 20°C and pH 3.
- Fig. 2.19** SEM images of beads: (j) Pure SA-N, (k) Pure SA-M, (l) SA-GO-N, and (m) SA-GO-M
- Fig. 2.20** SEM micrographs: (a) expanded graphene worm under microwave radiation, (b) 2D iron oxide decorated graphene, (c) graphene-carbon nanotube-iron oxide 3D nanostructures at the final stage, and (d) magnified 3D nanostructures; carbon

nanotubes are vertically grown on graphene sheet and iron oxide nanoparticles and are decorated on both graphene sheet and carbon nanotubes.

- Fig. 2.21** Interaction between Cr^{3+} , exfoliated GO and trioctylamine
- Fig. 2.22** Conceptual illustration of the affinity between (A) EGO and trioctylamine (B) TOA–EGO and chromium (VI).
- Fig. 2.23** The schematic representation for the metal ions removal on to GFC
- Fig. 2.24** Adsorption of MB on different ratios of pure Graphene and G/ Fe_3O_4 nanocomposites (different ratios: (S0.1, S0.2, S0.4, S0.6, S0.8 and S1, respectively).
- Fig. 2.25** SEM images of calcium alginate beads (a) and CA–Ni/Fe beads (b).
- Fig. 2.26** Field emission scanning electron micrographs (FESEM) of layered double hydroxide-loaded alginate beads (LDH-alginate beads): (a) cross-sectional view of pure alginate beads (0% LDH-alginate beads) (bar $\frac{1}{4}$ 100 mm); (b) X-ray spectrum (EDS) of pure alginate beads; (c) cross-sectional view of 8%LDH-alginate beads (bar $\frac{1}{4}$ 100 mm); (d) X-ray spectrum (EDS) of 8%LDH-alginate beads; (e) FESEM image of 8% LDH-alginate beads (bar $\frac{1}{4}$ 10 mm); (f) FESEM image of 8% LDH-alginate beads (bar $\frac{1}{4}$ 2 mm).
- Fig. 2.27** Field emission scanning electron micrographs (FESEM) of LDH-PVA/alginate beads: (a) cross-sectional view (bar, 200 μm), (b) FESEM image (bar, 2 μm), (c) X-ray spectrum. LDH: layered double hydroxide, PVA: polyvinyl alcohol.

- Fig. 2.28** SEM images of (a) pure alginate bead and (b) nanosized graphite carbon-impregnated calcium alginate bead.
- Fig. 2.29** SEM images of calcium alginate beads (a) and CA–Ni/Fe beads (b).
- Fig. 2.30** Schematic representation of cross-linked SAPAPN adsorbent
- Fig. 2.31** SEM images of LDH-coated zeolite-LTA by a hydrothermal treatment.
- Fig 4.1** FT-IR spectrum of zeolite synthesized from bentonite clay.
- Fig 4.2** FT-IR spectrum of zeolite synthesized from local clay.
- Fig. 4.3** FT-IR spectrum of zeolite synthesized from SiO₂ and Al₂O₃.
- Fig 4.31 c1)** XRD spectrum for zeolites synthesised from bentonite clay
- Fig 4.31 c2)** XRD spectrum for zeolites synthesised from local clay
- Fig 4.31 c3)** XRD spectrum for zeolites synthesised from silica and alumina
- Fig 4.31 c4)** Overlay of XRD spectrum of zeolites synthesised from different sources
- Fig. 4.4** FT-IR spectrum of magnetic Fe₃O₄ nanoparticles
- Fig 4.4 c)** XRD spectrum of magnetic iron oxide nanoparticles
- Fig 4.6 c)** XRD spectrum of magnetic nanocomposite
- Fig. 4.5** FT- IR spectrum of the Al-Zn LDH.
- Fig. 4.5 c)** XRD spectrum of Zn/Al layered double hydroxide

- Fig. 4.6** FT-IR spectrum of the zeolite from local clay mixed with activated charcoal and coated with Al-Zn LDH.
- Fig. 4.5 c)** XRD spectrum of Zn/Al layered double hydroxide
- Fig. 4.7** Adsorption of the 100 ppm phosphate solution
- Fig. 4.8** Adsorption of the 200 ppm phosphate solution
- Fig. 4.9** Adsorption of the 400 ppm phosphate solution
- Fig. 4.10** Adsorption comparison of phosphate using the magnetic nanocomposite.
- Fig. 4.11** Adsorption comparison of phosphate using the magnetic beads.
- Fig. 4.12** Langmuir isotherm for 100 ppm phosphate solution
- Fig. 4.13** Langmuir isotherm for 200 ppm phosphate solution
- Fig. 4.14** Langmuir isotherm for 400 ppm phosphate solution
- Fig 4.15** Langmuir isotherm comparison of phosphate using the magnetic nanocomposite.
- Fig 4.16** Langmuir isotherm comparison of phosphate using the magnetic beads.
- Fig 4.17** Freundlich isotherm for 100 ppm phosphate solution
- Fig 4.18** Freundlich isotherm for 200 ppm phosphate solution
- Fig 4.19** Freundlich isotherm for 400 ppm phosphate solution
- Fig 4.20** Freundlich isotherm comparison of phosphate using the magnetic nanocomposite.

- Fig 4.21** Freundlich isotherm comparison of phosphate using the magnetic beads
- Fig 4.22** Pseudo First Order kinetics of phosphate using the magnetic nanocomposite.
- Fig 4.23** Pseudo First Order kinetics of phosphate using the magnetic beads
- Fig 4.24** Pseudo Second Order kinetics of phosphate using the magnetic nanocomposite.
- Fig 4.26** Effect of the initial phosphate concentration and contact time using the magnetic nanocomposite.
- Fig 4.27** Effect of the initial phosphate concentration and contact time using the magnetic beads.
- Fig 4.28** Effect of the initial phosphate concentration and contact time using the magnetic nanocomposite.
- Fig 4.29** Percentage removal of phosphate against time using the magnetic nanocomposite.
- Fig 4.30** Percentage removal of phosphate against time using the magnetic beads.
- Fig 4.31** Thermodynamics studies of phosphate adsorption
- Fig 4.32** Adsorption of 100 ppm solution of chromium
- Fig 4.33** Adsorption of 200 ppm solution of chromium
- Fig 4.34** Adsorption of 400 ppm solution of chromium
- Fig 4.35** Percentage removal of chromium against time using the magnetic nanocomposite.

- Fig 4.36** Percentage removal of chromium against time using the magnetic alginate beads
- Fig 4.37** Effect of the initial chromium concentrations and contact time (Q_t vs time).
using the magnetic nanocomposite.
- Fig 4.38** Effect of the initial chromium concentrations and contact time (Q_t vs time) using
the magnetic alginate beads.
- Fig 4.39** Effect of the initial chromium concentrations and contact time (%R vs time)
using the magnetic nanocomposite.
- Fig. 4.40** Langmuir isotherm for 100 ppm solution of chromium
- Fig. 4.41** Langmuir isotherm for 200 ppm solution of chromium
- Fig. 4.42** Langmuir isotherm for 400 ppm solution of chromium
- Fig. 4.43** Langmuir isotherm comparisons of chromium using the magnetic
nanocomposite.
- Fig. 4.44** Langmuir isotherm comparisons of chromium using the magnetic beads
- Fig 4.45** Freundlich isotherm for 100 ppm solution of chromium
- Fig 4.46** Freundlich isotherm for 200 ppm solution of chromium
- Fig. 4.47** Freundlich isotherm for 400 ppm solution of chromium
- Fig.4.48** Freundlich isotherm comparisons of chromium using the magnetic
nanocomposite.

- Fig 4.49** Freundlich isotherm comparisons of chromium using the magnetic alginate beads.
- Fig 4.50** Pseudo First Order kinetics of chromium using the magnetic nanocomposite.
- Fig 4.51** Pseudo First Order kinetics of chromium using the magnetic alginate beads
- Fig 4.52** Pseudo Second Order kinetics of chromium using the magnetic nanocomposite.
- Fig 4.53** Pseudo Second Order kinetics of chromium using the magnetic alginate beads.
- Fig 4.54** Thermodynamics studies of chromium adsorption
- Fig 4.55** Adsorption of 100 ppm Copper solution
- Fig 4.56** Adsorption of 200 ppm Copper solution
- Fig 4.57** Adsorption of 400 ppm Copper solution
- Fig 5.58** Adsorption of Copper comparisons for magnetic nanocomposite
- Fig 4.59** Adsorption of Copper comparisons for magnetic beads
- Fig 4.60** Percentage removal of copper by magnetic nanocomposite
- Fig 4.61** Percentage removal of copper by magnetic beads
- Fig 4.62** Q_t against time for magnetic nanocomposite of copper
- Fig 4.63** Q_t against time for magnetic beads of copper
- Fig 4.64** Effect of the initial chromium concentrations and contact time (%R vs time) using the magnetic nanocomposite of copper

- Fig 4.65** Freundlich isotherm for 100 ppm solution of copper
- Fig 4.66** Freundlich isotherm for 200 ppm solution of copper
- Fig 4.67** Freundlich isotherm for 400 ppm solution of copper
- Fig 4.68** Langmuir isotherm for 100 ppm solution of copper
- Fig 4.69** Langmuir isotherm for 200 ppm solution of copper
- Fig 4.70** Langmuir isotherm for 400 ppm solution of copper
- Fig 4.71** Pseudo first order kinetics of copper for magnetic nanocomposite
- Fig 4.72** Pseudo first order kinetics of copper for magnetic beads
- Fig 4.73** Pseudo second order kinetics of copper for magnetic nanocomposites
- Fig 4.74** Pseudo second order kinetics of copper for magnetic beads
- Fig 4.75** Thermodynamics studies of copper adsorption
- Fig 4.76** Adsorption of 100 ppm solution of toluene
- Fig 4.77** Adsorption of 200 ppm solution of toluene
- Fig 4.78** Adsorption of 400 ppm solution of toluene
- Fig 4.79** Adsorption of toluene comparisons for magnetic nanocomposite
- Fig 4.80** Adsorption of toluene comparisons for magnetic beads.
- Fig 4.81** Q_t against time for toluene comparisons for magnetic nanocomposites.

- Fig 4.82** Q_t against time for toluene comparisons for magnetic beads.
- Fig 4.83** Percentage removal against time for toluene comparisons for magnetic nanocomposites.
- Fig 4.84** Percentage removal against time for toluene comparisons for magnetic beads.
- Fig 4.85** Percentage removal for toluene against initial concentration
- Fig 4.86** Langmuir isotherms for 100 ppm solution of toluene
- Fig 4.87** Langmuir isotherms for 200 ppm solution of toluene
- Fig 4.88** Langmuir isotherms for 400 ppm solution of toluene
- Fig 4.89** Freundlich isotherms for 100 ppm solution of toluene
- Fig 4.90** Freundlich isotherms for 200 ppm solution of toluene
- Fig 4.91** Freundlich isotherms for 400 ppm solution of toluene
- Fig 4.92** Pseudo first order kinetics of toluene for magnetic nanocomposite
- Fig 4.93** Pseudo first order kinetics of toluene for magnetic beads
- Fig 4.94** Pseudo second order kinetics of toluene for magnetic nanocomposite
- Fig 4.95** Pseudo second order kinetics of toluene for magnetic beads
- Fig 4.96** Thermodynamic studies for toluene adsorption

List of tables

- Table 4.1:** Isotherm parameters for adsorption of phosphate
- Table 4.2:** Kinetics parameters for adsorption of phosphate
- Table 4.3:** Thermodynamic parameters for the adsorption of phosphate
- Table 4.4:** Isotherm parameters for adsorption of chromium
- Table 4.5:** Kinetics parameters for adsorption of chromium
- Table 4.6:** Thermodynamic parameters for the adsorption of chromium
- Table 4.7:** Isotherm parameters for adsorption of copper
- Table 4.8:** Kinetics parameters for adsorption of copper
- Table 4.9:** Thermodynamics parameters for adsorption of copper
- Table 4.10:** Isotherm parameters for adsorption of toluene
- Table 4.11:** Kinetics parameters for adsorption of toluene
- Table 4.12:** Thermodynamics parameters for adsorption of toluene

List of abbreviations and symbols

Q_e or q_e	is the equilibrium adsorption capacity; (mg g^{-1})
Q_t or q_t	is the adsorption capacity at time, t (mg g^{-1})
q_m	is the maximum adsorption capacity; (mg g^{-1})
C_0	is the initial concentration of solution; (mgL^{-1})
C_e	is the concentration at equilibrium; (mgL^{-1})
K	is adsorption equilibrium constant of Langmuir isotherm;
K_F	is adsorption value, one of empirical constant of Freundlich isotherm;
n	is empirical constant of Freundlich isotherm;
ΔG°	is the Gibb's free energy change; (KJmol^{-1})
ΔH°	is the enthalpy change (KJmol^{-1});
ΔS°	is the entropy change;
R	is the universal gas constant, 8.314 J/mol K ;
T	is the absolute temperature, K ;
K_c	is equilibrium stability constant
R^2 or r^2	is the coefficient of determination.
MNP	magnetic nanoparticle
AC	activated carbon

1.0 INTRODUCTION

Industrial wastewater often contains both organic and inorganic compounds such as aromatic hydrocarbons and heavy metals (cations) and anions like nitrates, sulphates and phosphates and since the former comes from industrial use of organic compounds containing metal additives in the petroleum and organic chemical industries and the later from sewages, agricultural leach and laboratory wastes etc. [1]. Anionic compounds such as nitrate and phosphate are used as raw materials in compost as bacterial feed that is essential for the plant growth. These compounds are carcinogenic, and their presence in rivers and groundwater poses significant risks to the environment by increase of the biological oxygen demand as well as outgrowth of hyacinth and other sea weed(s). Among them, nitrate has more concern on a global scale due to its carcinogenic properties [102]. Different methods have been used for the removal of these pollutants but of particular interest is the use of adsorbents. Recently, most developed sorbents are useful for only one kind of pollutant removal. So treating wastewaters, containing different pollutants need several treatment cycles leading to be hard and cost-ineffectiveness. Therefore, since 2003, researchers have tried to introduce new complex sorbents for the simultaneous removal of different kinds of pollutants [48, 103]. Therefore, this research project seeked to develop a nanopore composite adsorbent of magnetic modified zeolites and powdered activated carbon (PAC) for the simultaneous removal of organic and inorganic pollutants in water.

1.1 JUSTIFICATION

In Zimbabwean urban and rural areas, there is shortage of clean water supplied to people because of high costs of chemicals for the purification of raw water. Therefore there is need to produce low-cost adsorbents for filters for domestic and industrial use. This research will benefit the community at large if the beads show excellent removal of inorganic and organic pollutants simultaneously from water.

Some pollutants are considered as potentially carcinogenic. As a matter of concern, the study will focus on the cheaper way of removing heavy metals, nitrates, phosphates and phenols in municipal wastewater and platinum mine processing plants.

In addition to the cost problem, another important factor pushing towards low-cost adsorbents is the availability of agricultural industrial waste products. In order to extend the life of waste materials without introducing into the environment new materials such as adsorbents can be prepared from them resulting in a reduction in the cost of waste disposal.

The specific objectives were

- i. To synthesise zeolites from different silica sources i.e. clay (local clay and Bentonite clay)
- ii. To modify the zeolite with layered double hydroxide, LDH
- iii. To make a nanopore composite of zeolite, magnetic iron oxide, activated charcoal and layered double hydroxide
- iv. To investigate the adsorption capacity of the composite adsorbent towards different heavy metals, nitrates, phosphates and cyclic hydrocarbon using the batch processes

- v. To find the kinetics of the adsorption process
- vi. To perform a thermodynamics study of the adsorption process by finding the effect of temperature on the adsorption process and analyse adsorption isotherms

2.0 LITERATURE REVIEW

Industrial and agricultural wastewaters are important source of groundwater and river pollution. They often contain both anionic and cationic compounds such as nitrates, phosphates, phenols and heavy metals [1]. Among cationic pollutants, heavy metal ions are sources of great concern in aquatic environments, because they are non- (bio) degradable and therefore persistent and should be removed from wastewaters before they are injected into water sources [2]. Aromatic compounds such as toluene are used as raw materials in many chemical productions and as solvents in manufacturing processes. These compounds are carcinogenic and their presence in water stream even at low concentrations poses significant environmental risks [1]. The risks of these contaminants cannot be overemphasized since they are well documented.

Adsorption process being very simple, economical, effective and versatile has become the most preferred method for the removal of toxic contaminants from wastewater [3]. Adsorption is operative in most natural physical, biological, and chemical systems, and is widely used in industrial applications using adsorbents such as activated charcoal, synthetic resins, zeolites, layered double hydroxides, natural polymers etc. Among other methods of water purification like reverse osmosis, U.V. irradiation, etc., adsorption is currently considered to be very suitable for wastewater treatment because of its simplicity, multiple applicability and cost effectiveness [4] [5].

Zeolites are crystalline materials made up of structures based on 3D frameworks of alumina and silica tetrahedral as shown in Fig. 2.1 and the SEM images of zeolites and modified zeolites showing the crystal morphology in Fig. 2.2. These typically anionic frameworks are populated by charge compensating cations to maintain neutrality.

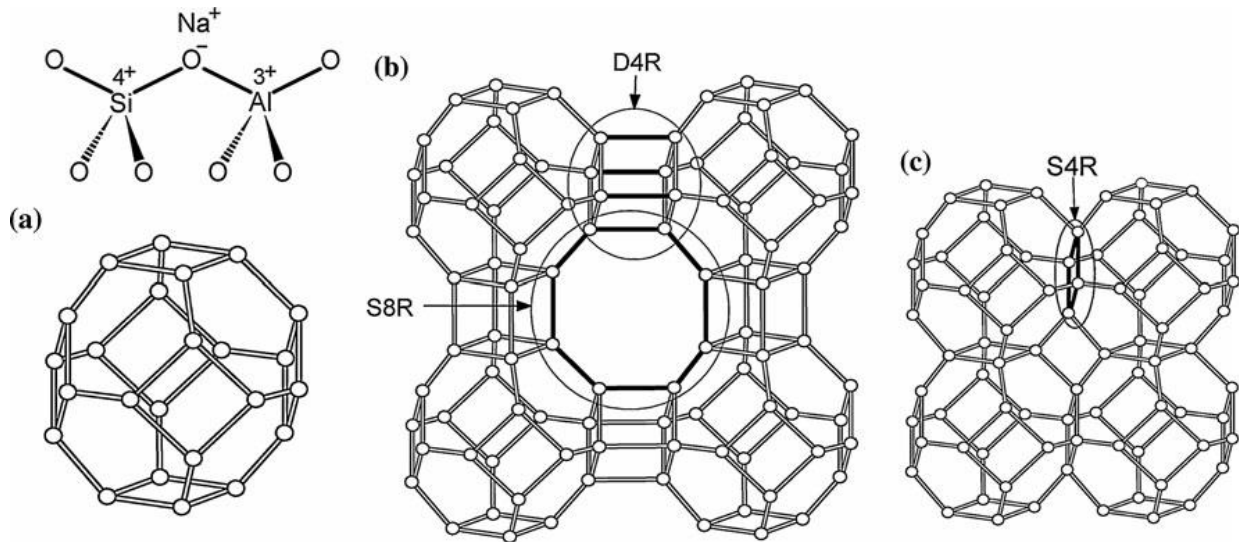


Fig 2. 1 Sodalite cage (a). Sod-cages connected through a double T4-rings (D4R) and a simple T8-ring (S8R) formed in zeolite A (b). Sod-cages connected through a simple T4-rings (S4R) in sodalite (c)

These compensating cations can participate in ion exchange processes where they often readily exchange with other metal ions when in aqueous solution hence zeolites act as ion exchange material.

Despite being good adsorbents in wastewater treatment, zeolites being crystalline, need to then be separated after they have been introduced in the waste water stream and this will possibly increase operational costs and this problem is solved by forming beads without affecting [6] but rather enhancing the adsorption capacity of the tetrahedron using natural polysaccharides for entrapment.

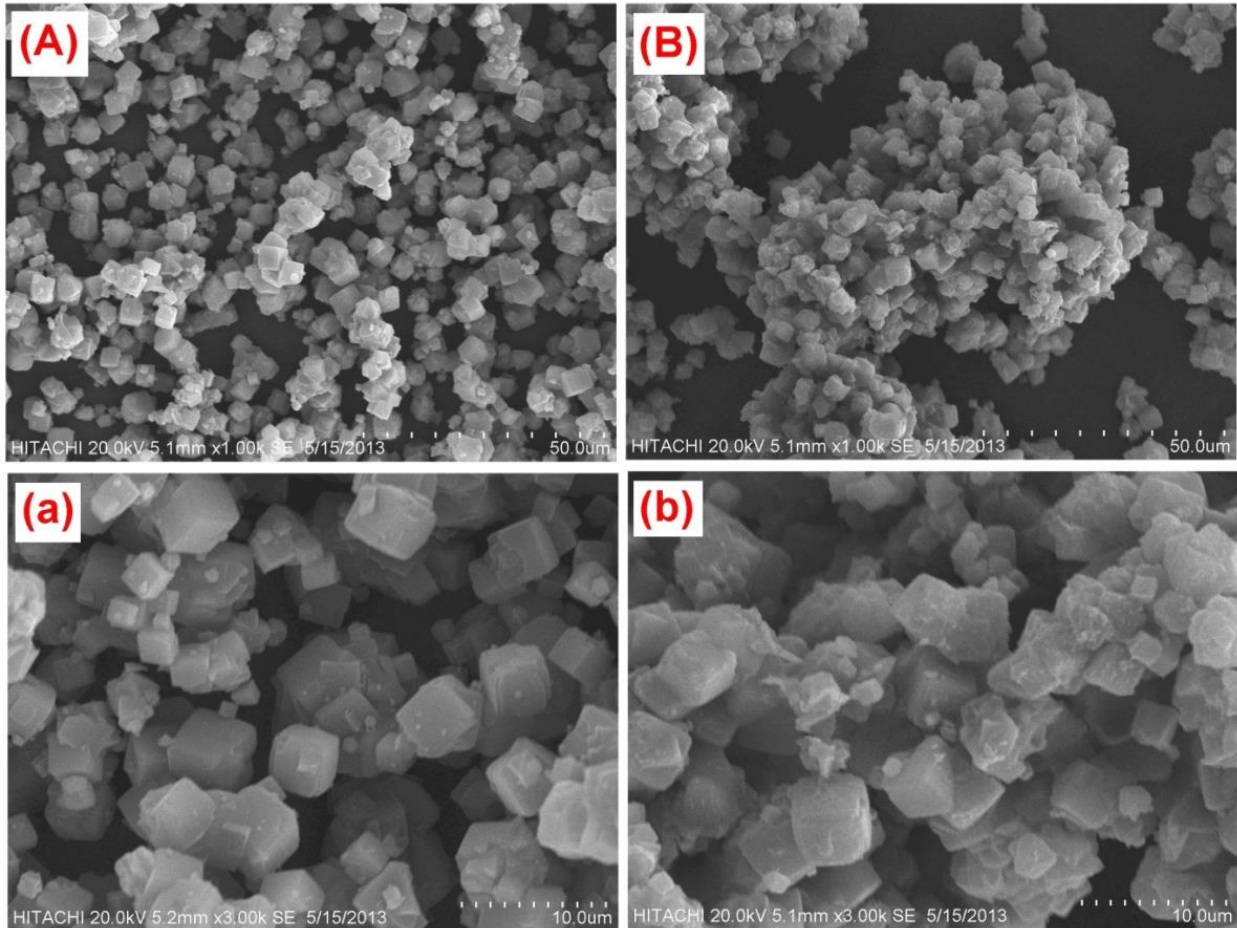


Fig 2.2. SEM images of zeolite (A), (a) and zeolite/Fe₃O₄ –Nanocomposites (NCs) (B), (b)[7]

Activated Carbon, AC is a microcrystalline, non-graphitic form of carbon with a nano porous structure that has been processed to develop its internal porosity. AC has a high degree of porosity, an extensive surface area of about 500 – 2000 m²/g and a high degree of surface reactivity. This large specific surface area leads to it being a very good adsorbent. Owing to its high degree of porosity, it has a large inner surface as shown in Fig. 2.3, which leads to high adsorption properties [9]. Since it comes in a powdered form, it is hard to separate from water after the purification process hence a method of immobilizing the AC will be ideal.

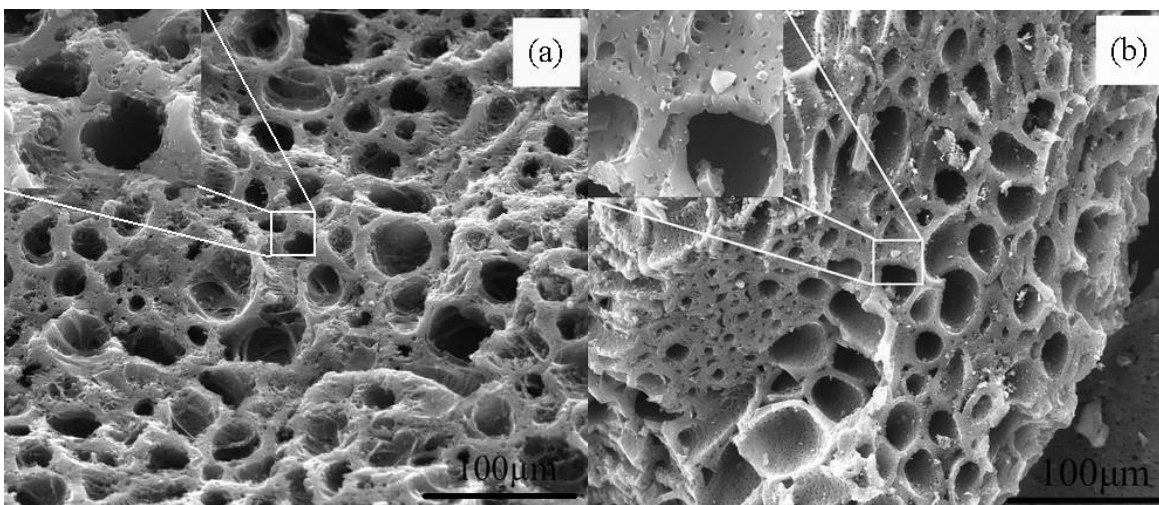


Fig 2. 3 SEM images (a) Nitrogen adsorption–desorption isotherms and (b) pore size distributions for coconut shell carbons [8].

Recently, layered double hydroxides (LDHs) or hydrotalcite-like compounds (HTlc) have become of interest from both industry and academia due to their unique anionic exchange properties hence are dubbed ‘anionic clays’, brucite-like structures [9]. Although LDHs exist as naturally occurring minerals, they are also relatively simple and economical to synthesize under laboratory conditions which can be scaled up. The structure of LDHs is based on positively charged sheets or layers of the hydroxides and the positive charges are balanced by intercalation of anions in the hydrated interlayer regions preferably nitrates which can be easily exchanged as shown in Fig. 2.4 and the SEM images in Fig. 2.5 showing the layers of the LDHs. LDHs have relatively weak interlayer bonding and because of that, they are organic and inorganic anion adsorbents. They also have a large surface area, high anion exchange capability (2–3 meq/g) which competes with those of other anion exchange resins and a very good thermal stability [10] [11]. LDHs have been studied extensively to assess their potential as adsorbents of anionic contaminants thus can be used as ion exchange adsorbents for water purification.

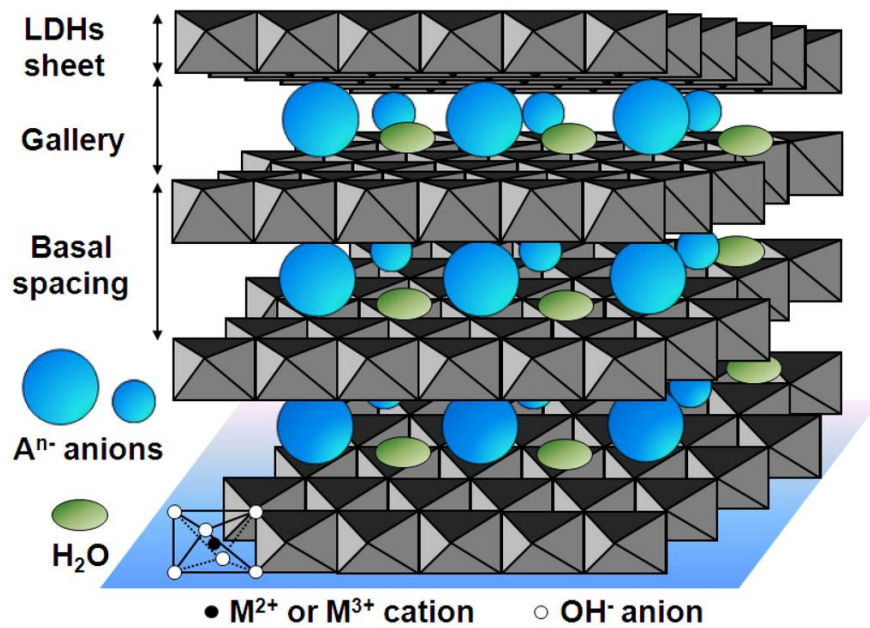


Fig. 2.4 schematic diagram of Layered Double Hydroxides

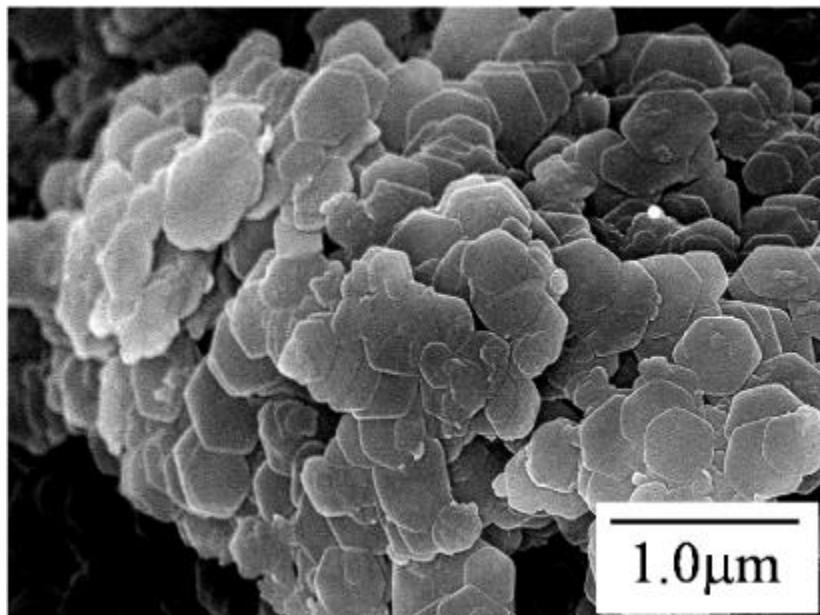


Fig 2.5 SEM image of LDH [12]

Alginate, a linear copolymer of α-L-guluronate (G) and α-D-mannuronate (M), is about 10–40% of the dry weight of all species of brown algae which forms insoluble beads when a solution containing Ca²⁺(aq.) ions is added to a solution of aqueous sodium alginate as

illustrated in Fig. 2.6. Alginate has widely been used for the immobilization of algal biomass, microorganisms, or entrapment of other specific sorbents (such as activated carbon, LDHs, zeolites, xanthan gum, silica gel) for various purposes, including deionization of water [13]. Though alginate has mostly been used as an immobilization/entrapment agent, it can also be used for metal sorption and has been discovered to have excellent sorption capacity towards several heavy metal ions.

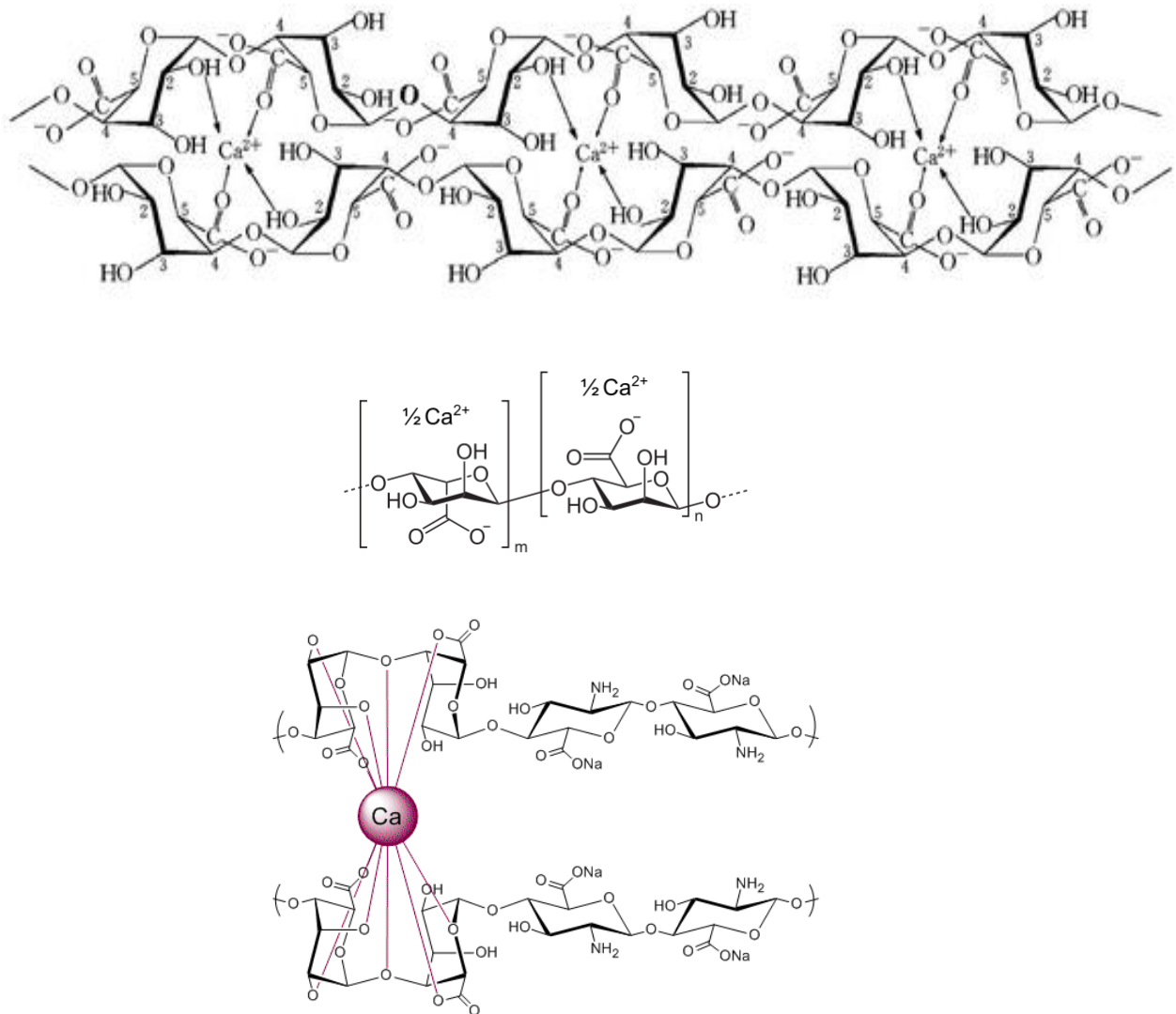


Fig. 2.6 Calcium alginate

In some studies that are recent, it has been shown that its sorption capacity greatly exceeds that of the actual sorbents entrapped in its matrix due to the presence of hydroxide groups for hydrogen bond formation and carboxylate groups for cation exchange [14]. Because of this, calcium alginate beads have been studied not only concerning their ability to bind metal ions and the mechanism of such [15] and its use as a sorbent due to its ability to adsorb metal ions [16] [17] but also as a composite membrane component in composite beads due to its ability to entrap other compounds in its matrix [18] [19]. Nonetheless, dry alginate beads used for heavy metal sorption are rigid materials which are not highly porous structure as shown in Fig. 2.7 and Fig. 2.8 thus the kinetics of sorption is somehow slow due to the low diffusion coefficient of the materials [20]. Hence some research has been done to increase the degree of porosity.

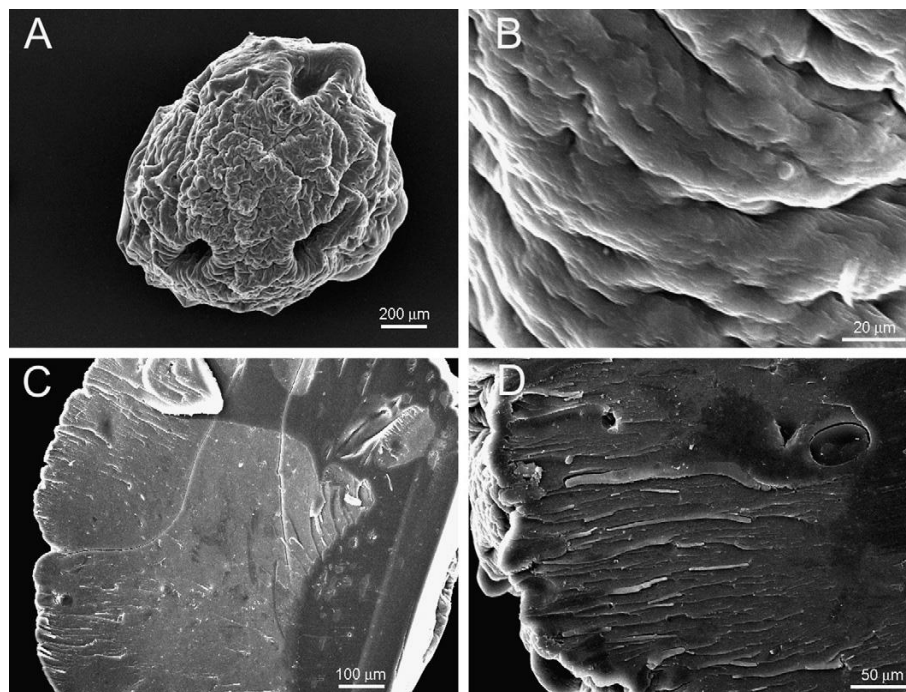


Fig. 2.7 SEM images of dry protonated calcium alginate beads: external surface (A and B); cross-section (C and D) [20]

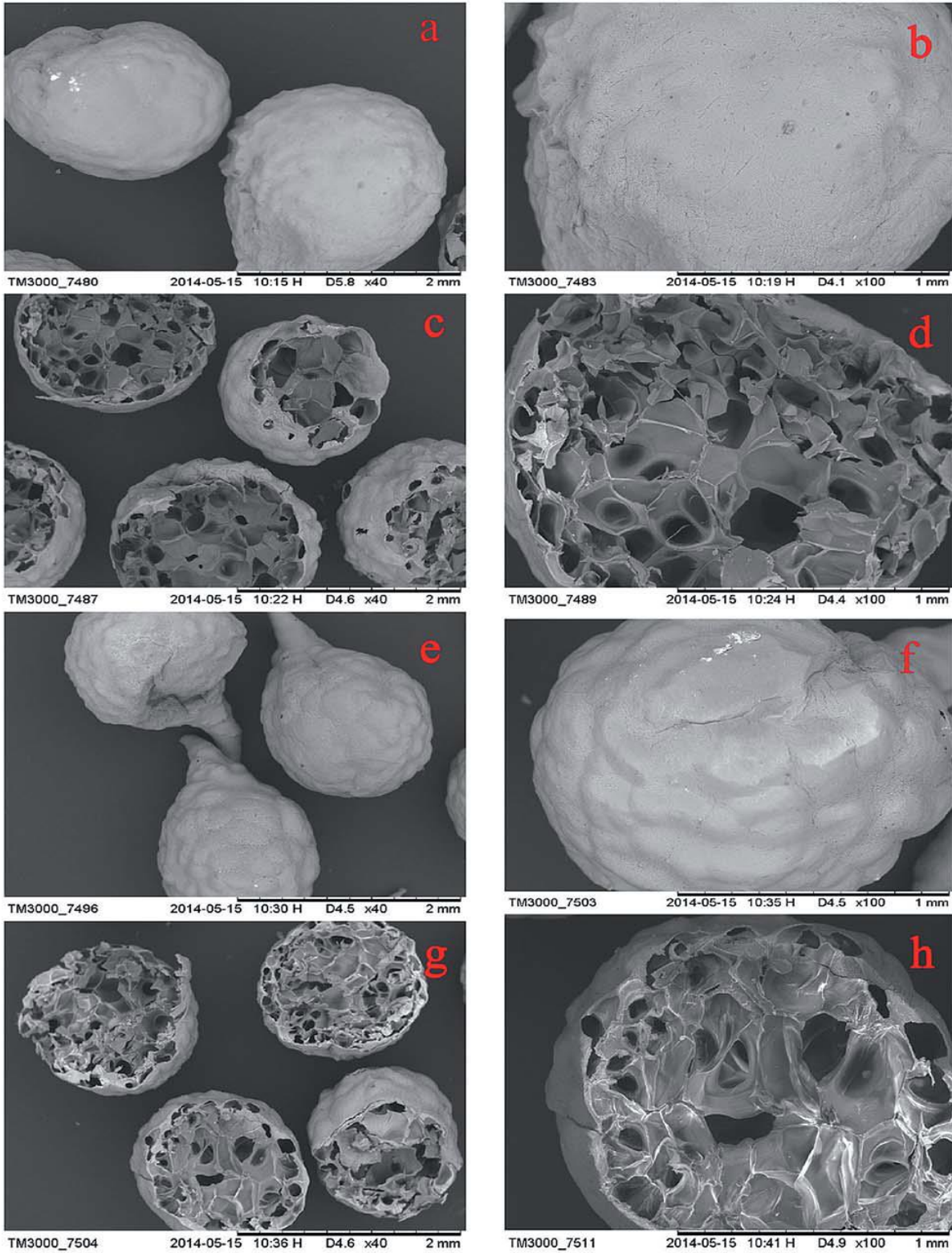


Fig. 2.8 SEM images of porous zirconium alginate beads and their cross section before adsorption (a–d) and after adsorption (e–h).[21]

Xanthan gum is a natural polysaccharide that is a product of secretion by the bacterium *Xanthomonas campestris* and is mostly used in the food industry for holding ingredients together so that they do not separate and it is mainly because of this property that it is used in composite beads. However, it also exhibits sorption of metal properties hence it helps in the remediation of wastewater [22]. It is composed of five saccharide repeating units, consisting of mannose, glucuronic acid and in the molar ratio 2:1:2 as shown in Fig. 2.9

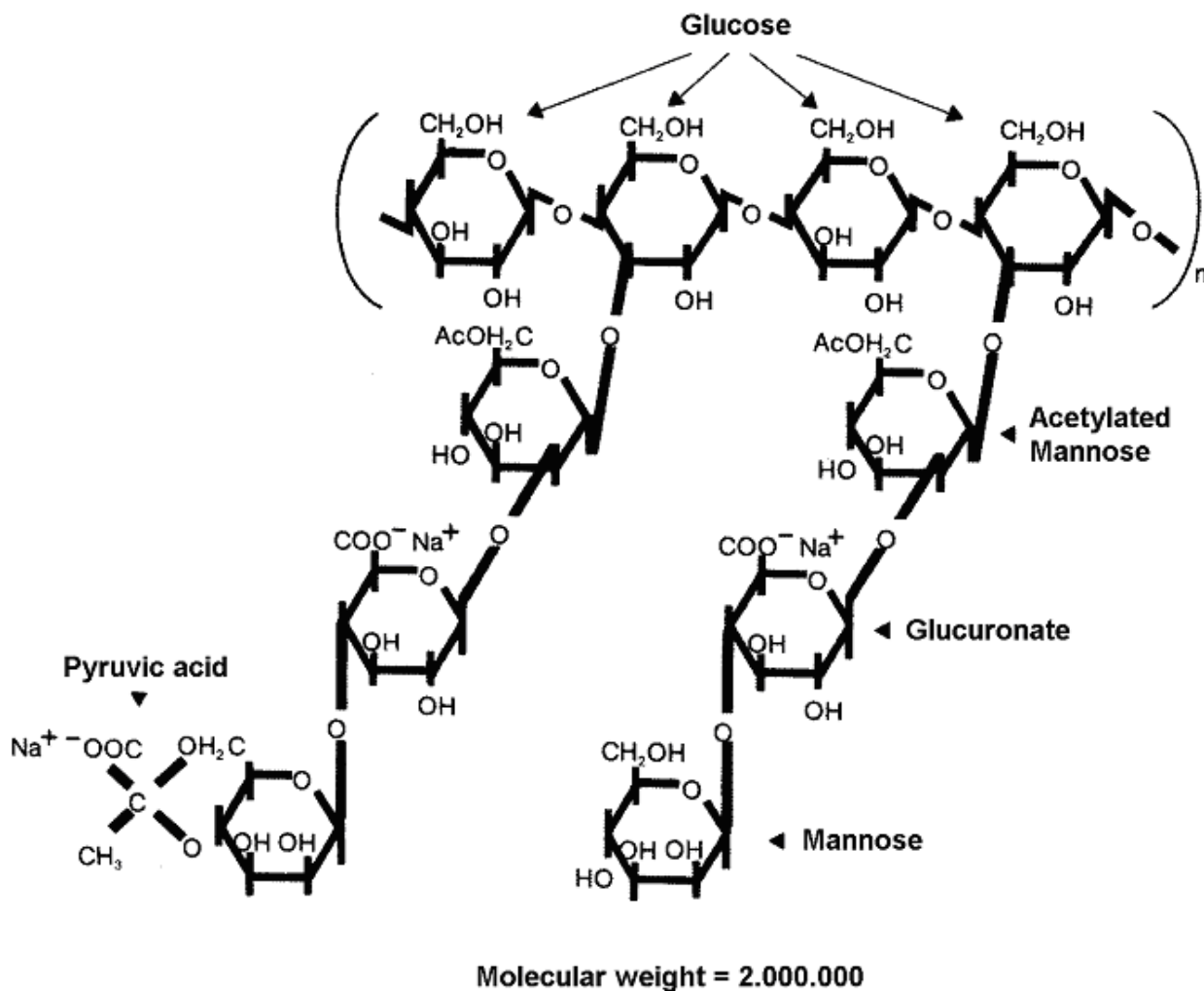


Fig. 2.9 Xanthan gum showing the penta saccharide repeat units

Xanthan gum also contains hydroxide, carboxylate and alkyl groups that can form hydrogen bonding, ionic bonds for ion exchange and Van der Waal forces respectively hence it also, like alginate can be used as an adsorbent.

2.1 Composite beads

2.1.1 Carbon containing composites

Combining zeolites and alginate, xanthan and activated carbon enhances the adsorption capacity. To achieve a high application potential for the alginate gel adsorbent, activated carbon-containing alginate bead adsorbent was developed by Park et al. [23]. Those authors tried to remove a broad range of heavy metal cations from synthetic solutions. Removal of Ni (II) cations from aqueous solutions through adsorption onto bio polymeric adsorbents, such as calcium alginate, chitosan-coated calcium alginate and chitosan-coated silica was studied by Vijaya et al. [24]. Nevertheless, Min and Hering [25] examined the fundamental aspects of a possible remediation strategy and removal of anionic metal species (arsenate) employing the biopolymer alginic acid pretreated with Ca(II) and Fe(III) cations, respectively [26]

Choi et al [1] attempted to develop a new adsorbent, alginate gel bead impregnated with zeolite and activated carbon for removal of mixed industrial contaminants. In order to examine the adsorption capacity of the alginate complex, both equilibrium and kinetic batch studies were performed on adsorption of zinc and toluene as target contaminants onto the alginate complex.

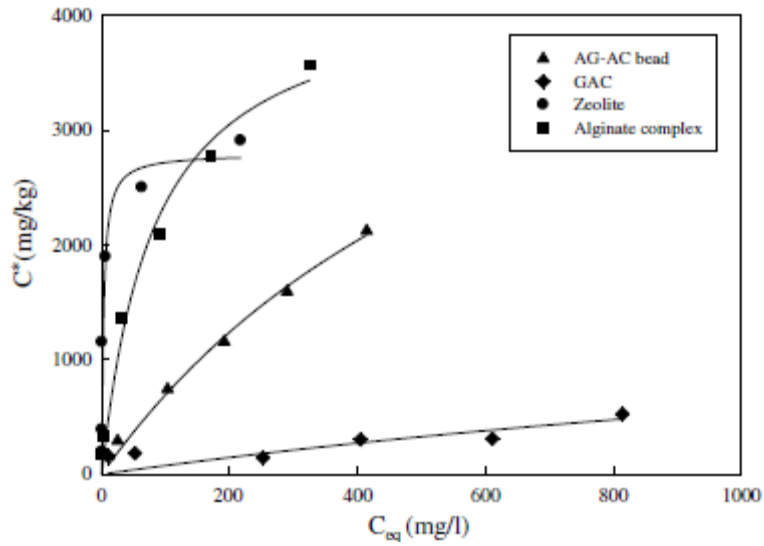


Fig. 2.10 Adsorption of zinc fitted with Langmuir isotherm on alginate impregnated with powdered activated charcoal (AG-AC beads), granular activated carbon (GAC), zeolite, alginate complex.

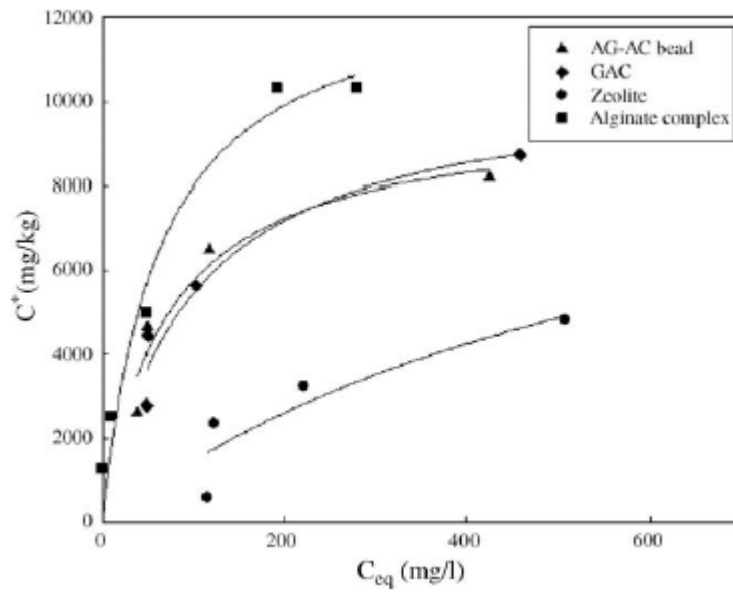


Fig. 2.11 Adsorption of toluene fitted with Langmuir isotherm on AG-AC beads, GAC, zeolite, alginate complex beads.

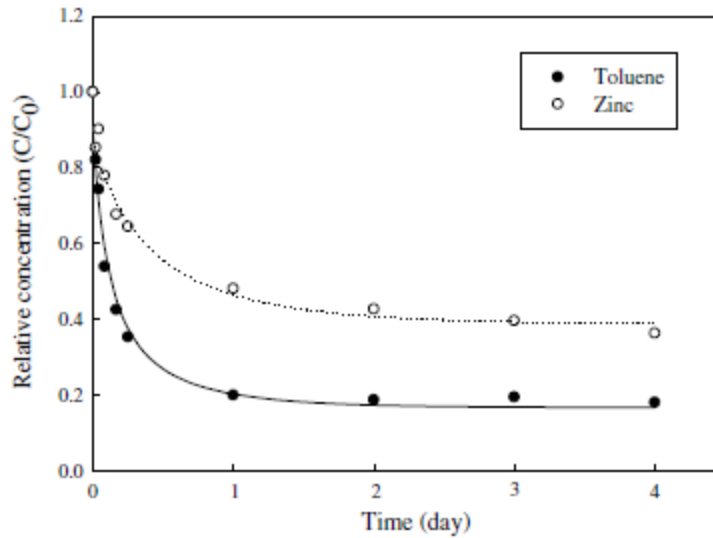


Fig. 2.12 Adsorption of zinc and toluene on alginate complex beads fitted with kinetic adsorption model (Eq. (2)).

After performing these tests, some results on Figs. 2.10 – 2.12, it was discovered that removal efficiency of zinc and toluene was 54 % and 86 % respectively from the starting concentrations of 250 mg/L, which was much higher for zinc compared to the values in literature and for toluene it was well close to that in literature. It was concluded that the composite complex can be used as simultaneous adsorbent remediating water with mixed contaminants.

Kamaruddin et al [27] researched on the preparation conditions for coconut shell activated carbon (CSAC) and clinoptilolite (Cl) composite adsorbent for colour removal from textile effluent focusing on the optimum conditions for preparation and the adsorption efficiency of the synthesized composite. A statistical approach and laboratory investigation were done in order to determine the factors influencing the preparation conditions of composite. An observation was made that the optimum CSAC/Cl composite adsorbent preparation conditions were obtained by using 5 % of CSAC and 63 % of Cl and the composite produced removed > 70 % of colour from actual textile wastewater. Various tests were conducted by varying the OPC (ordinary Portland cement) which was used as an adhesive to bind mixtures into granules

and it was observed that at 25 % of OPC content, maximum colour removal was still achieved. At an optimum shaking speed of 250 rpm, over 70 % of the colour was still removed.

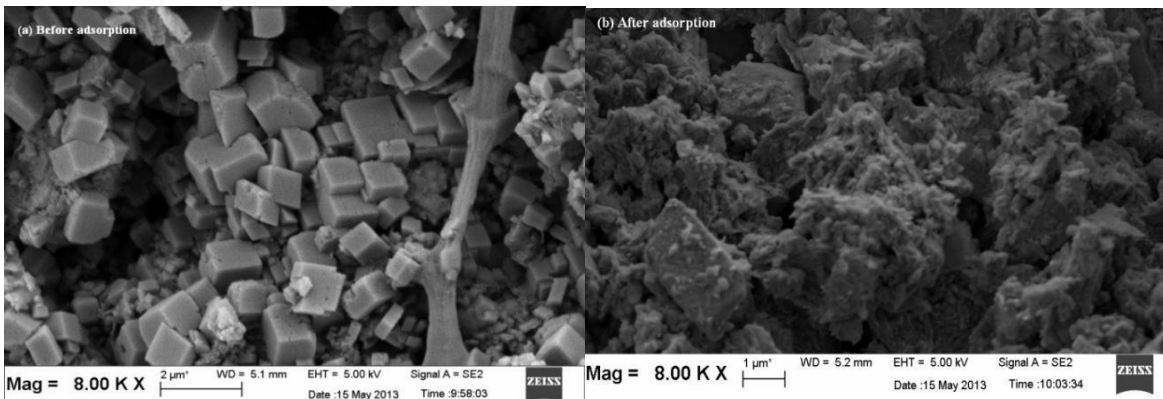


Fig. 2.13 (a) Before and, (b) after composite adsorbent adsorption of textile colour

The SEM images in Fig. 2.13 show that the optimum preparation conditions were sufficient to embed the Chloride onto the surface of the composite due to the presence of the rod like clods [27].

Jeon et al [30] made magnetic composites of carbon nanotubes (CNTs), alginate. Magnetic properties were due to the presence of the iron (III) oxide. The composite was used to remove Cu^{2+} ions from aqueous solution. The alginate and carbon nanotube were the adsorbent material and iron oxide made the composite magnetic thus the composite could be recovered easily from the water thereby preventing secondary pollution. SEM was used to determine the morphology of composites showing the carbon nanotubes and iron oxide entrapped in the alginate matrix. Both alginate and CNTs improved the Cu^{2+} ion removal efficiency by combining the properties of both adsorbent which are ion exchange between the calcium ions and the heavy metal and high absorption from surface complexation respectively. Comparing alginate beads and alginate beads impregnated with CNTs, the removal of Cu^{2+} ion improved

from 40 % for the alginate beads to over 60 % using alginate/CNT composite beads. The observation showed that impregnating alginate with CNTs results in more adsorption sites which are offered by the functional groups on CNTs introduced into the matrix hence synergistic effect of surface complexation and ion exchange of the calcium ion on the alginate matrix and the copper ion [28, 29]. The nano channels increased the surface complexation from the CNTs which helped in the adsorption of Cu^{2+} ions and also due to the more functional groups which increased ion exchange capacity between calcium ions and Cu^{2+} ions [30]. Magnetic separation is of a vital importance because it is environmentally friendly and the beads can be scaled up to remediate larger water reservoirs in a limited amount of time which can be used again after regeneration [31,32]. Nonetheless, the used of magnetic beads remains underutilized in this capacity [33].

Azari et al made nano composite of activated carbon and Fe/Ag nanoparticles for the removal of chromium (VI). The powdered activated carbon, (PAC) was magnetized using non zero valent iron (III) oxides for easy recovery and the iron oxide also acted as a reducing agent in reducing Cr^{6+} to Cr^{3+} . Due to its low reactivity, silver nanoparticles were used to speed up the reduction of chromium to Cr^{3+} . The Cr^{3+} was then adsorbed from the solution by the PAC.

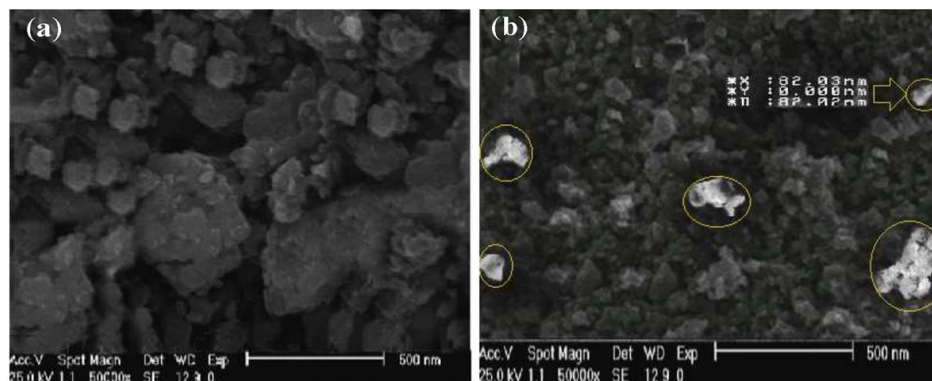


Fig. 2.14 SEM images of PAC (a) and PAC-Feo/Ag (b).

It was observed that maximum absorption of Cr (VI) happened at acidic pH, and was low at alkaline pH due to the fact that at higher pH the surface of the composite becomes negatively charged hence the $\text{Cr}_2\text{O}_7^{2-}$ ions are repelled from the surface of the composite thus less reactivity but at lower pH the opposite is true.

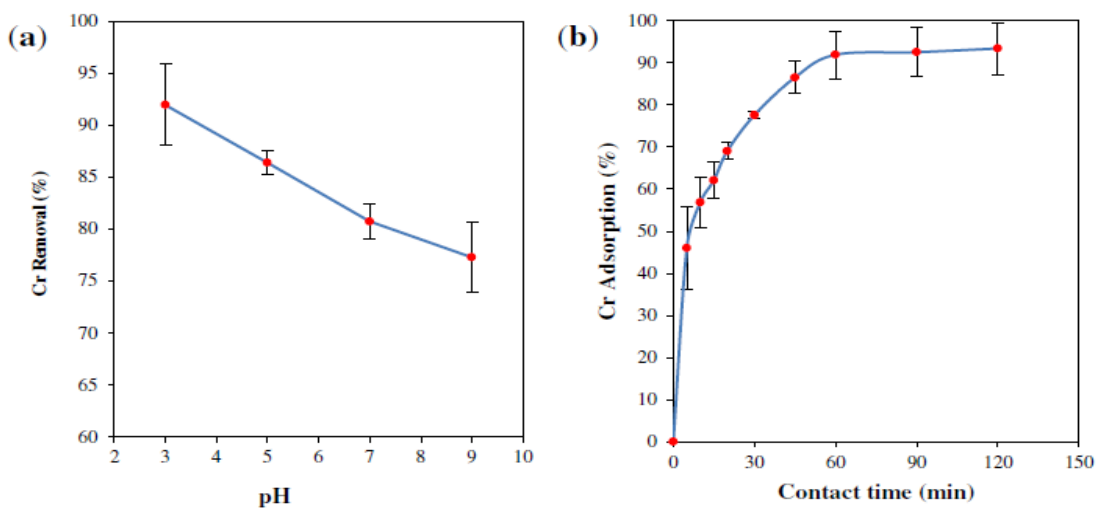


Fig. 2.15 Effect of pH (a) and contact time (b) on adsorption Cr(VI) onto PAC-Feo/Ag (200 rpm agitation speed, 0.3 g/l adsorbent 4 mg/L initial Cr(VI) concentration and $20 \pm 1^\circ\text{C}$).

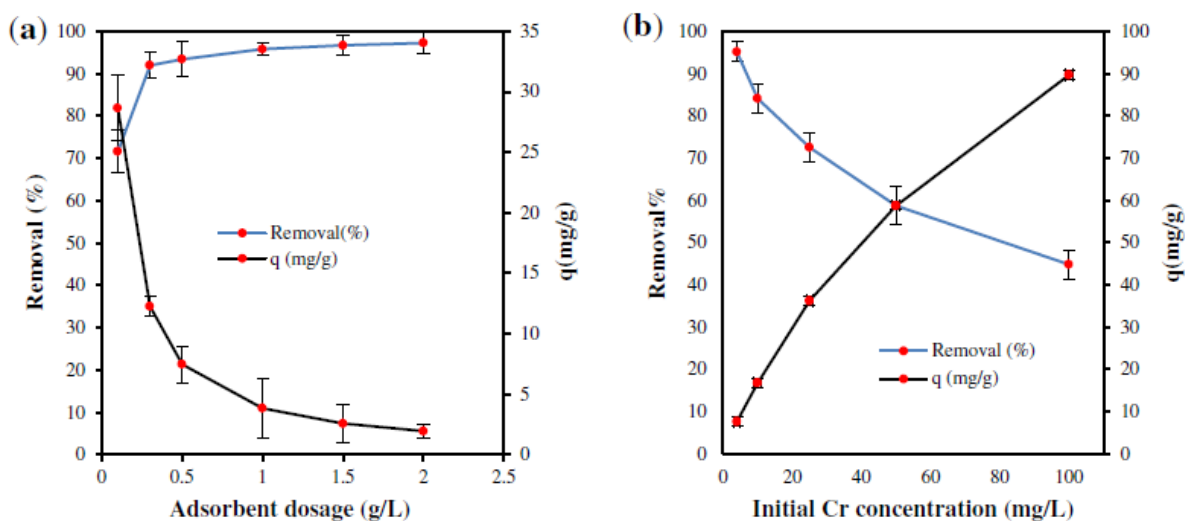


Fig. 2.16 Effect of adsorbent dosage (a) and initial Cr(VI) concentration (b) on removal efficiency and adsorption capacity of Cr using PAC-Feo/Ag (pH = 3.0 ± 0.1 , contact time = 60 min and $20 \pm 1^\circ\text{C}$).

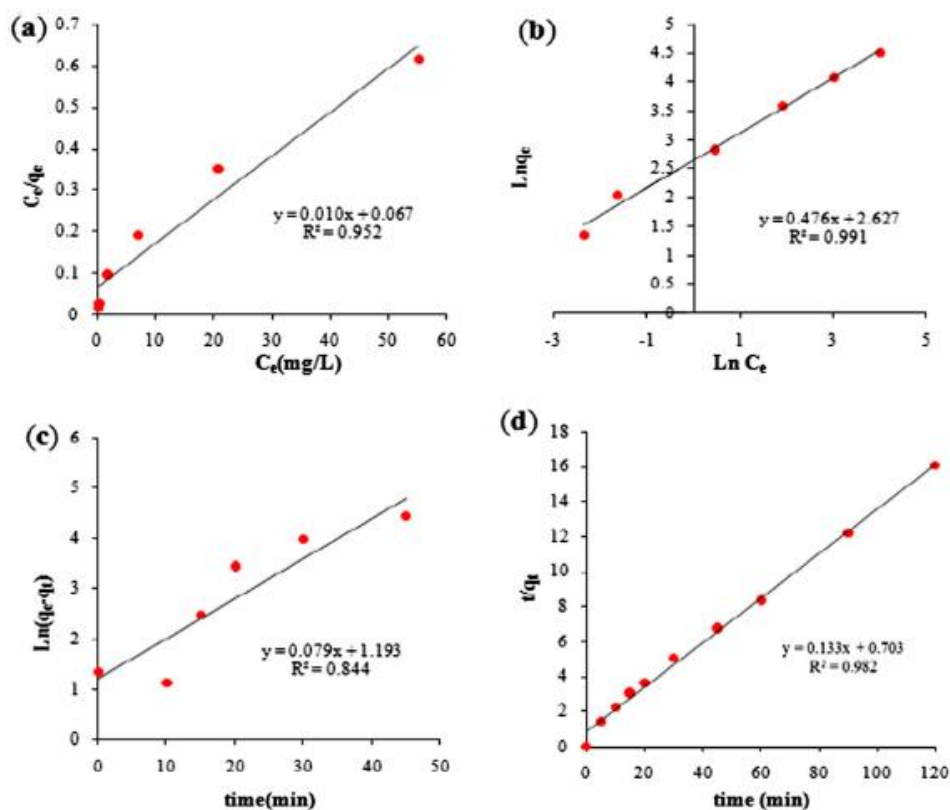


Fig. 2.17 The Langmuir (a), Freundlich (b) isotherm models and pseudo first-order (c) and pseudo second-order (d) kinetic models for the adsorption of Cr(VI) on PAC-FeO/Ag.

An optimum pH of 3 was observed where the highest absorption of 91.95 % was recorded. Other factors were tested i.e. contact time, Cr (VI) concentration, agitation speed, adsorbent dosage and equilibrium and kinetic models and it was shown that the equilibrium and kinetic studies of Cr(VI) adsorption followed the Freundlich isotherm and pseudo second order kinetic models [34].

Graphene, an allotrope of carbon has been also used as an adsorbent in nanopore composite beads where it enhanced the removal of anionic pollutants. Chandra et al were the first to use functionalized graphene as an adsorbent to remove ionic pollutants in water. They used highly selective adsorption of Hg^{2+} by a polypyrrole–reduced graphene oxide (PPy-RGO) composite

and they discovered that polymerizing the polypyrrole (PPy) onto the graphene sheets increased the adsorption surface area [35].

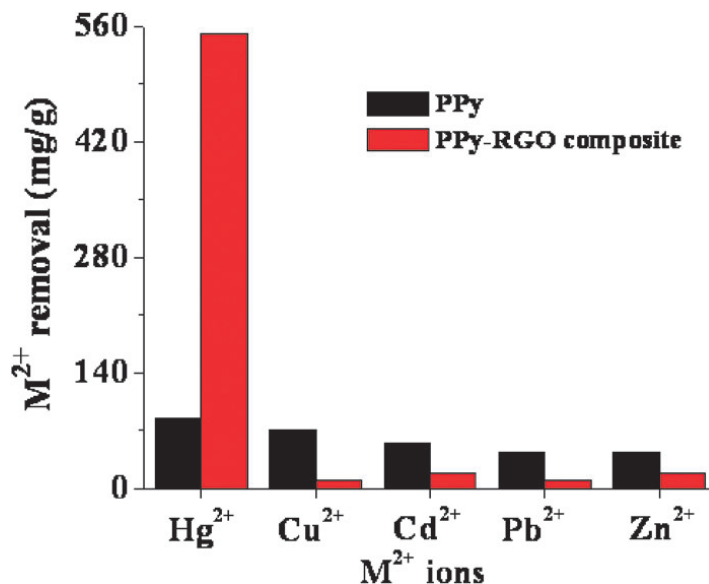


Fig. 2.18 M²⁺ removal on the PPy and the PPy–RGO composite from a mixed solution of metal ions at 20 °C and pH 3.

Later Chandra and colleagues also showed that arsenic can also be removed from contaminated water with an adsorption of over 99.9 % from an initial 1 ppb solution hence these can be used in arsenic removal from water. The composites can be recovered easily since they are superparamagnetic at room temperature. As compared to bare magnetite particles, the hybrids showed a high sorption towards As (III) and As (V) and this high sorption capacity was due to the increased adsorption sites in the M–RGO composite [36]. Sun and Bunshi prepared composites of graphene oxide (GO) impregnated in alginate. The adsorbent was used for sorption of a dye, acridine. Entrapping GO into the alginate improved the porosity of the alginate matrix as well as the absorption capacity

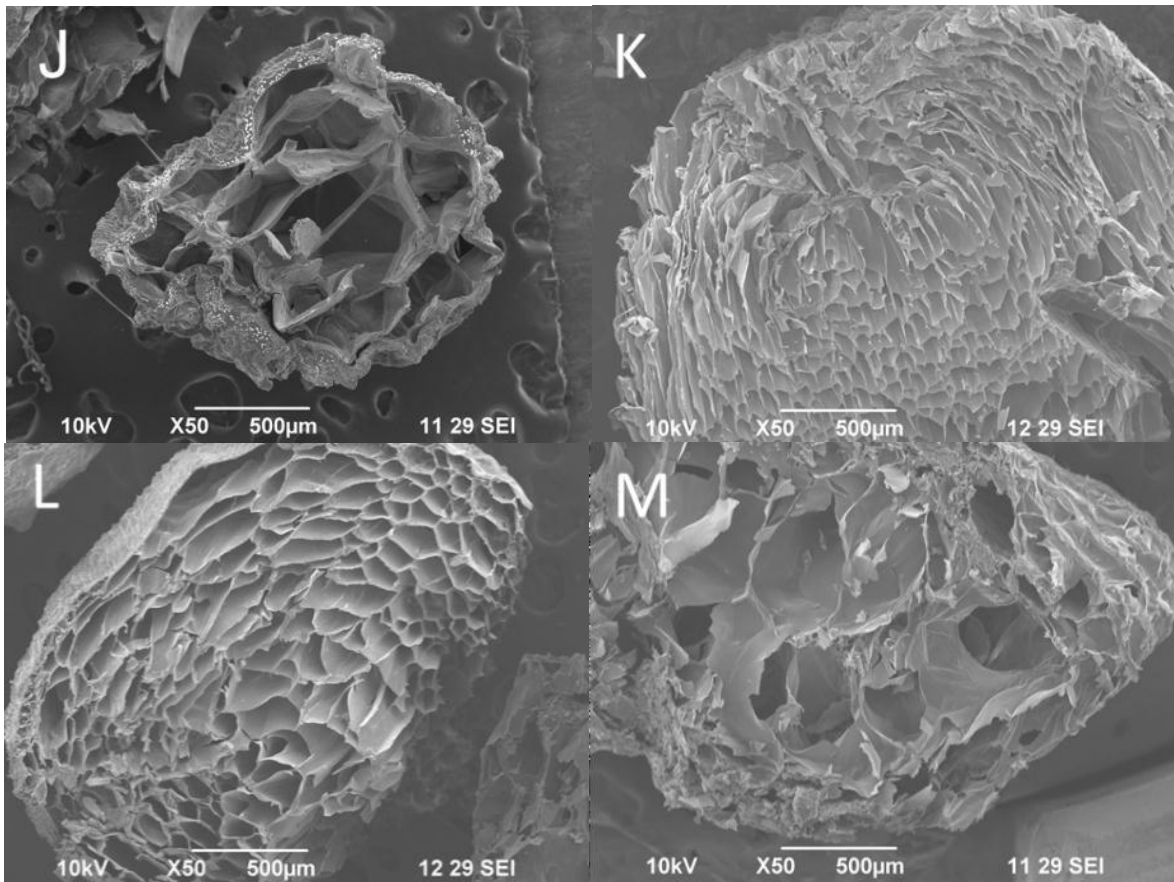


Fig. 2.19 SEM images of beads: (j) Pure SA-N, (k) Pure SA-M, (l) SA-GO-N, and (m) SA-GO-M

Kinetic studies followed the Langmuir isotherm, and higher maximum capacity was obtained in the presence of GO. Adsorption also increased with increase in pH because in acidic conditions the adsorption capacity of the alginate was greatly [37].

Vadahanambi et al synthesized, characterized and used three-dimensional graphene-carbon nanotube-iron oxide nanostructures for arsenic removal from contaminated water. Their nanostructure showed iron oxide nanoparticles deposited on both the carbon nanotubes which were vertically standing and on graphene sheets as shown on fig. 2.20. These nanostructures with iron oxide nanoparticles deposited on them had great adsorption capacity towards arsenic

due to their high surface area-to-volume ratio and open pore network of the graphene-carbon nanotube-iron oxide three-dimensional nanostructures [38].

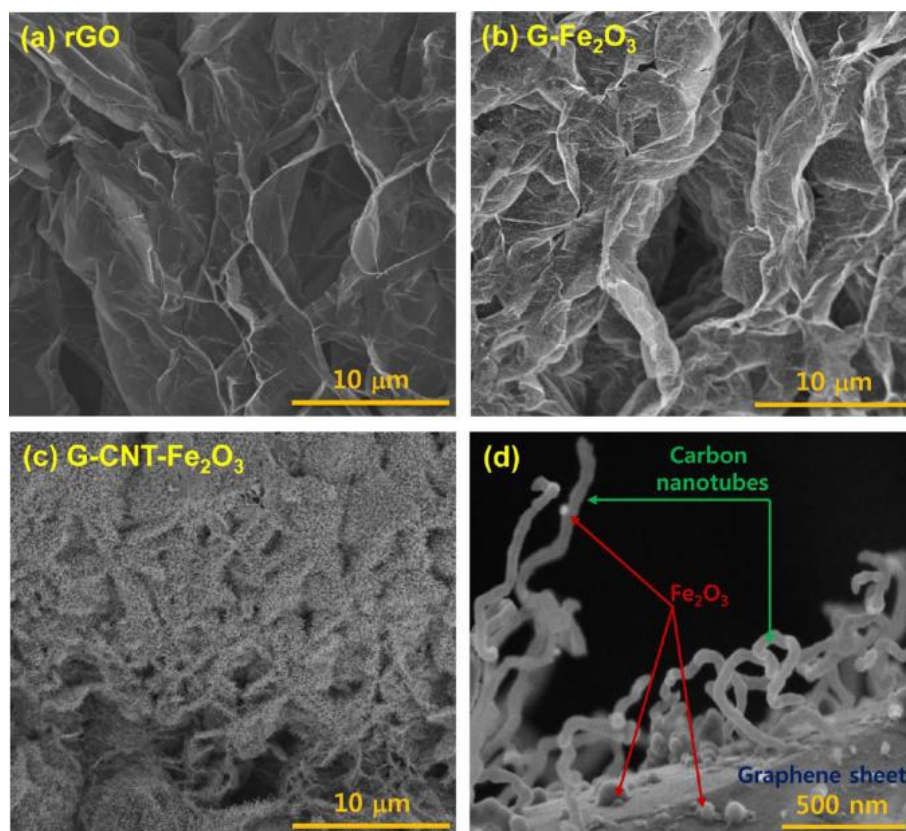


Fig. 2.20 SEM micrographs: (a) expanded graphene worm under microwave radiation, (b) 2D iron oxide decorated graphene, (c) graphene-carbon nanotube-iron oxide 3D nanostructures at the final stage, and (d) magnified 3D nanostructures; carbon nanotubes are vertically grown on graphene sheet and iron oxide nanoparticles and are decorated on both graphene sheet and carbon nanotubes.

Kumar et al worked on removal of toxic chromium based on the appealing interaction between exfoliated graphene oxide (EGO), trioctylamine (TOA) and Cr (VI). An adsorbent was made by impregnating graphene oxide with amine for the removal of hexavalent chromium. The nanocomposite adsorbent showed great adsorption of chromium with an adsorption capacity of 232.55 mg g⁻¹ which is quite high. The -NH_3^+ and the HCrO_4^- ions on the structure showed

affinity towards graphene oxide in the form of cation-pi and electrostatic interactions with adherence to second order kinetics.

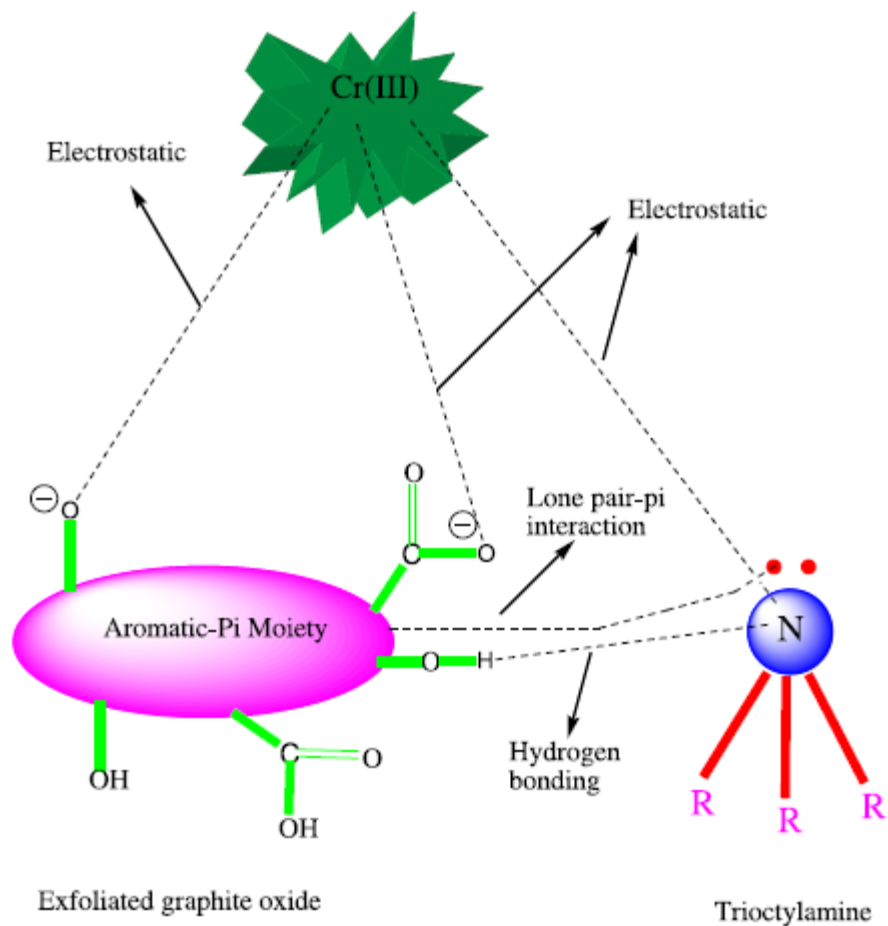


Fig. 2.21 Interaction between Cr^{3+} , exfoliated GO and trioctylamine

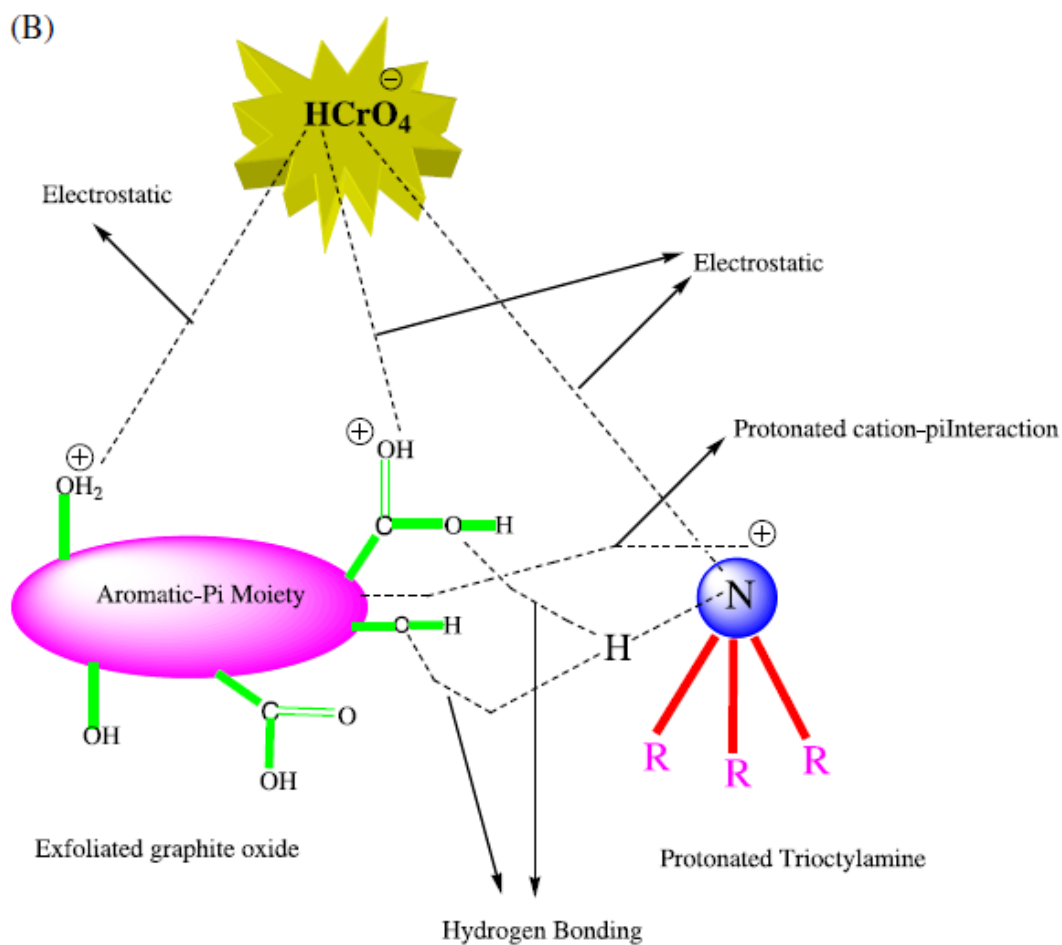


Fig. 2.22 Conceptual illustration of the affinity between (A) EGO and trioctylamine (B) TOA-EGO and chromium(VI).

The hexavalent and trivalent chromium can interact with this amine impregnated EGO adsorbent depending on the pH of the medium. The nanocomposite adsorbent has great potential in remediating wastewater samples [39].

Gan et al synthesized magnetic graphene oxide for removal of organic pollutants in water with specific attention to residual polybrominated diphenyl ethers. The purpose of the research was to make recyclable magnetic graphene composite absorbent. Iron oxide was used as the magnetic material, and the composite had an adsorption percentage of the polybrominated diphenyl ethers of 88.2 % – 99.1 % and still the percentage reached 80 % after recycling

(reusing). This nanocomposite can be considered cheaper since it maintained its adsorption capacity after reusing as well as easy recovery since its magnetic [40]. The same type of material was used to remove metals i.e. Ni^{2+} and Zn^{2+} by Muthukrishnaraj et al

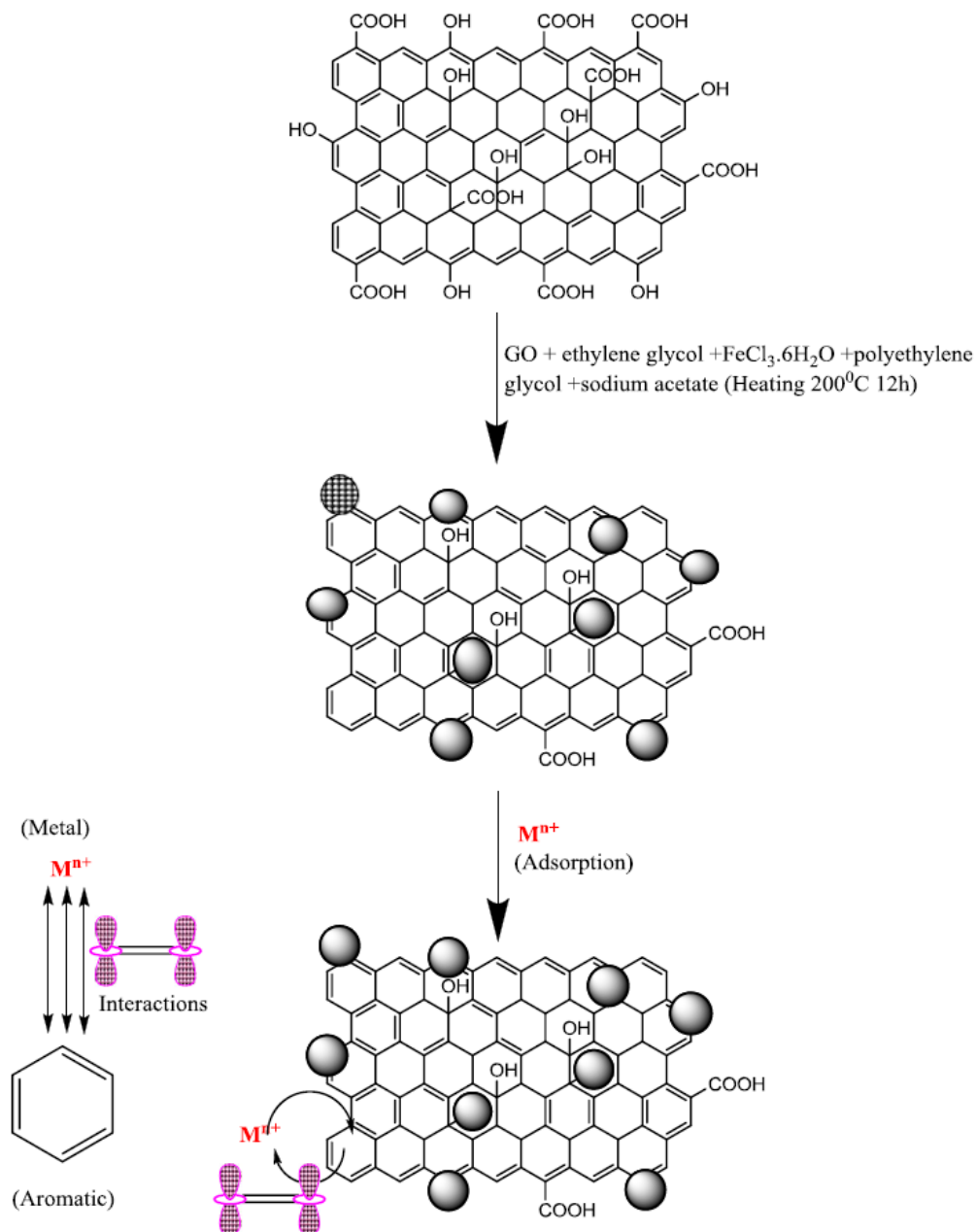


Fig. 2.23 The schematic representation for the metal ions removal on to magnetically recoverable graphene/Fe₃O₄ composite (GFC)

The nanocomposite showed high adsorption for the metal ions with the percentage removal of Zn^{2+} and Ni^{2+} at 96 % and 87 %, respectively [41]. On the same note, El-Din et al used magnetic graphene nanocomposites for removal of yet again an organic compound but this time methylene blue dye. The results of the experiment showed that increasing the ratio of the magnetic material on the graphene decreased the adsorption capacity but enhanced the magnetic properties of the composite [42].

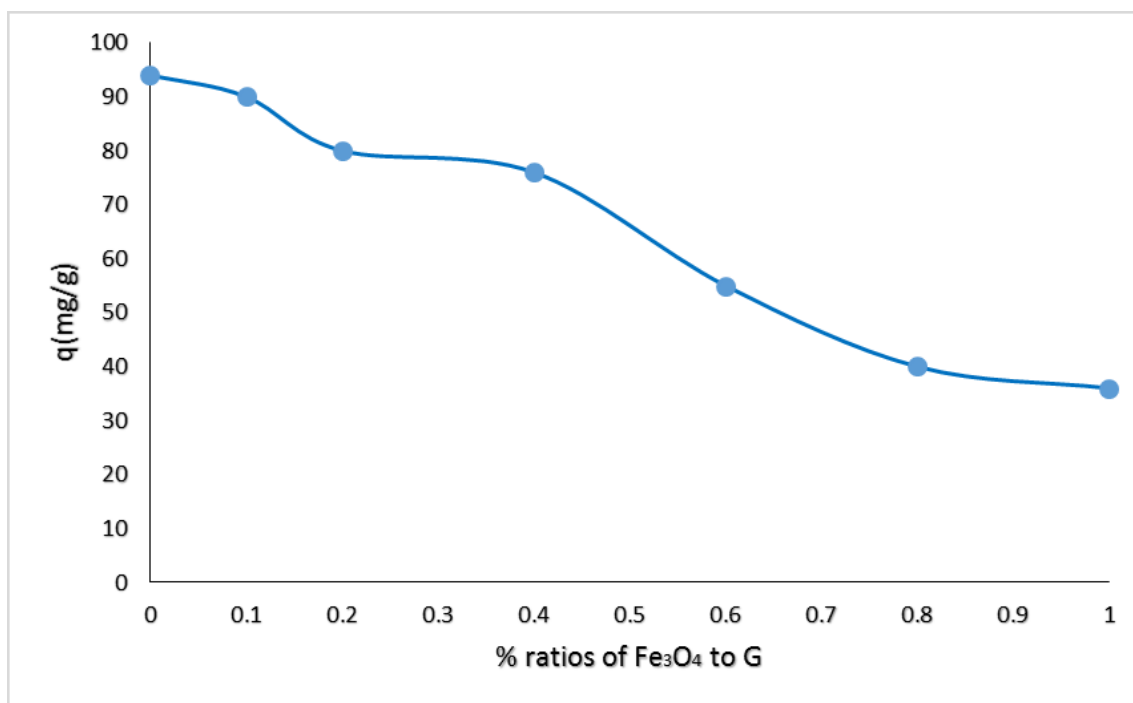


Fig. 2.24 Adsorption of MB on different ratios of pure Graphene and G/ Fe₃O₄ nanocomposites (different ratios: (Sample 0.1, Sample 0.2, Sample 0.4, Sample 0.6, Sample 0.8 and Sample 1, respectively).

Nandi et al incorporated manganese in the magnetic (iron oxide) graphene nanocomposite to remove arsenic from water. The composite showed a 99.9 % removal of carcinogenic As^{3+} from water [43]. Poursaberi et al incorporated copper nanoparticles in graphene for simultaneous adsorption and dechlorination of carbon tetrachloride. The composite was synthesised by reducing a mixture of graphene and Cu^{2+} ions. The copper ions were reduced to

copper nanoparticles which acted as catalysts in the degradation of the carbon tetrachloride. The composite showed a 99,2% removal of the carbon tetrachloride and the chloride ion concentration in solution increased with increasing remediation time. The chloride ions are a result of the degradation of the carbon tetrachloride thus this showed of the progress of carbon tetrachloride destruction [44].

Rogers et al investigated the adsorption organic compounds using nanomaterial functionalized papers. The papers were functionalized using carbon nanotube and graphene nanoplatelet and these functionalized papers were used to adsorb aromatic compounds from water. The experimental results showed that the hybrid paper adsorbent had a 25 % improvement towards adsorption than either adsorption of the singular materials though there is need for further study of the potential of this material [45].

2.1.2 Alginate containing composites

Alginates have been used as low cost adsorbents for wastewater remediation. During adsorption process. Alginates make a gel and appear to exchange with divalent and trivalent ions using their Ca^{2+} ions. Jodra and Mijangos impregnated activated carbon (AC) in various amounts into alginate beads for adsorption of organic compounds. They used synthetic solution containing phenol. Results showed that increasing the amount of AC in the beads increased the adsorption capacity [46]. Xiaoyan et al made porous zirconium alginate beads adsorbent to remove fluoride ions from water. The beads were prepared by mixing sodium alginate with zirconium ions. It was observed that the coexisting ions, HCO_3^- , SO_4^{2-} and PO_4^{3-} had a negative effect on the fluoride adsorption but however the research concluded that the material could potentially be used in the fluoride removal [47].

Another anion extensively studied is phosphate ion. Various composite beads have been developed to remove it from aqueous solutions. Mahmood et al developed alginate/calcium carbonate beads for removal of phosphate and it did effectively remove phosphate with a percentage removal of 83.2 % which showed that it is a great potential for the removal of phosphate [48]. Alginate beads were impregnated with silver nanoparticles by Lin and coworkers and the purpose of the silver nanoparticles (AgNPs) being to act as an antibacterial material. Conventional disinfection methods used powerful oxidants like chlorine, ozone and well as UV irradiation but these oxidants can react with natural organic molecules in water resulting in carcinogenic byproducts [49].

Simultaneous removal of metals and organic compounds in water reduces the steps of purification thereby cost. Chen et al impregnated calcium alginate with Ni and Fe nanoparticles and they investigated the nanocomposite as an adsorbent using synthetic solution containing Cu^{2+} and monochlorobenzene, MCB.

The encapsulation increased the adsorption properties from 83.9 % to 86.7 % for Cu^{2+} and 94.7 % to 99.1 % for MCB compared with pure Ni/Fe nanoparticles at a faster rate even because the alginate also acts as an adsorption material thus encapsulating nanomaterials in alginate beads does not reduce activity of Ni/Fe nanoparticles [50].

Adsorption of Cu^{2+} ions was also achieved using magnetic calcium alginate hydrogel beads (m-CAHB). The beads were magnetized by Fe_2O_3 for easy recovery. The adsorption capacity was ~ 100 % under the optimum conditions with pH 2.0, 2.0 g L^{-1} adsorbent dosage for 334 and 250 mg L^{-1} initial Cu^{2+} ion concentration. The incorporation of magnetic nanoparticles did not reduce the sorption properties of the calcium alginate towards Cu^{2+} [51].

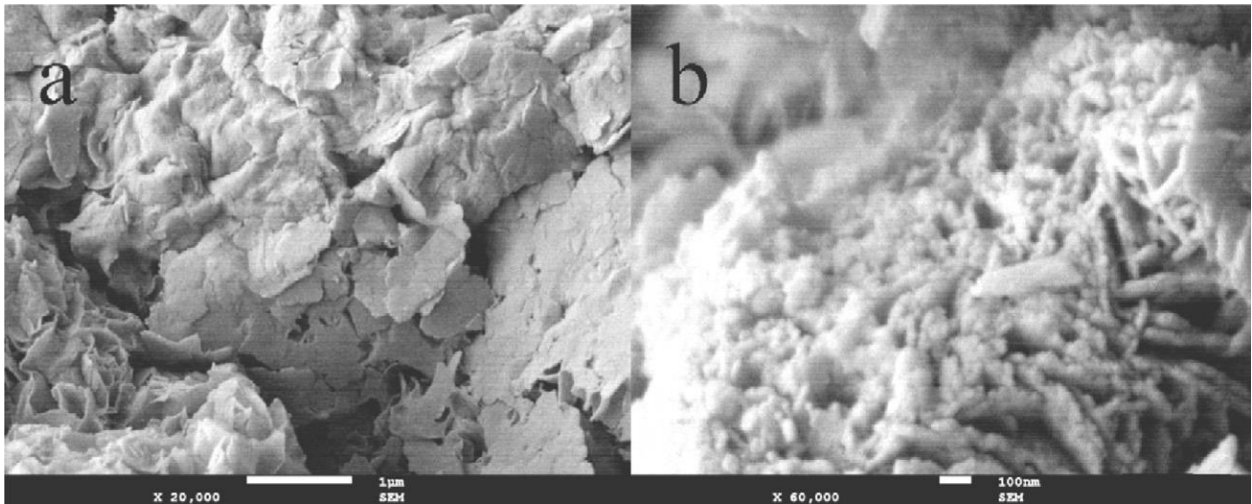


Fig. 2.25 SEM images of calcium alginate (CA) beads (a) and CA–Ni/Fe beads (b) [51]

The anion adsorption capacity can be enhanced by impregnating composite beads with layered double hydroxides (LDHs) because the positive charge of hydroxide layers in LDH has strong affinity for the aqueous negative anions [52] which makes LDH a promising adsorbent for the removal of anionic pollutants [10, 53, 54]. Huang et al impregnated magnetic alginate beads with millimeter sized magnesium and aluminum LDH nanoflakes (LDH-n-MABs) for sorption of fluoride in water. The investigation was on whether alginate was an effective material for the immobilization of Mg–Al-LDH and also to investigate the feasibility of fluoride removal using LDH-n-MABs. The results showed that the nanocomposite beads had a high adsorption capacity for the fluoride ion for both synthetic and real fluoride contaminated ground water without any leaching thus these beads have great potential in anionic contaminant removal in water [55]. Kim et al entrapped magnesium-aluminum LDH (Mg–Al-LDH) in calcium alginate beads but without magnetic material. They used this nanocomposite for phosphate removal

from contaminated water using batch and flow-through column experiments. Experimental results showed that Mg-Al LDH-alginate beads were effective in the removal of phosphate.

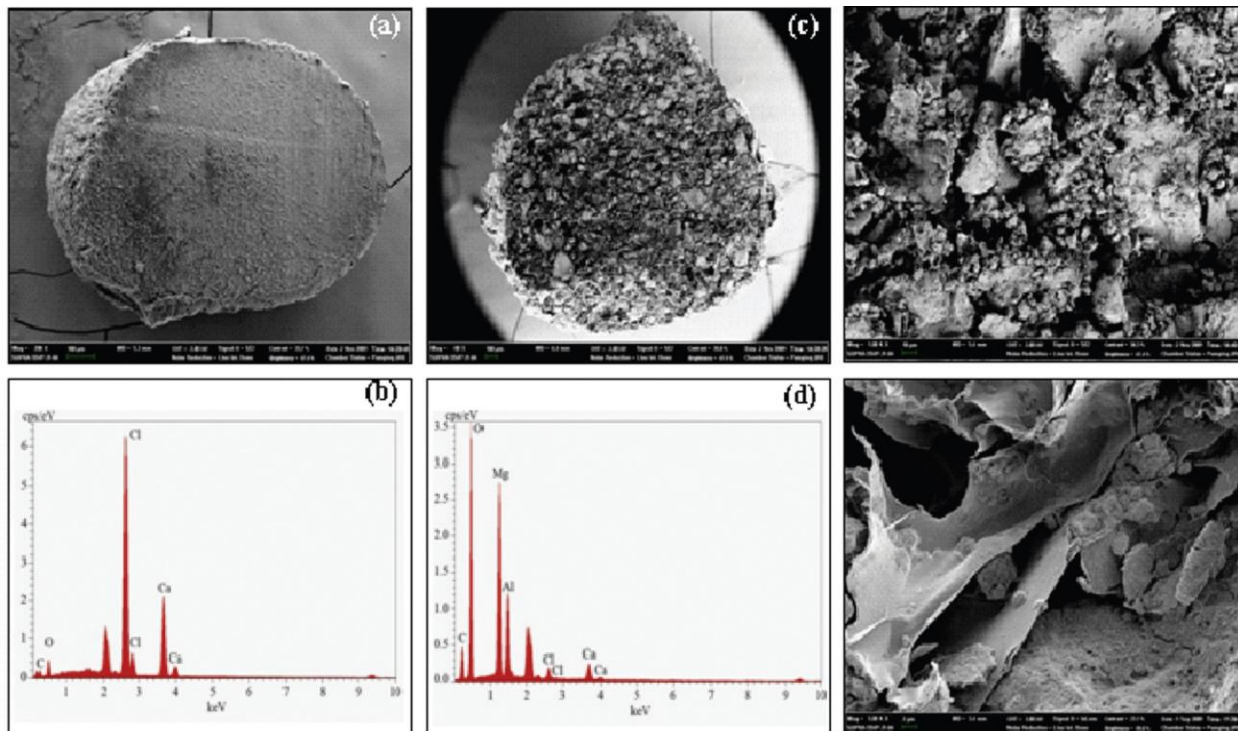


Fig. 2.26 Field emission scanning electron micrographs (FESEM) of layered double hydroxide-loaded alginate beads (LDH-alginate beads): (a) cross-sectional view of pure alginate beads (0% LDH-alginate beads) (bar $\frac{1}{4}$ 100 mm); (b) X-ray spectrum (EDS) of pure alginate beads; (c) cross-sectional view of 8%LDH-alginate beads (bar $\frac{1}{4}$ 100 mm); (d) X-ray spectrum (EDS) of 8%LDH-alginate beads; (e) FESEM image of 8% LDH-alginate beads (bar $\frac{1}{4}$ 10 mm); (f) FESEM image of 8% LDH-alginate beads (bar $\frac{1}{4}$ 2 mm).

The sorption increased from 14.1 % without the LDH to 99.1 % at a 10 % LDH-alginate composition by mass which was a sharp shoot but however at 10% LDH-alginate there was clogging at the opening of the syringe during synthesis of the bead hence 8 % LDH-alginate beads were used which still had a high percentage removal of phosphate at 98.6 % thus it follows that an increase in LDH content increases percentage adsorption without affecting the sorption properties of the alginate [56]. Han et al synthesized polyvinyl alcohol/alginate

hydrogel beads containing Mg-Al layered double hydroxide (LDH-PVA/alginate beads) for phosphate removal.

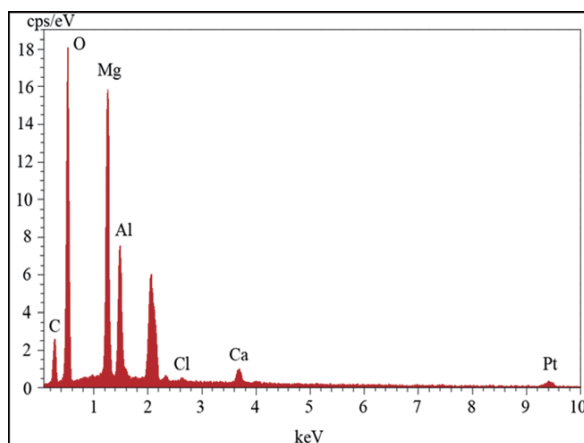
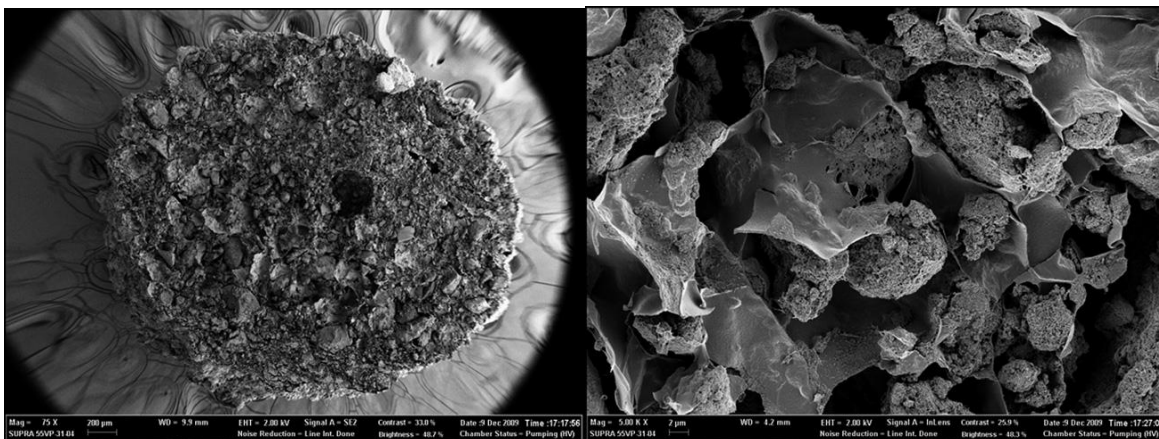


Fig. 2.27 Field emission scanning electron micrographs (FESEM) of LDH-PVA/alginate beads: (a) cross-sectional view (bar, 200 μm), (b) FESEM image (bar, 2 μm), (c) X-ray spectrum. LDH: layered double hydroxide, PVA: polyvinyl alcohol.

Results showed that by combining PVA with the LDH-alginate beads improved the adsorption of phosphate to about 99.2 % as compared to the one by Kim et al in 2011 of 98.6 % and also improved the stability of the bead in a phosphate solution as well that the adsorption was not sensitive to the pH of the phosphate solution. This study demonstrated that LDH-PVA/ alginate beads with a higher chemical stability against phosphate have the potential for phosphate removal as adsorptive material [57]. Phuong used them for nitrate removal from water. Batch

adsorption and adsorption isotherms experiments done and showed that the nitrate sorption process on the Mg–Al LDH-alginate/PVA beads followed pseudo-second-order reaction kinetic model and the Langmuir isotherm. The percentage removal of nitrate by column was 67.1 % [58].

Cho et al impregnated nanosized graphite into calcium alginate beads (AB) to make nanosized graphite carbon-impregnated calcium alginate bead (NGCAB) for removal of Pb^{2+} and Ni^{2+} .

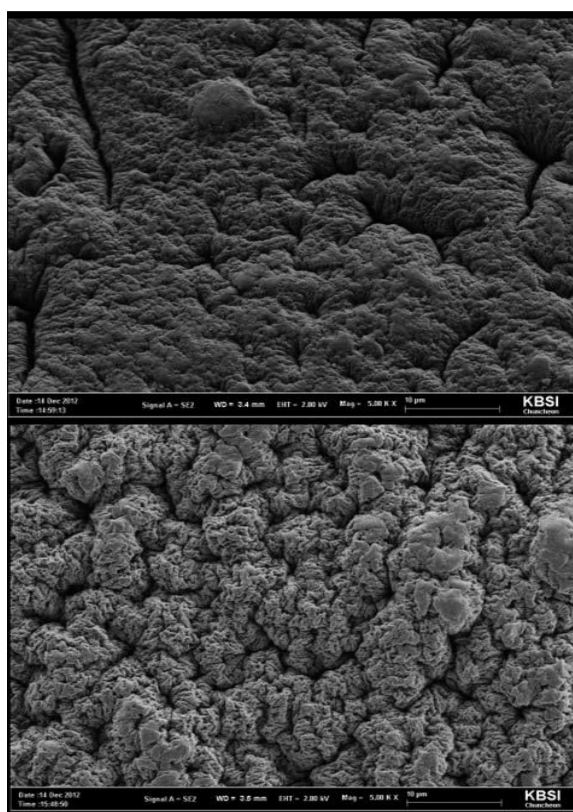


Fig. 2.28 SEM images of (a) pure alginate bead and (b) nanosized graphite carbon-impregnated calcium alginate bead.

Adsorption kinetics studies were done and it was discovered that the beads followed a pseudo second order kinetics and Langmuir isotherm model fitted well for the adsorption isotherm of Pb^{2+} onto AB, while Freundlich isotherm model showed a good prediction for NGCAB and the adsorption isotherm for Ni^{2+} followed the Freundlich isotherm [59].

Bezbaruah et al entrapped iron nanoparticles into calcium alginate beads for removal of nitrate ions in groundwater. The bare non-zero valent iron (nZVI) nanoparticles reduced the nitrate ion levels by a percentage almost the same as the entrapped nZVI thus entrapment gives a better option since bare nZVI tend to amalgamate due to magnetic and Van der Waals forces and form larger particles that sediment into aquifer media pores. The amalgamated particles have decreased activity because they have decreased specific surface area unlike the entrapped ones. None Zero valent iron has an advantage over the zero valent iron (ZVI) of having a high surface area thus faster and more complete reactions and can be easily injected into the aquifer [60]. Non-zero valent iron can also be used to reduce cations with high oxidation states e.g. Cr^{6+} . Kim et al used iron-iron oxide nanocomposites for sorption of chromium (VI) in water but however the composite can also reduce the Cr^{6+} to Cr^{3+} at a neutral pH using the non-zero valent iron since effort is being made to synthesis composites that can both adsorb and reduce Cr^{6+} [61].

Chmielewska et al impregnated alginate with zeolite clinoptilolite pellets so as to improve the adsorption performance of the zeolites. They used synthetic solutions of nitrates, sulphate and Zn^{2+} . Results of the experiments showed that adsorption was higher than other mostly natural adsorbents examined towards similar pollutants thus showing that the alginate zeolitic beads had great potential for remediating polluted water [62].

Kim et al developed an alginate complex for simultaneous removal of mixed contaminants containing both organic and inorganic compounds. The alginate complex was synthesized by entrapping synthetic zeolite and powdered activated carbon (PAC) into alginate gel bead. Synthetic solutions of zinc and toluene were used as target contaminants. The equilibrium and kinetic batch tests showed that the adsorption of two contaminants followed Langmuir isotherm

and that the nanocomposite had a percentage removal of zinc and toluene of 54 % and 86 % for the initial solution concentrations of 250 mg/L, respectively which was far better compared to the individual adsorbents and also better than alginate impregnated with PAC (AG-AC bead) [1].

A novel nanopore biopolymer was produced by Esmailian et al. They developed an alginate gel bead impregnated with surfactant-modified zeolite (SMZ) and powdered activated carbon (PAC) for simultaneous removal of nitrate and cadmium ions from wastewaters and the beads showed a 56 % and 99.8 % removal percentage respectively. Different aspect ratios were used [2].

Papageorgiou et al investigated the effect of porosity in Cu^{2+} and Cd^{2+} ion sorption by developing porous alginate aerogel beads and compared them with their non-porous aerogel analogues. The beads showed a 20 % higher sorption capacity attributed to increased functional groups accessibility combined with increased flexibility due to the effect of porosity [63].

The nanoparticle impregnated beads had a greater removal efficiency compared to the bare alginate beads and the nanocomposite beads retained their sorption properties even after three time regeneration [50]. Wu et al made magnetic alginate beads to determine the absorption capacity of these beads towards lanthanum using batch and column flow techniques. The magnetic material was iron oxide and the magnetic properties were mainly for easy recovery and the beads could be regenerated easily using 0.05 mol/L CaCl_2 effectively. The experimental data showed that the magnetic alginate beads are effective adsorbents for the uptake of La^{3+} from aqueous chloride medium and chemisorption was considered to be a key of process and adsorption mechanism could be concluded to be complexation, ion exchange and electrostatic

interaction [64]. Hammouda and et al used these magnetic alginate beads for removal of organic contaminants by using synthetic 3-methylindole from aqueous solution and applying the Fenton process. The nanoparticles of Fe_2O_3 also worked as catalysts for the decomposition of 3-methylindole besides being the magnetic material with a low leaching of the nanoparticles. However, the nanocomposite worked at carefully chosen operating conditions and a deviation from these reduced the activity of the beads. The beads showed great sorption properties with a total removal of the indole thus the beads have great potential for water remediation [65]. The magnetic alginate was also used for removing Uranium with a 98 % percentage removal but however an organic extractant tri- n -butyl phosphate (TBP) was also impregnated together with the magnetic nanoparticles [65]

Cataldo et al made beads by mixing alginate/pectate sorbent materials and used them in gel phase for Cd^{2+} and Cu^{2+} removal from aqueous solutions. The sorption process of these ions with concentration ratios was investigated using kinetic and equilibrium tests and it was shown from kinetic tests that sorption of Cd^{2+} and Cu^{2+} occurred prevalently by ion exchange and that it was higher for the mixed alginate/pectin gel beads compared to the calcium alginate polymer gel and that the sorption process followed a pseudo second-order kinetic model. The activity of the nanocomposite increased with an increase in the amount of pectin in the mixed alginate/pectate gel system according to the trend $\text{Ca-AP2} > \text{Ca-AP1.5} > \text{Ca-AP1}$ [66].

Rao et al developed a new sodium alginate-gelatin (SAG))-g-poly (acrylic acid)/polyaniline (SAPAPN) by cross-linking with glutaraldehyde then grafting by free radical polymerization with poly (acrylic acid) and polyaniline. The beads showed great potential in sorption of Ni^{2+} and Cu^{2+} and recyclability thus they can be used for the said purpose.

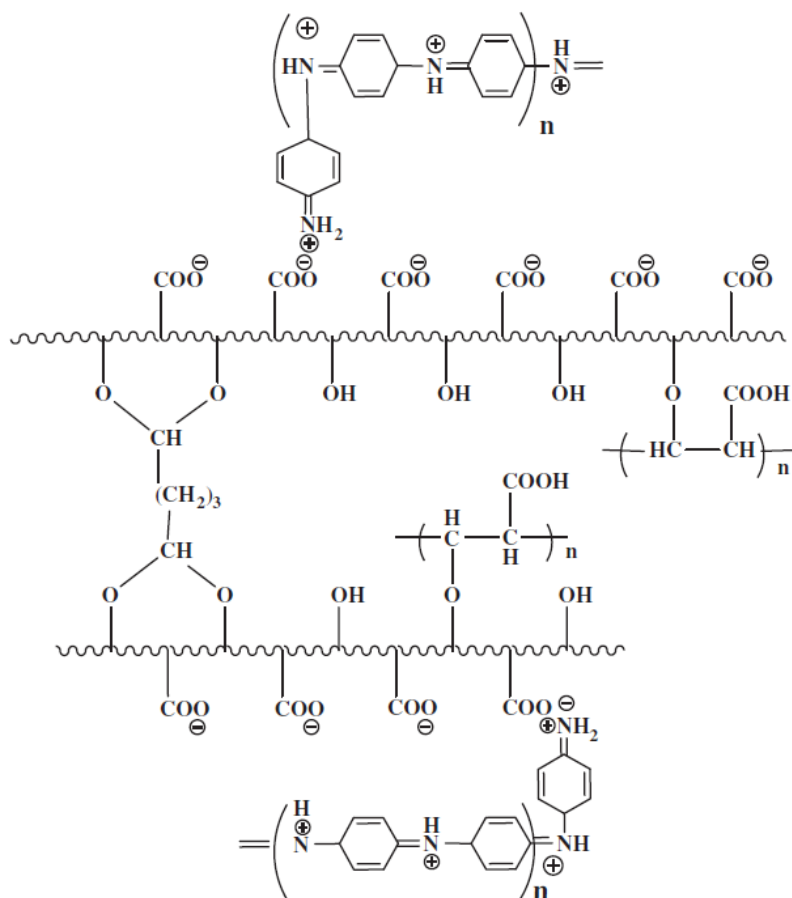


Fig.2.30 Schematic representation of cross-linked SAPAPN adsorbent [67]

Lee and Kim synthesized magnetic alginate-layered double hydroxide composites which were used for phosphate removal. It was discovered that both the magnetic Fe_2O_3 and the Mg-Al LDH had sorption properties towards the phosphate ion thus it's an added advantage for the magnetic material to also adsorb the phosphate ions. This showed the great potential for the nanocomposite bead [68].

2.1.3 Other nanocomposites

There are various other combinations of adsorbent materials that can be amalgamated into a nanocomposite bead. Ghorai and colleagues developed a biodegradable nanocomposite of the combination of xanthan gum and silica for removal of Pb^{2+} ions in water. The physical and

chemical characteristics of the nanocomposite showed stronger interaction of silica nanoparticles with xanthan gum and a high sorption of Pb^{2+} compared to other reported adsorbents which could be attributed to higher hydrodynamic radius and hydrodynamic volume. The experimental evidence also showed that the nanocomposite could be easily regenerated [69]. The researchers also went on to investigate whether the nanocomposite could be used for organic compounds with a particular emphasis on removal of Congo red (CR) dye from aqueous solution. Experimental results showed that the nanocomposite had excellent adsorption capacity for CR dye ($Q_e = 209.205 \text{ mg g}^{-1}$), which is considerably high and the beads could be regenerated of this pollutant as well [70]. Other dyes were removed by other different nanocomposites some of them magnetic i.e. malachite green dye onto novel kappa-carrageenan-g-polyacrylic acid/ $\text{TiO}_2\text{-NH}_2$ hydrogel nanocomposite [71], methylene blue sorption by humic acid-coated Fe_3O_4 nanoparticles [72], reactive Blue 5 using magnetic composite of activated carbon and iron oxide [73], methyl violet blue using halloysite-magnetite-based composite [74] and methylene blue using gum and silica hybrid organic-inorganic hydrogel nanocomposite [75] Xanthan gum was also impregnated with magnetic nanocomposites of iron oxide for removal of malachite green from aqueous solution [76] and also the cationic azo dye crystal violet was adsorbed by magnetite nanoparticles coated with waste sourced bio-based substances synthesized by Magnacca et al [77].

Some magnetic nanocomposite beads can be made using molecular imprinted materials. Molecular imprinting can be defined as the assembly of a cross-linked polymer matrix around an imprint molecule that is held in place by either chemical or physical bonds from the functional monomers. The removal of the imprint molecule then produces an imprint cavity of a specific size and shape complementary to the imprint molecule [78] which is also capable of

reuptake of the imprint if the template is due to ionic interactions since it can be selectively recognized by the sites wherewith it once was [79]. This then is called the molecularly imprinted polymer (MIP) which can be made into various shapes during synthesis in its gel form for different applications [80]. These imprint sites act the same as the active sites of biological receptor molecules such as antibodies and enzymes [81]. The idea of molecular imprinting was first introduced in 1931 and in 1972, Wulffand Sarhan, and Klots and Takagishi synthesized organic polymers with imprinted sites for ligand selectivity [82] and in decades that followed, more research has been ongoing on the applications of MIPs as polymeric antibodies in both analysis and remediation of wastewater [83]. MIPs also found application for sorption of various selective organic water pollutants [84, 85] and also selective sorption of various metal ions. Ion imprinted polymers, IIPs, operate the same way as MIPs since they can recognize metal ions after imprinting [86] thus IIPs have potential use for selective sorption of inorganic pollutants [87,88] even in weakly acidic solutions [89]. Ion imprinted polymers besides being simple and easy to have predetermined selectivity and also low cost, they are stable and can be employed in a wider pH range, solvents and temperatures without structural or chemical changes [90, 91]. Selectivity of IIPs comes from the specificity of the ligand on the coordination geometry of the ion-template complex, coordination number of the ions, charges on the ions and on their sizes [92].

Magnetizing the IIPs with Fe_3O_4 results in easy and economical recovery process [92,93,94 and 95]. The concept of making magnetic composite beads for easy recovery after use has attracted interest over the past decade or so since it is easy, convenient and economical and ecofriendly [96]. Tawengwa synthesized magnetic ion imprinted polymers with high recognition for uranyl ion (UO_2^{2+}) in the presence of competing ions and the selectivity order was $\text{UO}_2^{2+} > \text{Fe}^{3+} >$

$\text{Pb}^{2+} > \text{Ni}^{2+} > \text{Mg}^{2+}$. Anions were also investigated with a selectivity order as follows $\text{Cr}_2\text{O}_7^{2-} > \text{SO}_4^{2-} > \text{F}^- > \text{NO}_3^-$ thus even in the presents of other competing ions, cation or anions alike, selectivity was enhanced for the imprinted ions [96,97].

Gum is another adsorbent used in nanocomposites as reported by Mittal et al (2014) when they used gum ghatti-grafted poly (acrylamide-co-acrylonitrile). The nanoporous composite was used for sorption of Pb^{2+} and Cu^{2+} which proved to be efficient and cost effective though highly pH dependent [98]. Yamada et al coated zeolites with LDH which were used for Ca^{2+} and NH_4^+ removal in water and the experimental results showed great sorption properties and hence the nanocomposite could be used for remediation of polluted water [12].

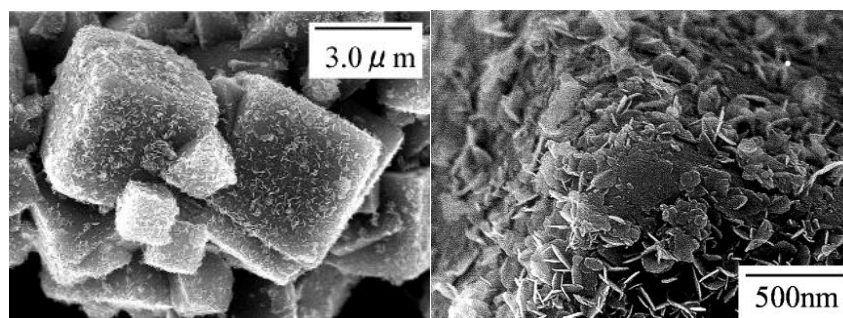


Fig. 2.31 SEM images of LDH-coated zeolite-LTA by a hydrothermal treatment. [12]

Hristodor and researchers entrapped nanoparticles in clay to make clay nanocomposites. This was done by using Al^{3+} and Fe^{3+} nitrate solution as starting material wherewith the solutions were mixed with clay and NaOH added dropwise to form the composite. These composite were used to remediate radioactive waste containing Cs. The nanocomposite clay showed great sorption properties for radioactive waste [99]. Kalantari et al combined clay and Fe_3O_4 nanoparticles. The nanocomposite were used for sorption of Pb^{2+} , Cu^{2+} and Ni^{2+} ions and reported a percentage removal efficiency of 89.72 %, 94.89 % and 76.15 % respectively

showing a potential for remediation of the latter [100]. Adding Cd^{2+} , Cr^{2+} , Co^{2+} , and Mn^{2+} to the a solution containing the afore mentioned ions, then sorption of the latter using 2,4-Dinitrophenylhydrazine (DNPH) immobilized on sodium dodecyl sulfate coated nano-alumina was investigated by Afkhami et al and experimental data showed that though the nanocomposite had great sorption efficiency, it was affected by pH, contact time and adsorbent dosage [101,102, 103]

3.0 METHODOLOGY

3.1 Materials

All the reagents used were of analytical grade. Absolute ethanol, iso-propyl alcohol, sodium hydroxide pellets, hydrochloric acid (32 %) and chromium (III) chloride were supplied by Glassworld. EDTA and sodium alginate ($C_6H_7O_6Na$) were supplied by Techno pharm Chem, India. Zinc nitrate and ferrous sulphate were supplied by Associated Chemical Enterprises. Potassium dichromate and calcium chloride were supplied by UniLab. Xanthan gum and copper (II) sulphate were supplied by Skylabs. Aluminium nitrate, cadmium oxide and disodium hydrogen phosphate were supplied by MERCK. Ascorbic acid was supplied by M.C. Scientific. Ammonium molybdate and aluminium oxide were supplied by Hopkins and Williams. Cobalt sulphate was supplied by M&B and potassium dihydrogen orthophosphate was supplied by SAR Chem.

3.2 Synthesis of Zeolite

3.2.1 Synthesis of zeolites from bentonite clay

Bentonite clay was calcined for 2 hours at $700\text{ }^{\circ}\text{C}$. After cooling, 30 g of the calcined clay was mixed with 5 M NaOH in a 1g: 5 mL ratio in a 250 mL beaker. The mixture was stirred for 5 hours at $100\text{ }^{\circ}\text{C}$ and then transferred into a Teflon lined hydrothermal synthesis autoclave for 18 hours at $150\text{ }^{\circ}\text{C}$. The final mixture after cooling was filtered and washed with distilled water until the pH of the eluent was 10 [104].

Another zeolite was synthesized from bentonite clay but at a temperature of $200\text{ }^{\circ}\text{C}$ using the same procedure as above.

3.2.2 Synthesis of zeolites from local clay

Local clay was calcined at 700 °C. After cooling, 40 g of the calcined local clay was mixed with 5 M NaOH in a 1g: 5 mL ratio in a 500 mL beaker and stirred for 5 hours at 100 °C. The mixture was transferred into a Teflon lined hydrothermal synthesis autoclave at 150 °C for 18 hours. The final mixture after cooling was filtered and washed with distilled water until the pH of the eluent was 10 [104].

3.2.3 Synthesis of zeolites from silica and Al₂O₃

Silica rock was pulverized into fine powder and sieved (~ 70 microns). NaOH (1.66 g) was added slowly to deionized water (28 mL) in a 250 mL beaker and stirred until a clear homogenous solution which appeared after about 5 mins. To 0.75 g of Al₂O₃ was added 2 mL of the prepared NaOH. The mixture was stirred at 100 °C until a homogenous mixture was obtained. To 1.54 g of silica was added 5.5 mL of NaOH and the mixture was stirred at 100 °C until a homogenous mixture was obtained. After homogenization, the two mixtures were mixed together and stirred vigorously for 5 hours until homogenization was obtained. The resulting homogenous mixture was transferred into a Teflon lined hydrothermal synthesis autoclave at 150 °C for 18 hours. The final mixture after cooling was filtered and washed with distilled water until the pH of the eluent was 10 [104].

3.3 Synthesis of magnetic nanoparticles (MNPs), Fe₃O₄

Ferric chloride (FeCl₃.6H₂O), (5.75 g) was mixed with 15.33 g of sodium acetate in a 500 mL beaker. To the mixture was added 320 mL of diethylene glycol under mechanical stirring. After homogeneity, the yellow solution was transferred into a Teflon lined hydrothermal synthesis autoclave, sealed and heated at 200 °C for 8 hours. The black magnetic precipitate was washed

with ethanol and deionized water then dried using acetone [40]. The product was characterized by FT-IR.

3.4 Synthesis of Aluminium – Zinc Layered Double Hydroxides (LDH)

A solution of a mixture of Zn^{2+}/Al^{3+} was made by adding 17.85 g of $Zn(NO_3)_2 \cdot 6H_2O$ and 11.34 g of $Al(NO_3)_3 \cdot 9H_2O$ and 5.10 g of $NaNO_3$ to 300 mL of deionized water in a 500 mL beaker and stirred with a magnetic stirrer until all salts were completely dissolved. To this solution, 2 M NaOH was added dropwise from a burette with vigorous stirring at ambient temperature until the pH reached 10.70. The mixture was left stirring for 24 hours. After 24 hours of stirring, the mixture was filtered using a vacuum pump and a Buchner flask and washed with deionized water until pH of the filtrate reached 9. The residue was dried in an oven at 80 °C for 24 hours. The Al/Zn LDH was characterized using FT-IR.

3.5 Coating mixture of zeolite, MNPs, activated charcoal with Zn/Al Layered Double Hydroxide (LDH)

A zeolite mixture was made by mixing zeolites synthesized from bentonite clay, local clay and silica/aluminium oxide in a 1:1:1 ratio. A portion of this zeolite mixture (9.48 g) was mixed with 3.20 g of activated charcoal and 4 g of MNPs in a 1000 mL beaker. Zinc nitrate, $Zn(NO_3)_2 \cdot 6H_2O$ (17.85 g) and 11.34 g of aluminium nitrate, $Al(NO_3)_3 \cdot 9H_2O$ and 5.10 g of sodium nitrate, $NaNO_3$ were also added to the mixture in the 1000 mL beaker and 300 mL of deionized water was added. The mixture was stirred with a magnetic stirred until a homogenous mixture was obtained. Sodium hydroxide (2 M) was added dropwise with vigorous stirring until the pH reached 10.7. The mixture was stirred for 24 hours at ambient temperature. Afterwards the mixture was filtered and washed with deionized water until the pH

of the eluent was 9.4. The mixture was then dried in an oven at 100 °C for 24 hours. After drying the granules were ground in a mortar and pestle.

3.6 Synthesis alginate beads impregnated with the magnetic nanocomposite

A solution of 3 % w/v of sodium alginate was prepared by mixing 9.00 g of sodium alginate powder with 300 mL deionised distilled water. The mixture was stirred with a magnetic stirrer until it was homogenous. After it was homogenous, 12.00 g of the magnetic nanocomposite (Fe₃O₄ MNP, zeolite, activated charcoal and LDH) and 1,0 g of xanthan gum were added to the 3 % w/v of sodium alginate solution in an aspect ratio of 3:4:1 (alginate: nanocomposite: xanthan gum). The aspect ratio was selected on the basis of work by Esmailian et al [2]. The mixture was stirred with a magnetic stirrer until it was homogenous. The mixture remained stationary for 1 hour for degassing. The mixture was poured into a burette and added dropwise to a 500 mL solution of 4 % CaCl₂ to form the magnetic nanocomposite beads. The calcium alginate complex gel beads were formed upon contact with the cross linker solution and were kept in the solution for 24 hours to mature and stabilize. The beads were filtered from the solution and washed with 2.5 L deionised water and dried in an oven at 60 °C for 24 hours [2].

3.7 Preparation of the stock solutions for adsorption studies

Solutions containing cations, anions and aromatic organic compounds were made for adsorption studies. Three solutions were made i.e. 100 ppm /10% toluene, 200 ppm/ 15% toluene and 400 ppm of Cu²⁺, PO₄³⁻, Cr₂O₇²⁻ into 3 different volumetric flasks.

3.7.1 The 100 ppm solution

The 100 ppm solution was prepared by adding 0.14945 g of Na_2HPO_4 ; 0.39281 g of $\text{CuSO}_4 \cdot 5\text{H}_2\text{O}$ and 0.13622 g of $\text{K}_2\text{Cr}_2\text{O}_7$ to 200 mL of deionized water. The solution was transferred into a 1000 mL volumetric flask and 100 mL of toluene was added using a 100 mL measuring cylinder and the mixture was made to the mark using absolute ethanol. The final pH was 0.98

3.7.2 The 200 ppm solution

The 200 ppm solution was prepared by adding 0.2989 g of Na_2HPO_4 ; 0.7858 g of $\text{CuSO}_4 \cdot 5\text{H}_2\text{O}$ and 0.2724 g of $\text{K}_2\text{Cr}_2\text{O}_7$ to 200 mL of deionized water. The solution was transferred into a 1000 mL volumetric flask and 150 mL of toluene was added using a 100mL measuring cylinder and the mixture was made to the mark using absolute ethanol. The final pH was 0.94

3.7.3 The 400 ppm solution

The 400 ppm solution was prepared by adding 0.5978 g of Na_2HPO_4 ; 1.5716 g of $\text{CuSO}_4 \cdot 5\text{H}_2\text{O}$ and 0.544 g of $\text{K}_2\text{Cr}_2\text{O}_7$ to 200 mL of deionized water. The solution was transferred into a 1000 mL volumetric flask using a 100 mL measuring cylinder and the mixture was made to the mark using absolute ethanol. The final pH was 0.96

NB - The prepared solutions turned into green from yellowish orange due to the reduction of $\text{Cr}_2\text{O}_7^{2-}$ by the ethanol under acidic condition to Cr^{3+} . All the dichromate was reduced to Cr^{3+} since the alcohol was in excess.

3.8 Batch adsorption studies

Batch adsorption studies were performed to investigate the efficiency of the LDH – coated zeolite – MNP – activated charcoal nanocomposite and the alginate beads impregnated with the nanocomposite material.

3.8.1 Batch adsorption methods for phosphate

A gram of adsorbent was weighed into each of the 100 mL conical flask. After that, 100 mL of the 100 ppm solution was added to each flask at a pH of 0.98 at ambient temperature. The flasks were shaken using an agitator for 10, 15, 30, 45, 60, 120, 180, 240 and 300 mins. The experiment was repeated using 200 ppm and 400 ppm solutions. The remaining concentration of phosphate in each of the flask was determined using the colourimetric method.

3.8.1 Preparation of reagents for the colourimetric determination of phosphate ions

Reagents were prepared for the colourimetric determination of phosphate using UV VIS.

Reducing solution preparation

The reducing solution was made by mixing 39 mL of ammonium heptamolybdate, $(\text{NH}_4)_2\text{Mo}_7\text{O}_{24}\cdot 4\text{H}_2\text{O}$ (1 g in 50 mL), 60 mL of ascorbic solution (1 % w/v in H_2O) and 125 mL of diluted sulphuric acid (0.90 M) into a 250 mL volumetric flask and making upto the mark using deionised water.

Standard solutions preparation

A standard stock solution of phosphate (1000 ppm) was prepared by dissolving 1.433 g of potassium dihydrogen phosphate, KH_2PO_4 in 1L of deionised water in a 1000 mL volumetric flask and from this, aliquots of the stock solution for preparing working standards of 0.0, 0.4,

0.8, 1.6, 2.4 and 3.2 ppm PO_4^{3-} were transferred into six 50 mL volumetric flasks. Into nine other 50 mL volumetric flasks, was pipetted 2 mL from the samples in their order of 10, 15, 30, 45, 60, 120, 180, 240 and 300 mins for the 100 ppm solution. To each of the 15 flasks was added 20 mL of the reducing solution and filled up to the mark using deionised water. The flasks were then heated in a water bath at 50 °C. The absorbance was measured at 830 nm using a UV-VIS (Shimadzu UV-3101PC). The procedure was repeated for the 200 ppm and 400 ppm solutions.

3.8.2 Batch adsorption for Chromium (III)

A gram of adsorbent was weighed into each of the 100 mL conical flask. After that, 100 mL of the 100 ppm solution was added to each flask at a pH of 0.98 at ambient temperature. The flasks were shaken using an agitator for 10, 15, 30, 45, 60, 120, 180, 240 and 300 mins. The experiment was repeated using 200 ppm and 400 ppm solutions. The remaining concentration of chromium (III) in each of the flask was determined using the colourimetric method.

3.8.2.1 Preparation of reagents for chromium (III) determination.

Preparation of Standard solution.

A 1000 ppm stock solution of Cr was made by dissolving 5.124 g of $\text{CrCl}_3 \cdot 6\text{H}_2\text{O}$ in 1000 mL of deionised water. Working standards of 5, 10, 20, 40 and 50 ppm was made by pipetting 0.5, 1.0, 2.0, 4.0, 5.0 mL respectively, of the 1000 ppm stock solution into each of the 100 mL volumetric flasks and made up to the mark using a 0.15 M solution of EDTA (55.826 g in 1000 mL of deionised water). The flasks were heated for 30 mins at 100 °C and absorbance was recorded at 575 nm.

Preparation of samples

For each of the samples, 10 mL of each of the samples were pipetted into each of the 50 mL volumetric flask and made up to the mark using a 0.15 M solution of EDTA (55.826 g in 1000 mL of deionised water). The flasks were heated for 30 mins at 100 °C and absorbance was recorded at 575 nm using a UV-VIS (Shimadzu UV-3101PC). The procedure was repeated for the 200 ppm and 400 ppm solutions.

3.8.3 Batch Adsorption of copper

A gram of adsorbent was weighed into each of the 100 mL conical flask. After that, 100 mL of the 100 ppm solution was added to each flask at a pH of 0.98 at ambient temperature. The flasks were shaken using an agitator for 10, 15, 30, 45, 60, 120, 180, 240 and 300 mins. The experiment was repeated using 200 ppm and 400 ppm solutions. The remaining concentration of copper in each of the flask was determined using the Flame Atomic Absorption Spectroscopy.

3.8.3.1 Preparation of reagents for determination of copper (II)

Preparation of Standard solution.

A 1000 ppm stock solution of Cu was made by dissolving 3.9281 g of $\text{CuSO}_4 \cdot 5\text{H}_2\text{O}$ in 1000 mL of deionised water. Working standards of 2, 4, 8, 16 and 24 ppm were made by dilutions of the 1000 ppm stock solution into each of the 100 mL volumetric flasks and made up to the mark using deionised water. Absorbance was recorded at 324.8 nm with a slit width of 0.5 and lamp mode BGC-D2 using a SHIMADZU AA-6701 FAAS.

3.8.4 Batch Adsorption of Toluene.

A gram of adsorbent was weighed into each of the 100 mL conical flask. After that, 100 mL of the 100 ppm solution was added to each flask at a pH of 0.98 at ambient temperature. The flasks were shaken using an agitator for 10, 15, 30, 45, 60, 120, 180, 240 and 300 mins. The experiment was repeated using 200 ppm and 400 ppm solutions. The remaining concentration of toluene in each of the flask was determined using Gas Chromatography.

3.8.4.1 Preparation of reagents

Preparation of Standard solution.

A set of 10 %, 20 %, 30 % and 40 % toluene standards were made by dilution of pure toluene in 5 mL volumetric flasks and making to the mark using ethanol. The determination of toluene was then done on a VARIAN STAR 3400 CX Series Gas Chromatography.

4.0 RESULTS

4.1 Characterization of zeolites

Zeolites were characterized using FT IR (Thermo Fischer Scientific Nicolet 6700), Scanning electron microscopy (SEM) , energy dispersive X-ray spectroscopy (EDX) and x-ray diffraction spectroscopy (XRD).

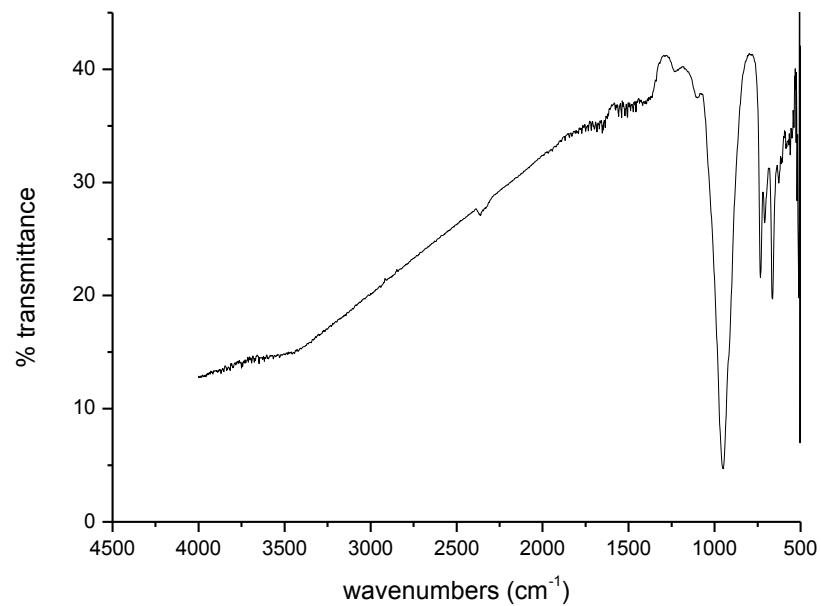


Fig 4.1 FT-IR spectrum of zeolite synthesized from bentonite clay.

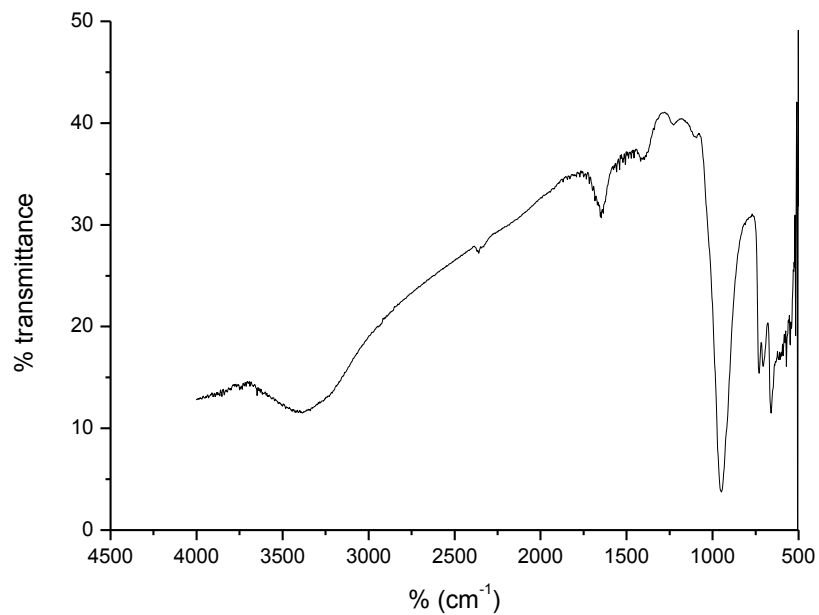


Fig 4.2 FT-IR spectrum of zeolite synthesized from local clay.

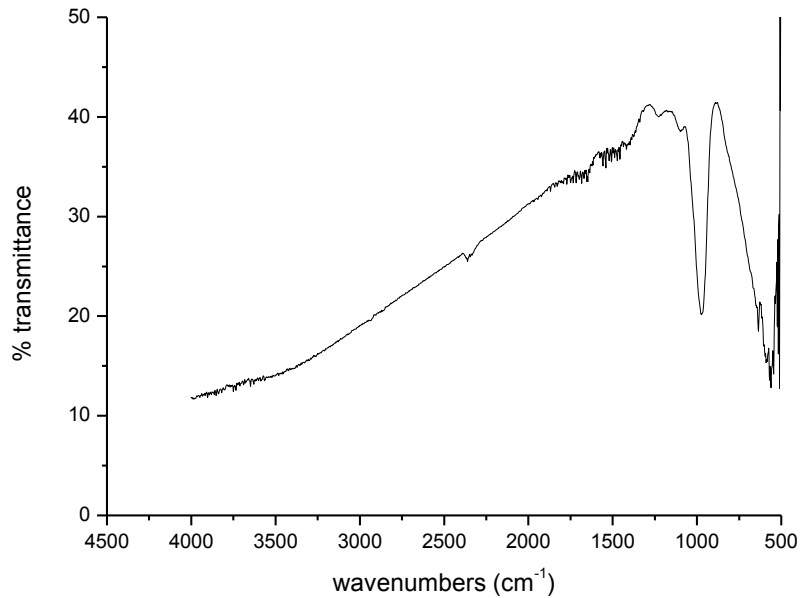


Fig. 4.3 FT-IR spectrum of zeolite synthesized from SiO₂ and Al₂O₃.

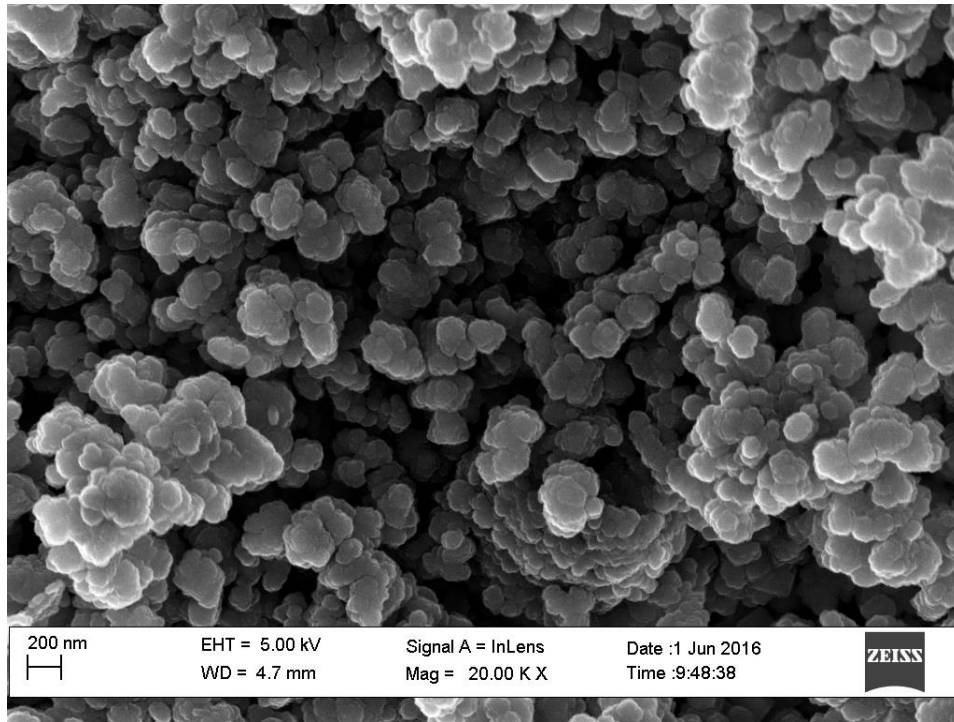


Fig 4.3 a1) SEM image for zeolite synthesised from bentonite clay

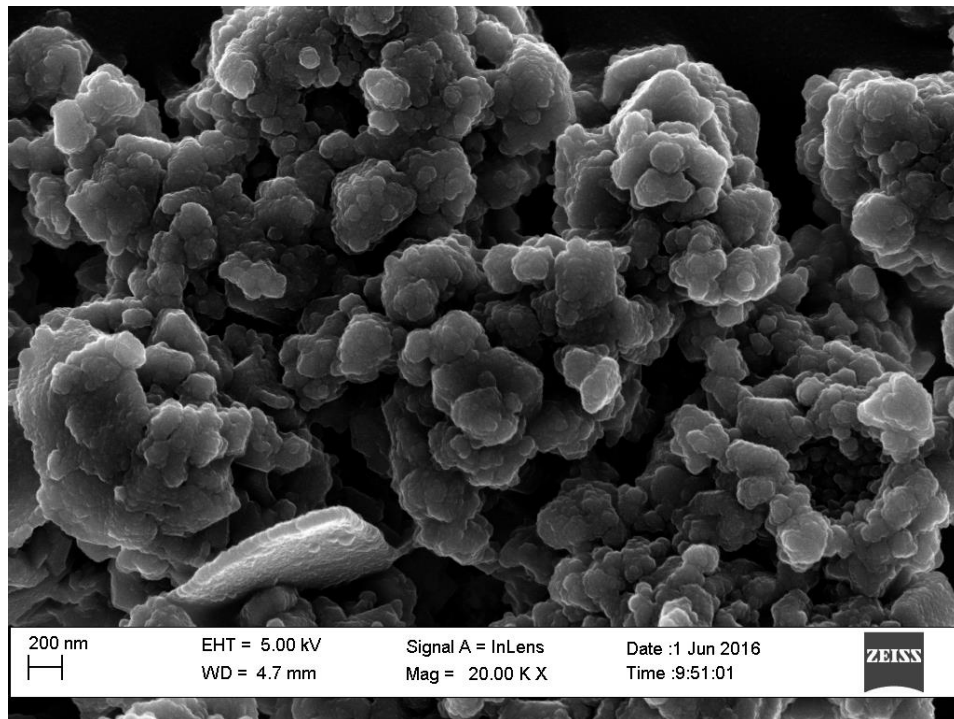


Fig 4.3 a2) SEM image for zeolite synthesised from local clay

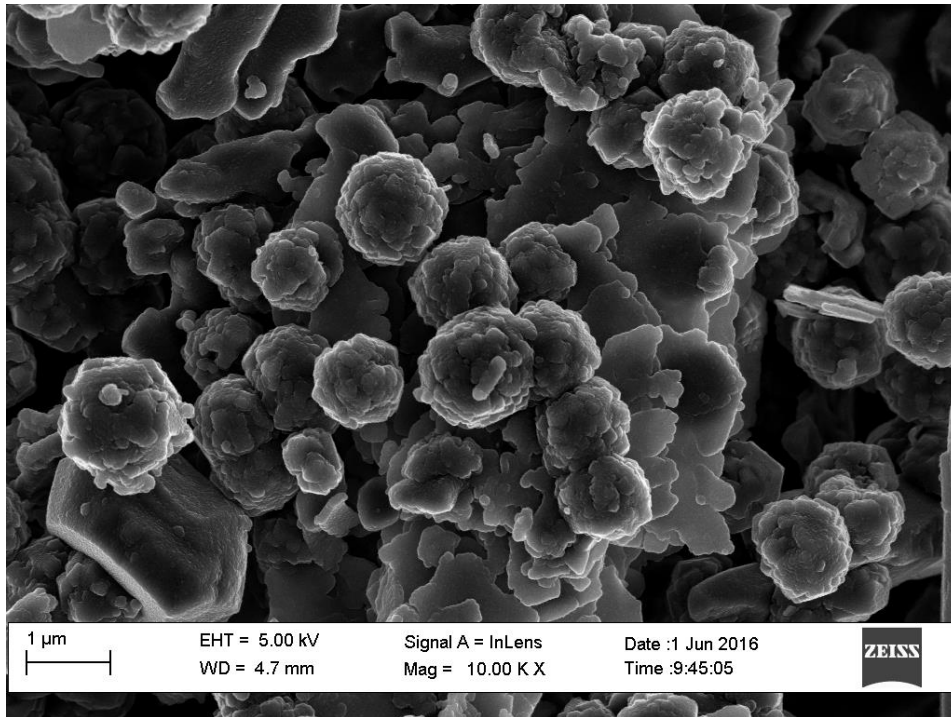


Fig 4.3 a3) SEM image for zeolite synthesised from silica and Al_2O_3

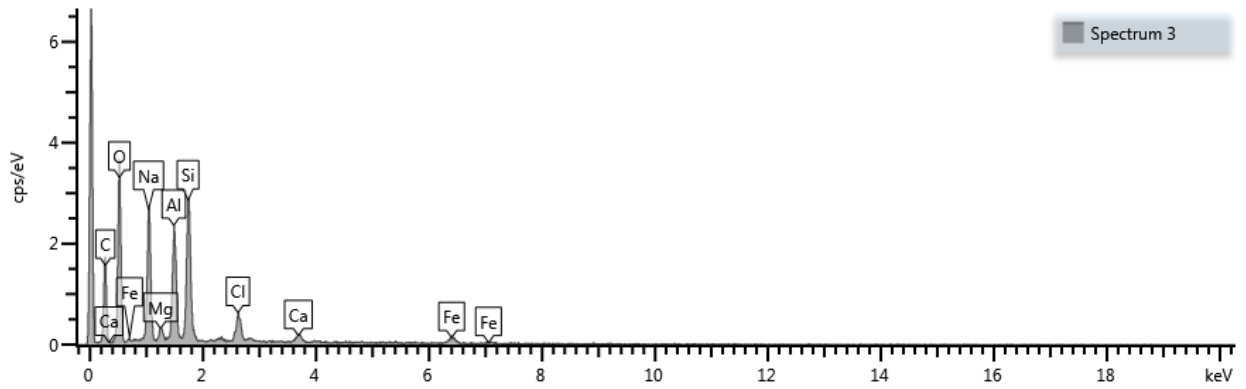


Fig 4.3 b1) EDX spectrum for zeolite synthesised from bentonite clay

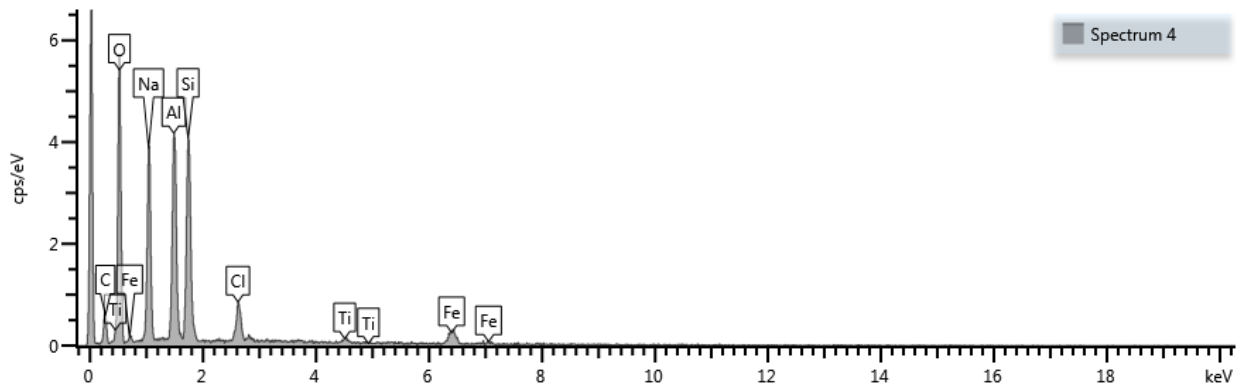


Fig 4.3 b2) EDX spectrum for zeolite synthesised from local clay

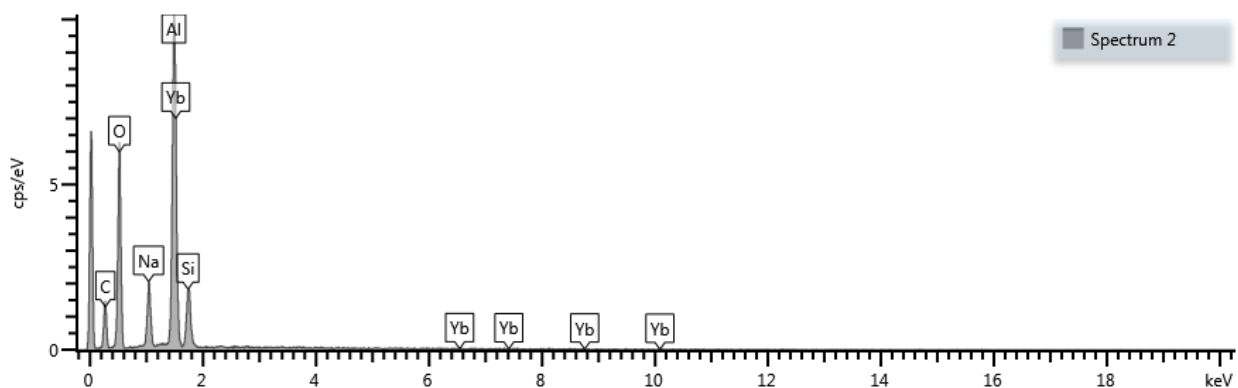


Fig 4.3 b3) EDX spectrum for zeolite synthesised from silica and Al₂O₃

Table 4.1 EDX weight percentage and sigma percentage of zeolites

zeolite from bentonite clay			zeolite from local clay			zeolite from silica and alumina		
Element	Wt%	Wt% Sigma	Element	Wt%	Wt% Sigma	Element	Wt%	Wt% Sigma
O	42,48	0,73	O	42,41	0,58	O	47,3	0,56
Na	17,82	0,47	Na	17,35	0,36	Na	8,85	0,29
Mg	1,71	0,22	Al	15,27	0,32	Al	34,74	0,47
Al	12,67	0,38	Si	16,28	0,34	Si	9,12	0,31
Si	17	0,43	Cl	3,48	0,18	Yb	0	0
Cl	3,86	0,24	Ti	0,79	0,15	Total:	100	
Ca	1,36	0,18	Fe	4,42	0,31			
Fe	3,1	0,35	Total:	100				
Total:	100							

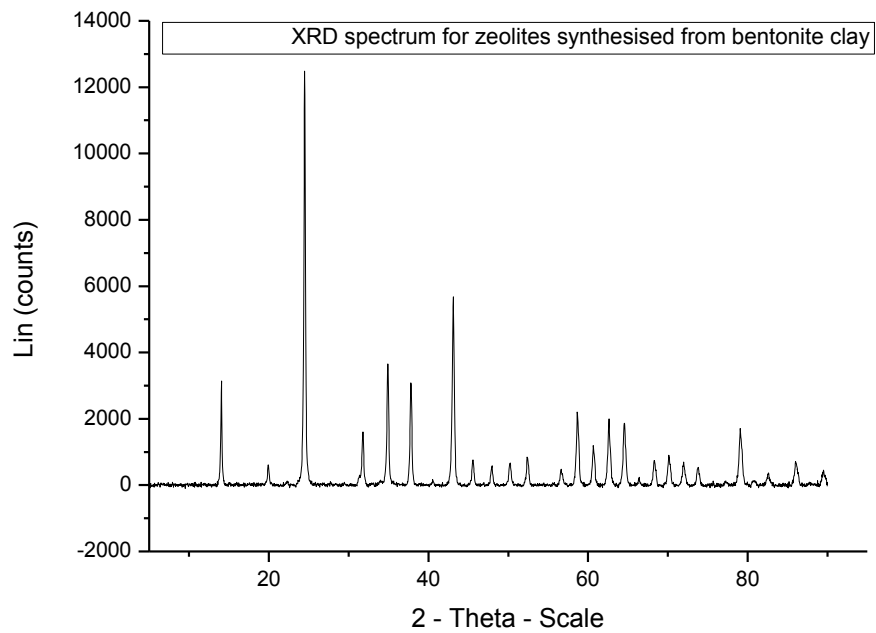


Fig 4.3 c1) XRD spectrum of zeolites synthesised from bentonite clay

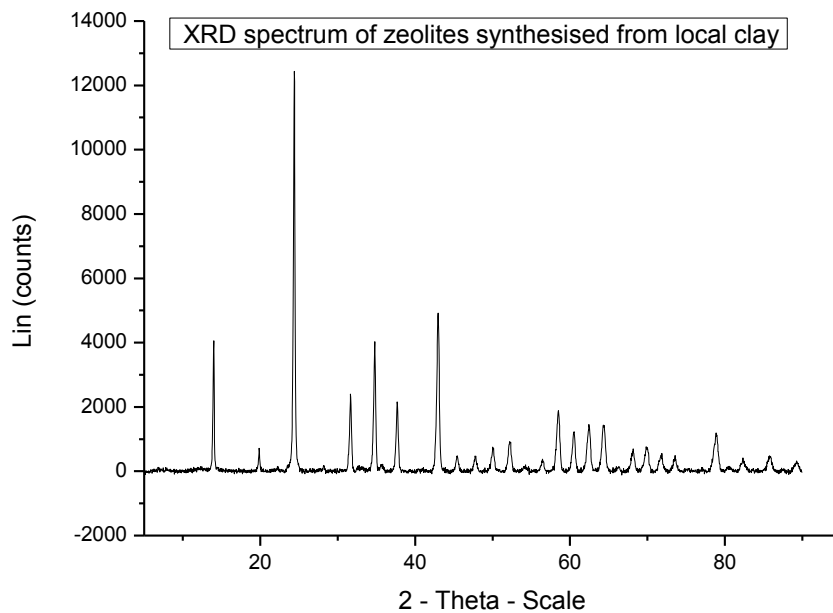


Fig 4.3 c2) XRD spectrum of zeolites synthesized from local clay

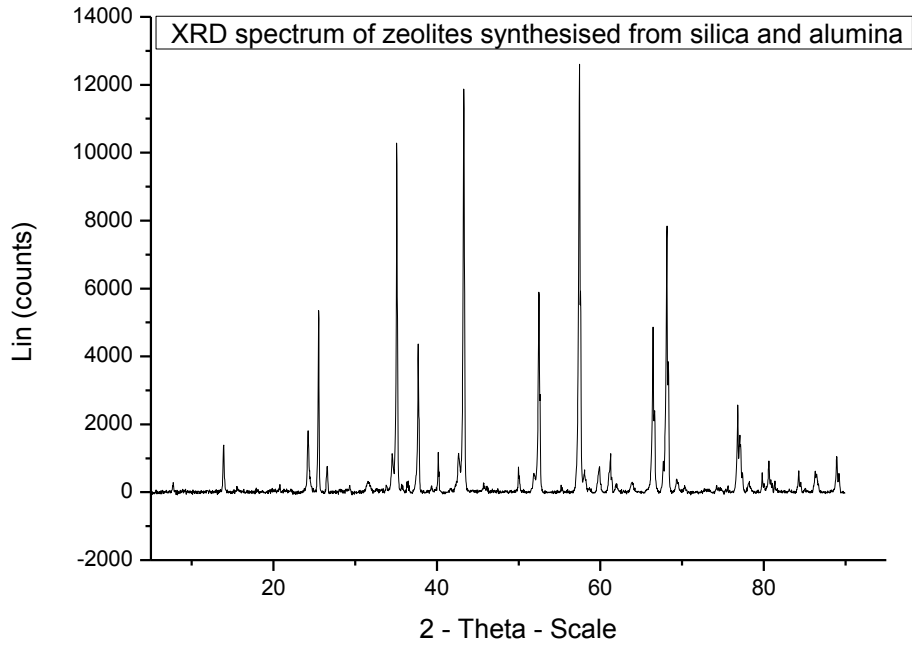


Fig 4.3 c3) XRD spectrum of zeolites synthesized from silica and alumina

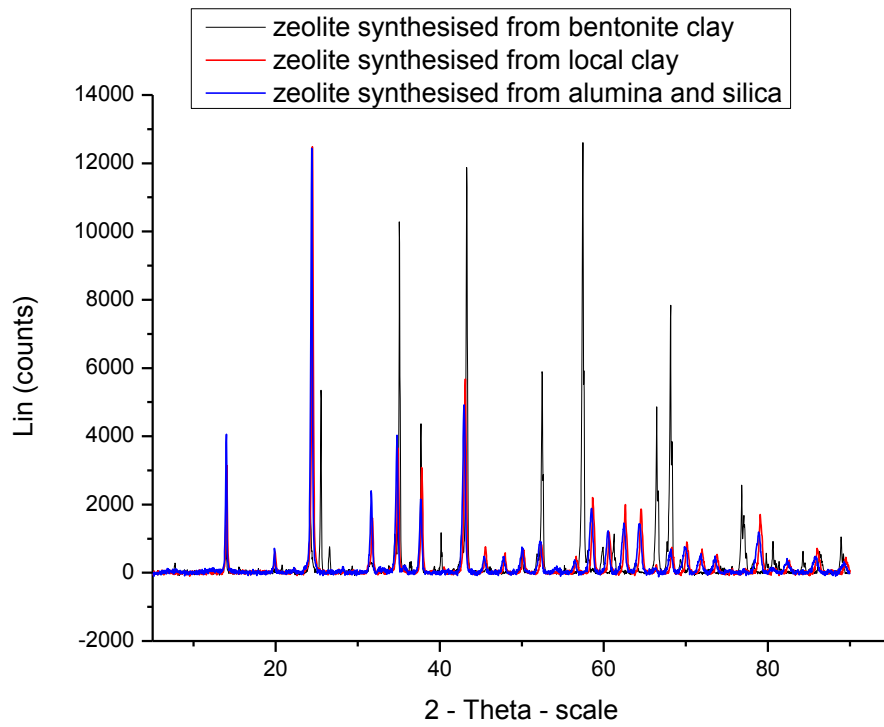


Fig 4.3 c4) Overlay of XRD spectrum of zeolites synthesized from different materials

4.2 Characterization magnetic nanoparticles

Magnetic nanoparticles were characterized using FT IR (Thermo Fischer Scientific Nicolet 6700) , scanning electron microscopy (SEM) , energy dispersive X-ray spectroscopy (EDX) and x-ray diffraction spectroscopy (XRD).

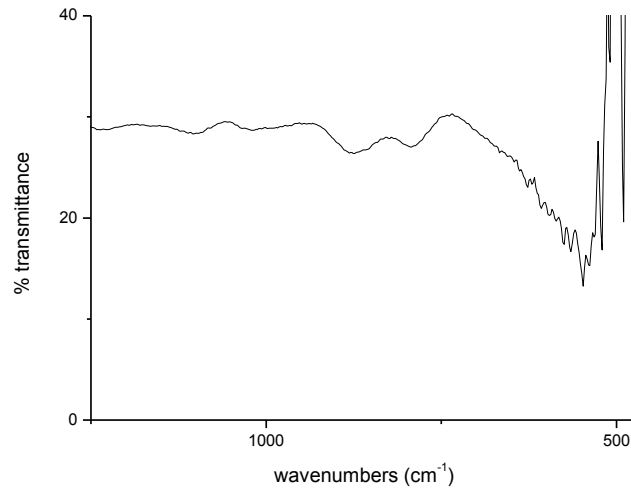


Fig 4.4 FT-IR spectrum of magnetic Fe₃O₄ nanoparticles

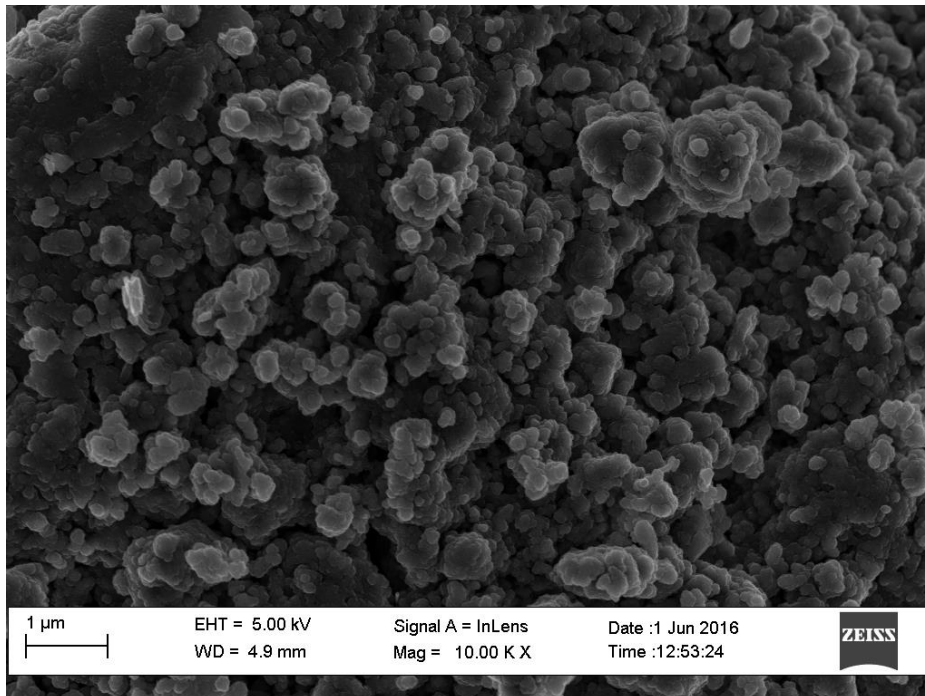


Fig 4.4 a) SEM image for magnetic nanoparticles (Fe₃O₄)

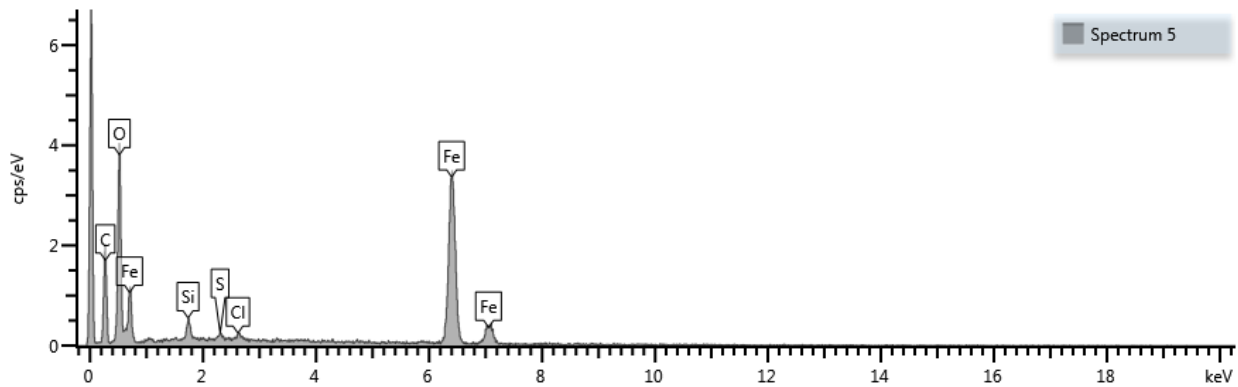


Fig 4.4 b) EDX spectrum for magnetic nanoparticles (Fe_3O_4)

Table 4.2: EDX weight percentage and sigma percentage of magnetic nanoparticles (Fe_3O_4)

magnetic nanoparticles					
element	O	Si	S	Cl	Fe
Wt %	27,39	2,24	0,59	0,54	69,23
Wt % sigma	0,58	0,2	0,15	0,15	0,61

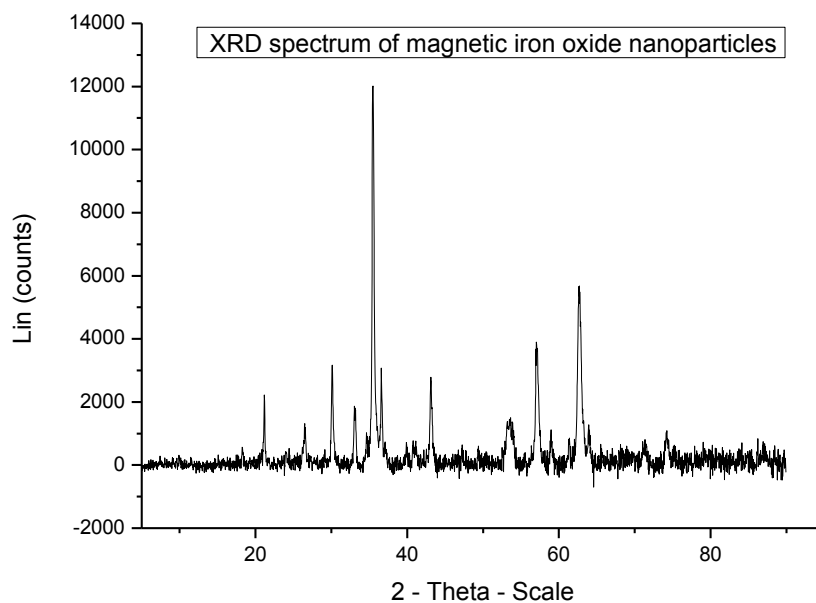


Fig 4.4 c) XRD spectrum of magnetic iron oxide nanoparticles

4.3 Characterization of LDHs

Layered double hydroxides were characterized using FT IR (Thermo Fischer Scientific Nicolet 6700) , scanning electron microscopy (SEM), energy dispersive X-ray spectroscopy (EDX) and x-ray diffraction spectroscopy (XRD).

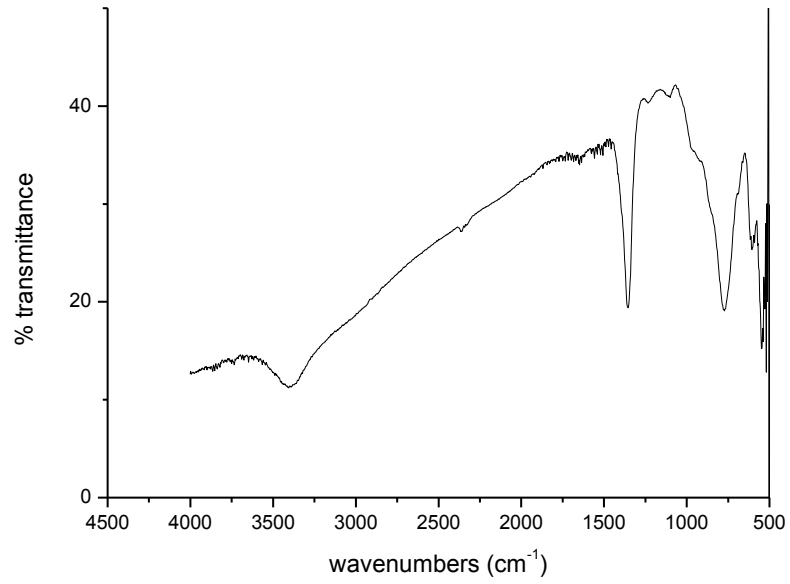


Fig. 4.5 FT-IR spectrum of the Al-Zn LDH.

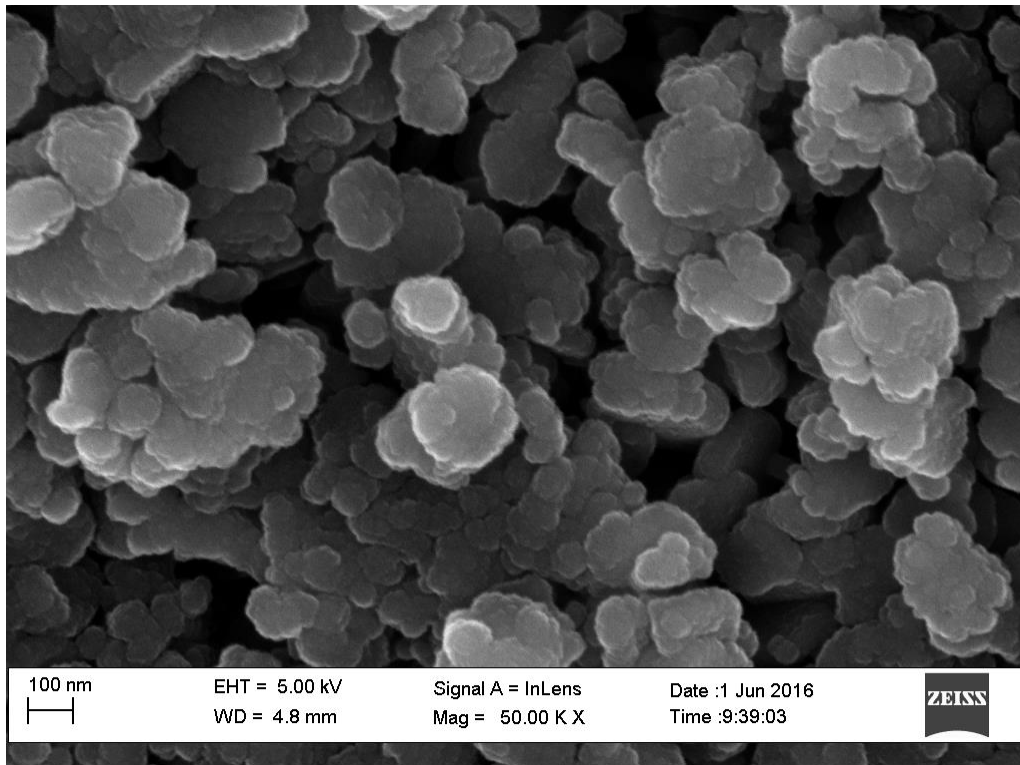


Fig 4.5 a) SEM image for Zn/Al Layered Double Hydroxides

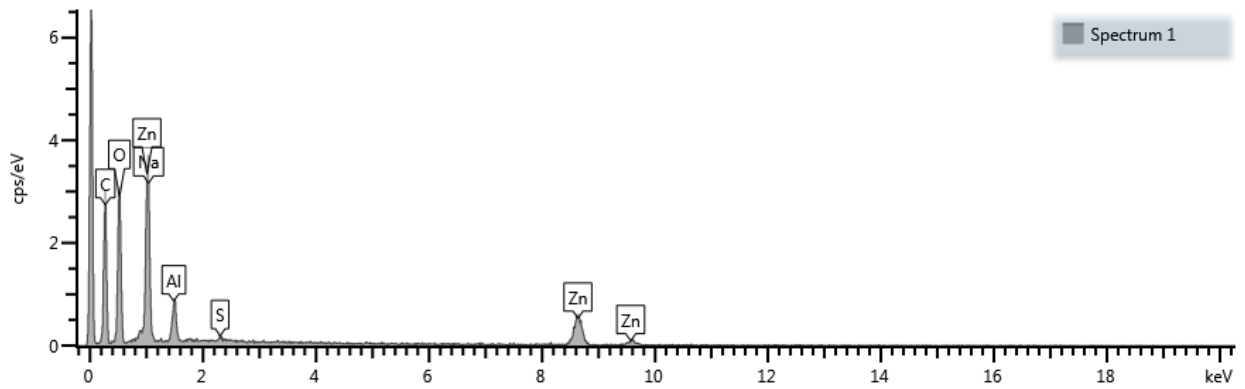


Fig 4.5 b) EDX spectrum for Zn/Al Layered Double Hydroxides

Table 4.3: EDX weight percentage and sigma percentage of Zn/Al LDH

Zn/Al LDH					
element	O	Na	Al	S	Zn
Wt %	37,82	10,77	8,8	0,72	41,89
Wt % sigma	1,06	1,26	0,49	0,2	1,22

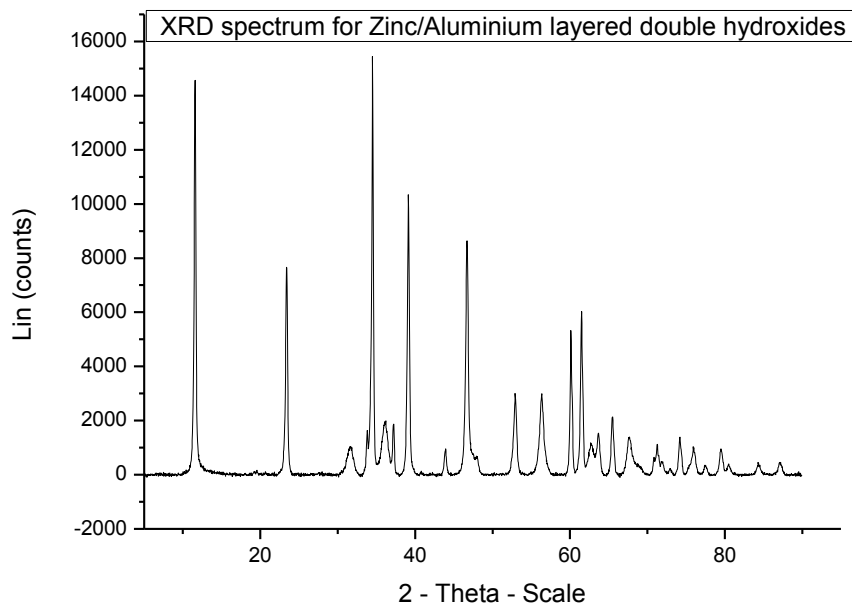


Fig. 4.5 c) XRD spectrum of Zn/Al layered double hydroxide

4.4 Characterization of magnetic nanocomposite

The magnetic nanocomposite was characterized using FT IR (Thermo Fischer Scientific Nicolet 6700), scanning electron microscopy (SEM), energy dispersive X-ray spectroscopy (EDX) and x-ray diffraction spectroscopy (XRD).

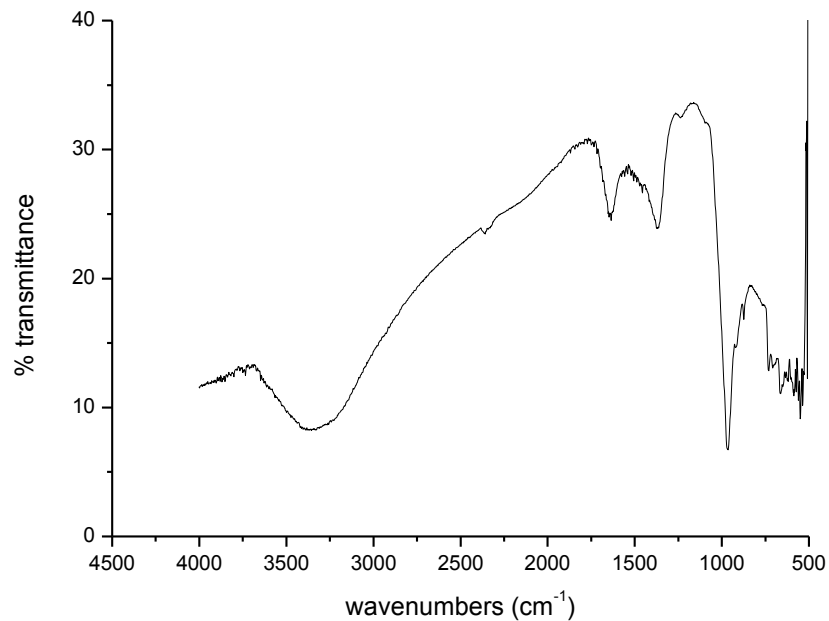


Fig. 4.6 FT-IR spectrum of the zeolite from local clay mixed with activated charcoal and coated with Al-Zn LDH.

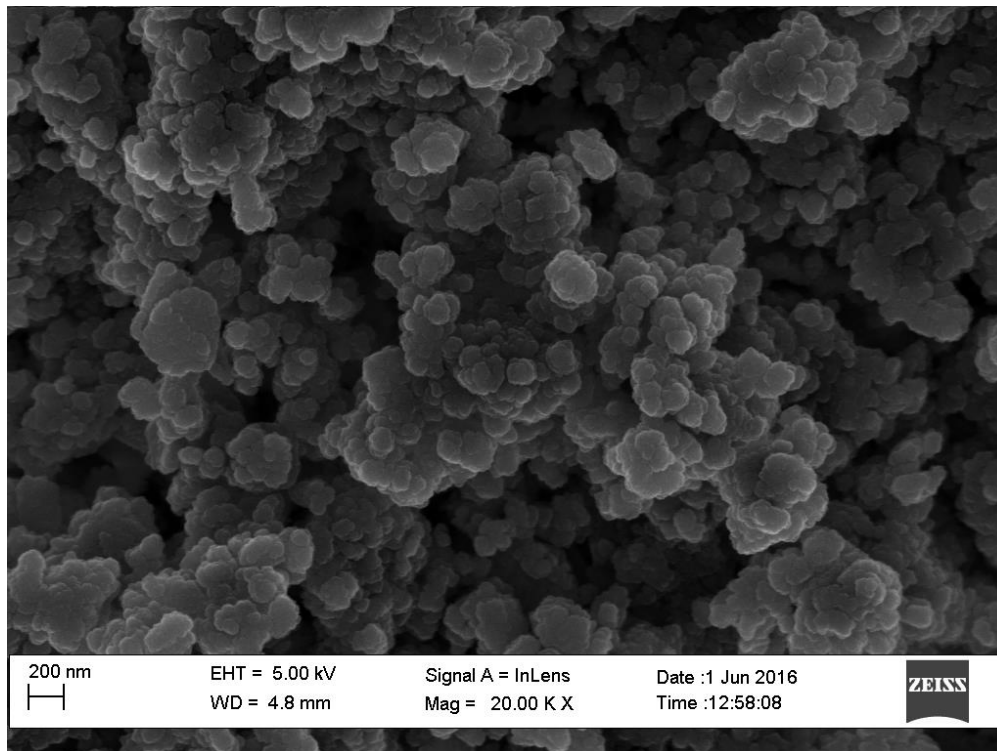


Fig 4.6 a) SEM image for magnetic nanocomposite

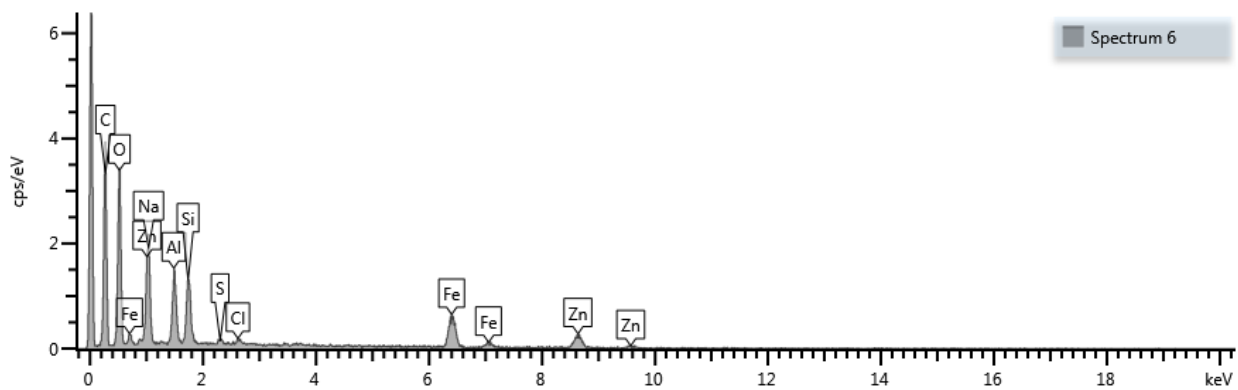


Fig 4.6 b) EDX spectrum for magnetic nanocomposite

Table 4.4: EDX weight percentage and sigma percentage of magnetic nanocomposite

magnetic nanocomposite								
element	O	Na	Al	Si	S	Cl	Fe	Zn
Wt %	37,16	10,78	10,23	9,33	0,71	0,63	15,79	15,37
Wt % sigma	0,85	0,78	0,42	0,39	0,17	0,17	0,62	0,88

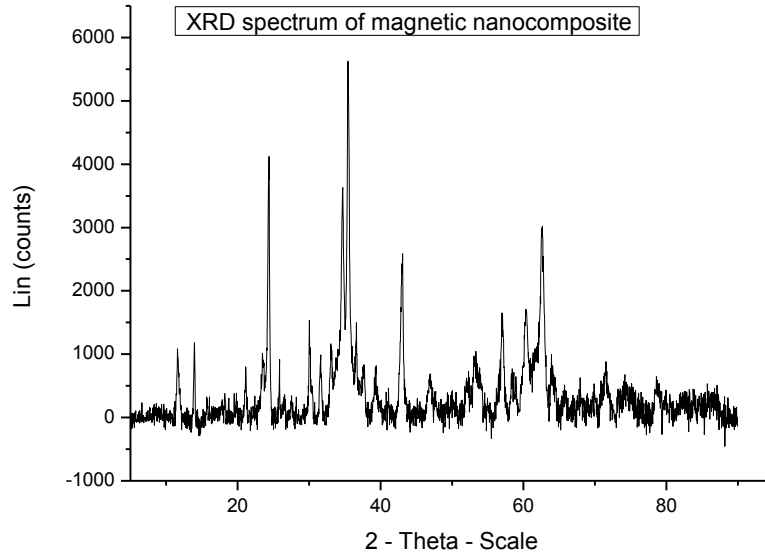


Fig 4.6 c) XRD spectrum of magnetic nanocomposite

4.5 Adsorption studies of phosphate

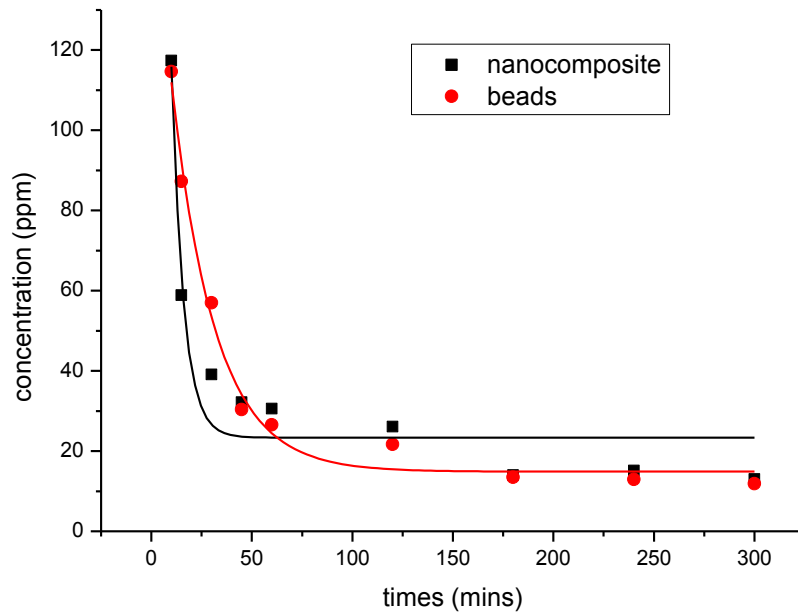


Fig. 4.7 Adsorption of the 100 ppm phosphate solution

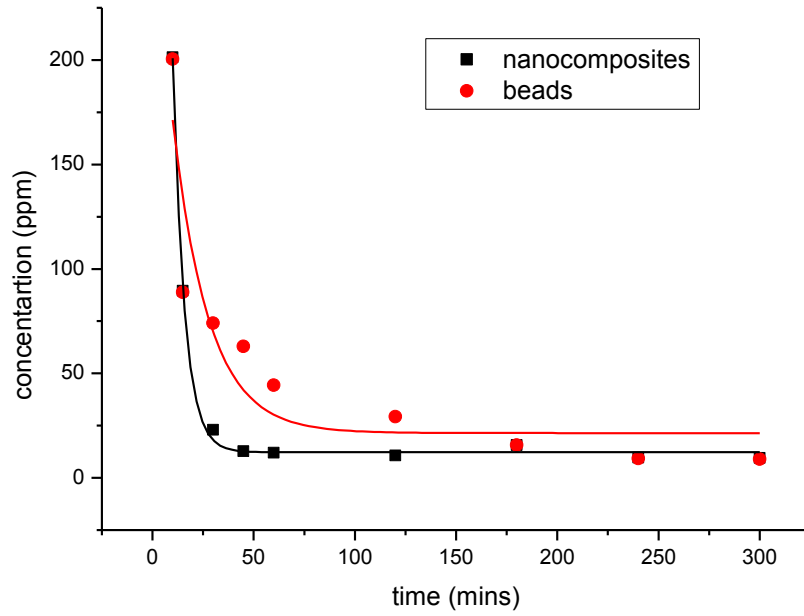


Fig. 4.8 Adsorption of the 200 ppm phosphate solution

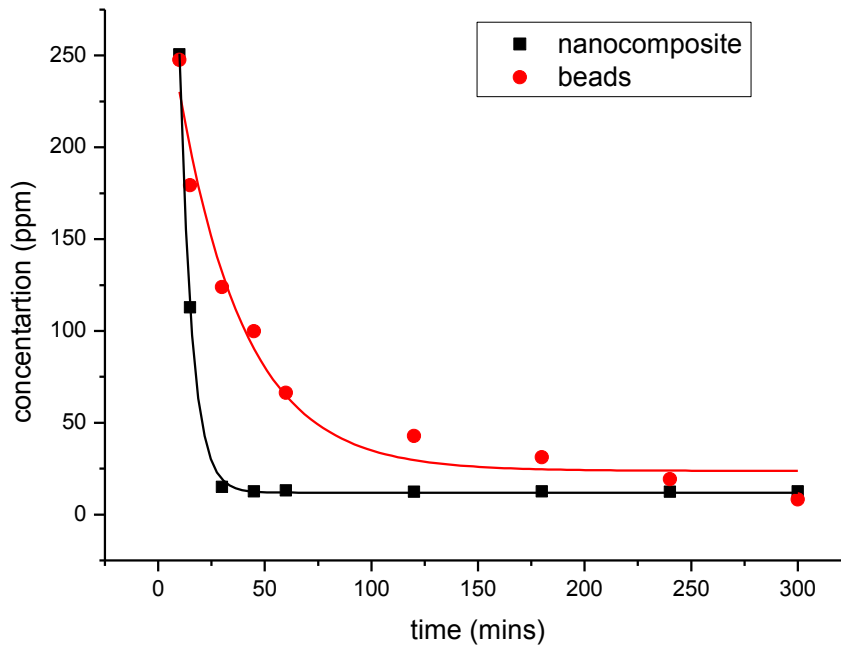


Fig. 4.9 Adsorption of the 400 ppm phosphate solution

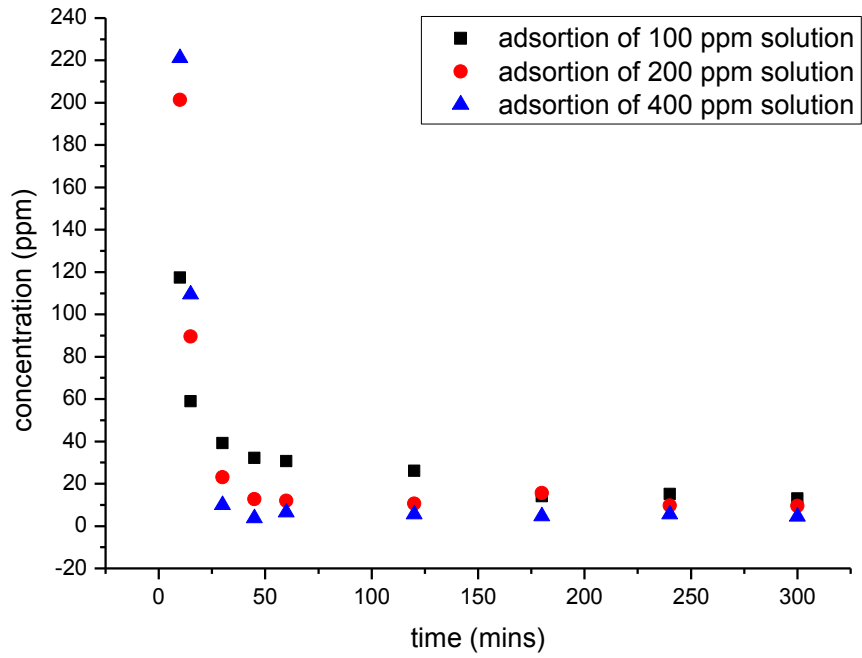


Fig. 4.10 Adsorption comparison of phosphate using the magnetic nanocomposite.

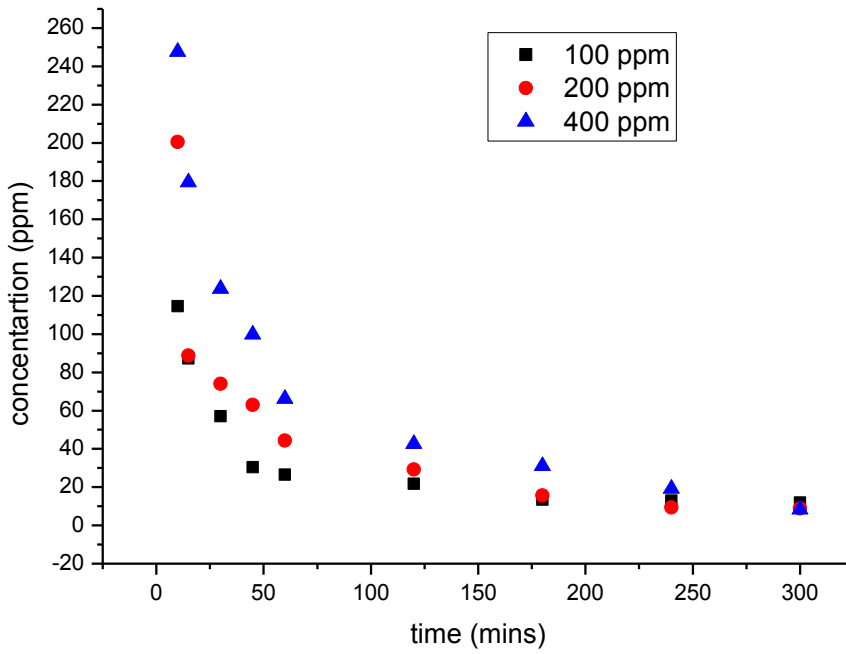


Fig. 4.11 Adsorption comparison of phosphate using the magnetic beads.

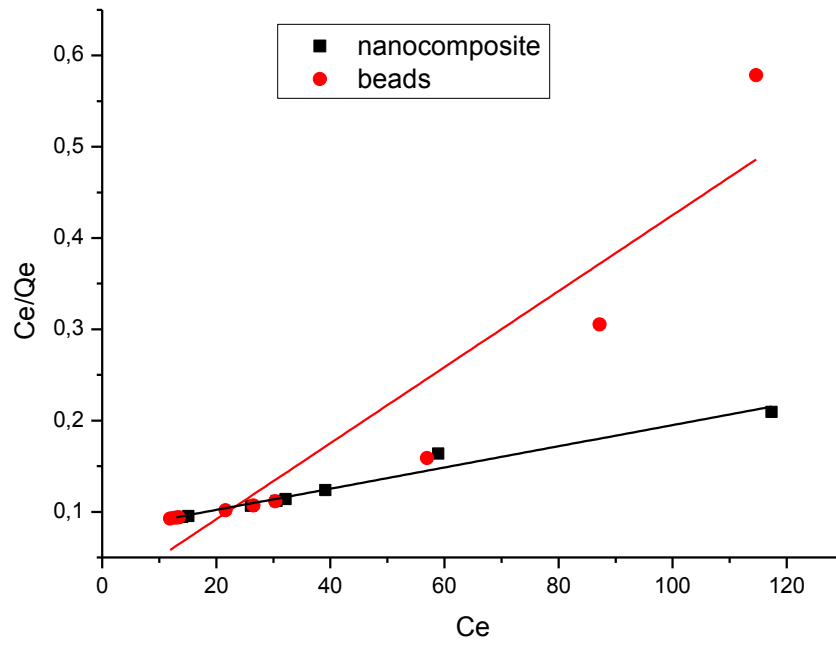


Fig. 4.12 Langmuir isotherm for 100 ppm phosphate solution

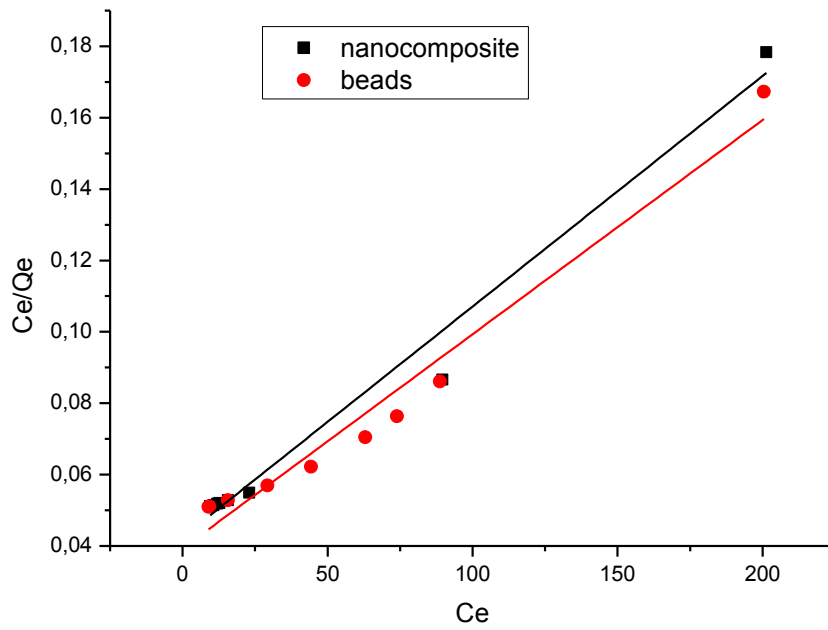


Fig. 4.13 Langmuir isotherm for 200 ppm phosphate solution

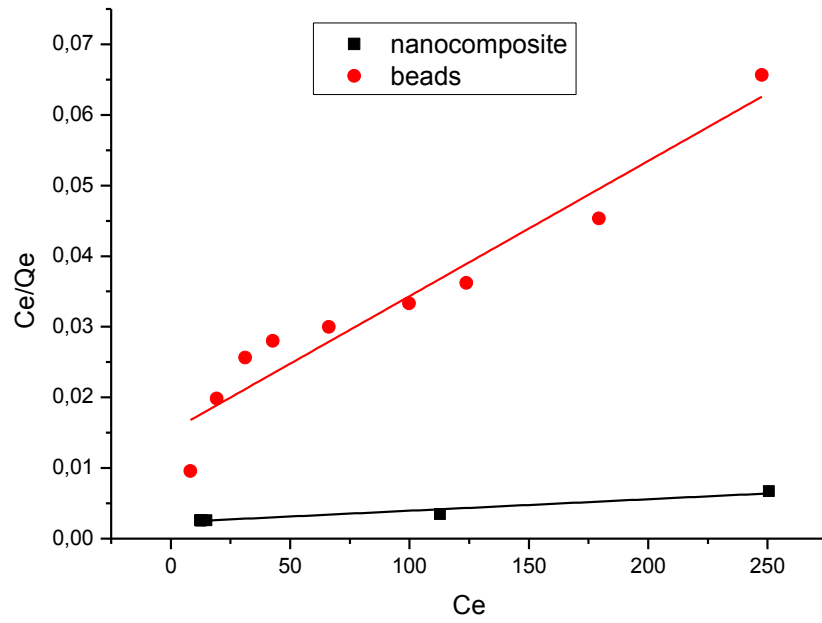


Fig. 4.14 Langmuir isotherm for 400 ppm phosphate solution

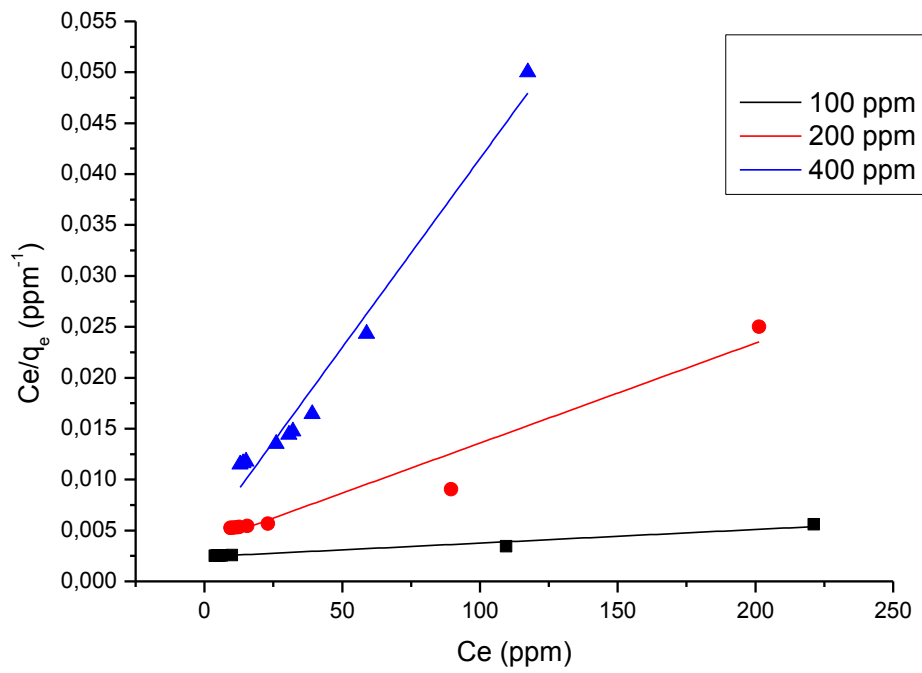


Fig 4.15 Langmuir isotherm comparison of phosphate using the magnetic nanocomposite.

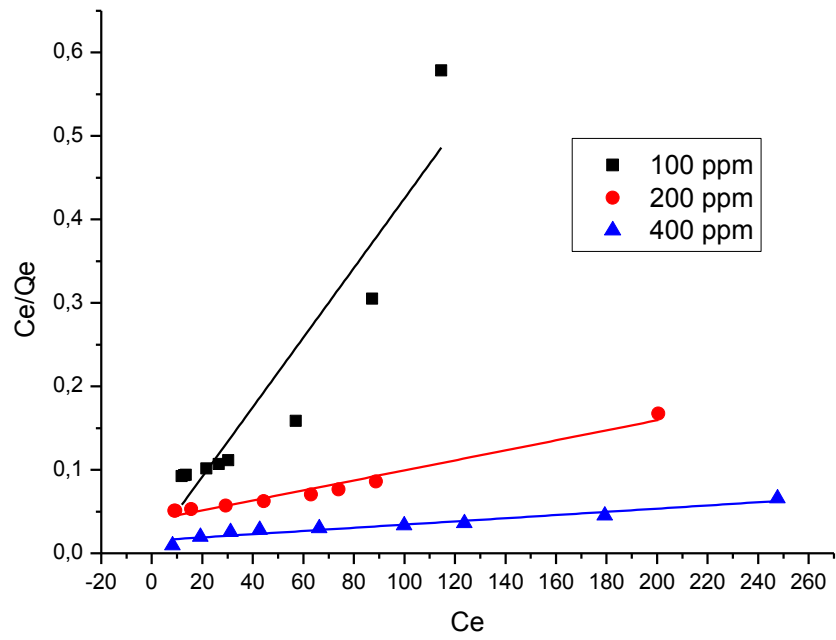


Fig 4.16 Langmuir isotherm comparison of phosphate using the magnetic beads.

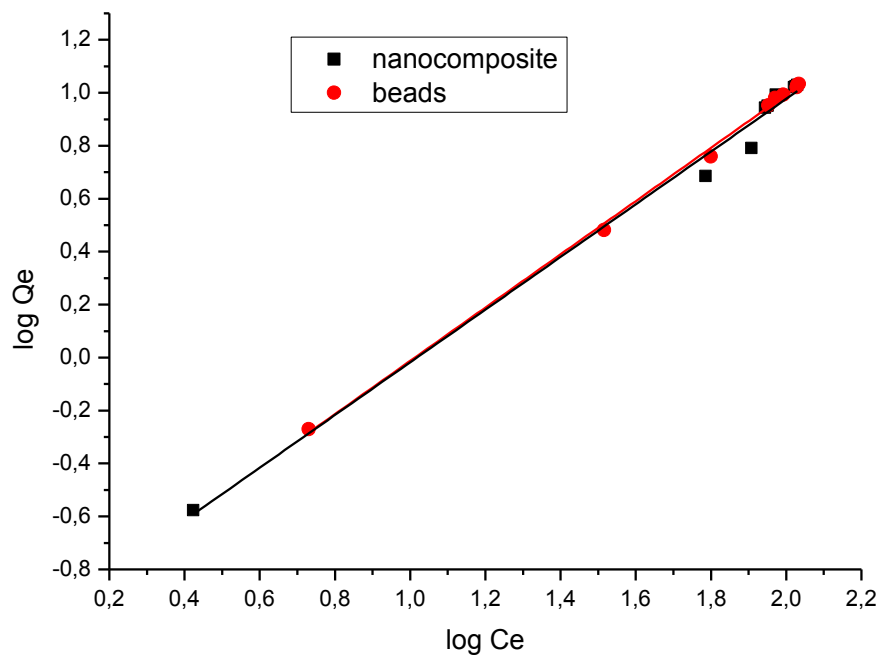


Fig 4.17 Freundlich isotherm for 100 ppm phosphate solution

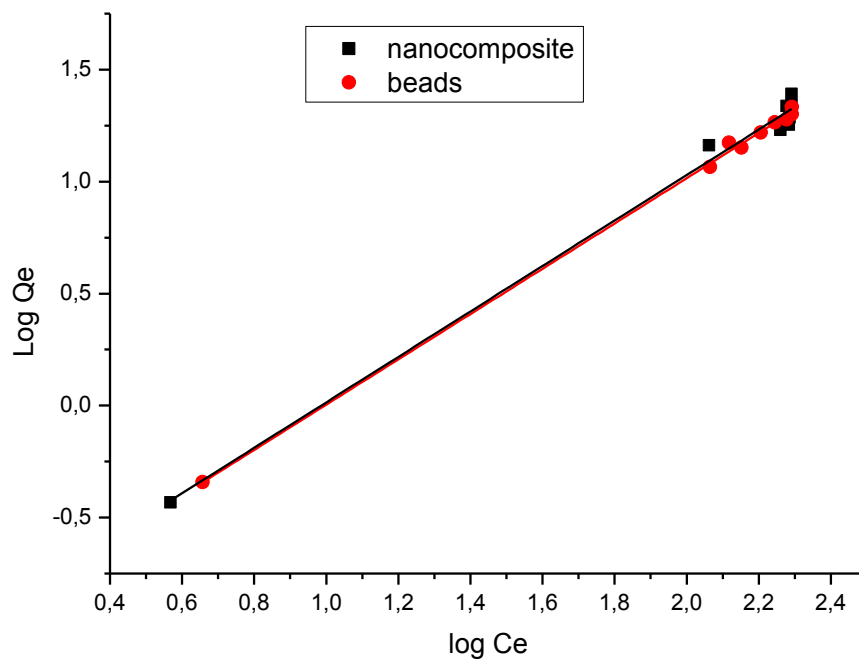


Fig 4.18 Freundlich isotherm for 200 ppm phosphate solution

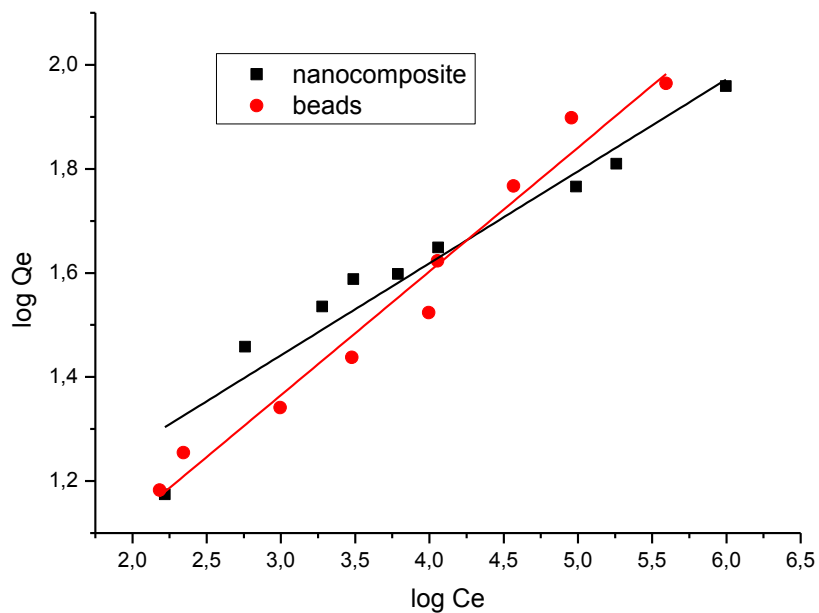


Fig 4.19 Freundlich isotherm for 400 ppm phosphate solution

Table 4.7: Isotherm parameters for adsorption of phosphate

isotherm	parameter	value					
		100		200		400	
		NC	BD	NC	BD	NC	BD
Freundlich		0,962	1,0059	1,0016	1,011	1,1845	0,2379
	K_F	0,1256	0,36	0,101	0,365	0,038	1,918
	R^2	0,971	0,998	0,995	0,998	0,978	0,97
langmuir	q_m	223,7	12,678	265,01	25,432	411,53	23,54
	K	11,948	65,517	38,294	65,533	180,402	65,757
	R^2	0,971	0,969	0,9472	0,967	0,648	0,98

NOTE* NC – magnetic nanocomposite; BD – magnetic alginate beads and thus represented as such onwards

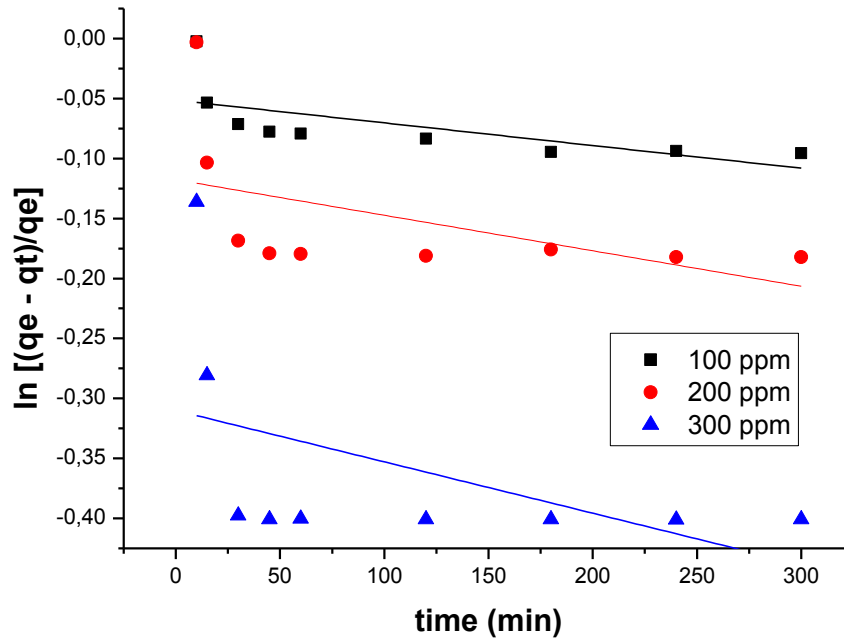


Fig 4.22 Pseudo First Order kinetics of phosphate using the magnetic nanocomposite.

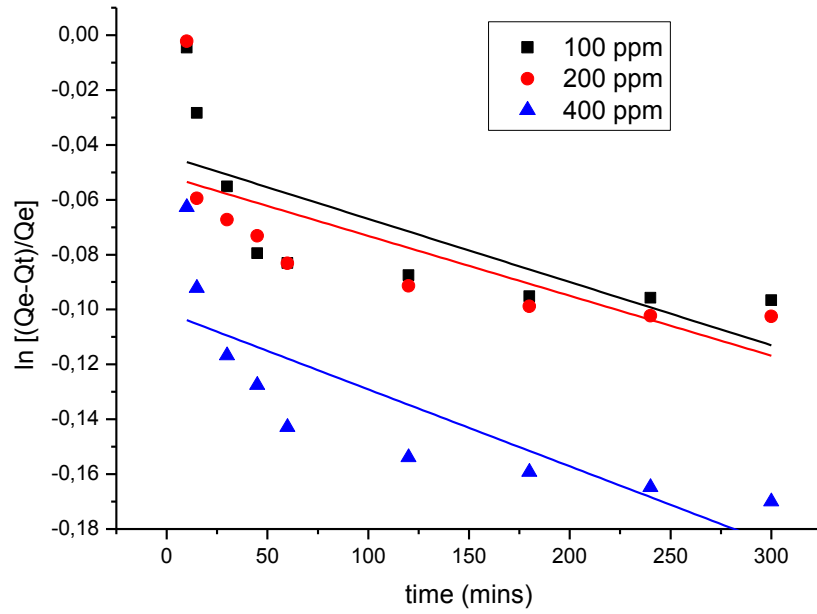


Fig 4.23 Pseudo First Order kinetics of phosphate using the magnetic beads

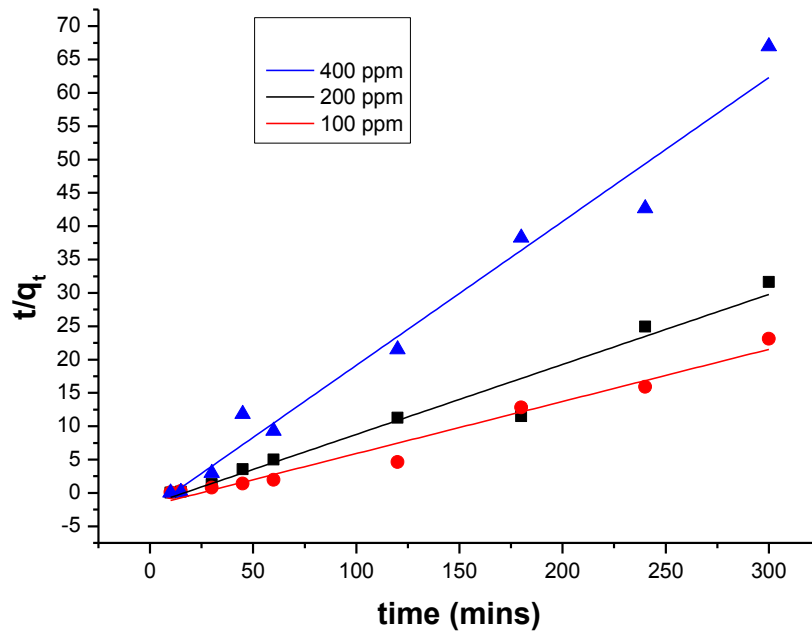


Fig 4.24 Pseudo Second Order kinetics of phosphate using the magnetic nanocomposite.

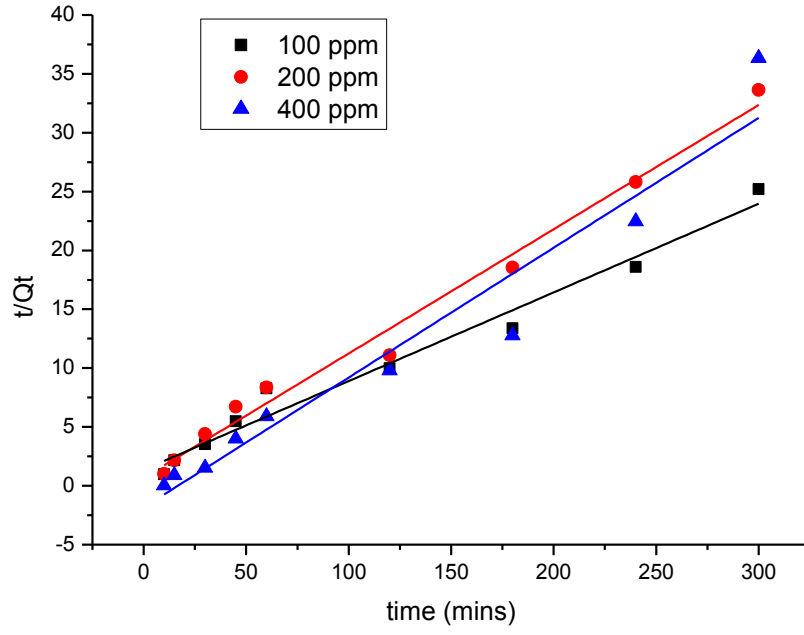


Fig 4.25 Pseudo Second Order kinetics of phosphate using the magnetic beads.

Table 4.8: kinetics parameters for adsorption of phosphate

	initial sorbate concentration					
	100		200		400	
	NC	BD	NC	BD	NC	BD
Q_e (exp)(mg /g)	12,99	11,901	9,49	8,921	12,601	8,256
Pseudo-first-order						
Q_e (calc)	0,95	0,957	0,889	0,95	0,733	0,904
$k_1 \times 10^{-4}$	1,89	2,303	2,96	2,182	4,28	2,804
R^2	0,3893	0,478	0,1632	0,47	0,1361	0,629
Pseudo-second-order						
R^2	0,9742	0,973	0,95712	0,987	0,9692	0,986
Q_e (calc)	4,631	13,28	9,5057	9,07	12,674	9,47
$1/(k^2Q_e^2)$	-2,45	-1,365	-1,73	-1,837	-1,922	-0,682

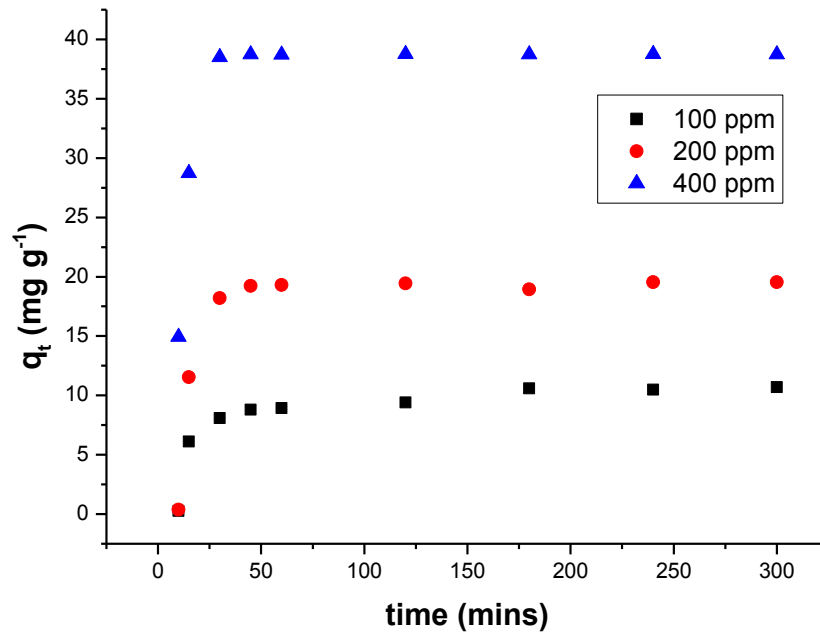


Fig 4.26 Effect of the initial phosphate concentration and contact time using the magnetic nanocomposite.

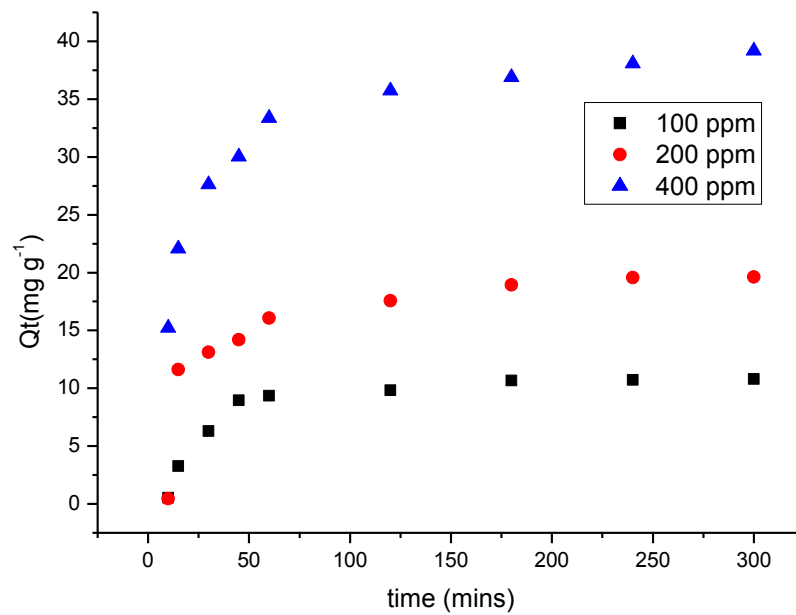


Fig 4.27 Effect of initial phosphate concentration against contact time using the magnetic beads.

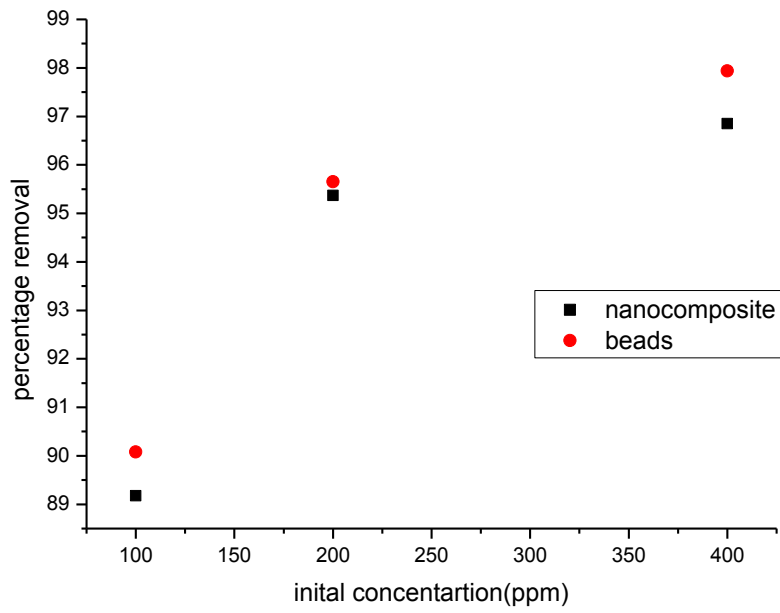


Fig 4.28 Effect of the initial phosphate concentration against contact time using the magnetic nanocomposite.

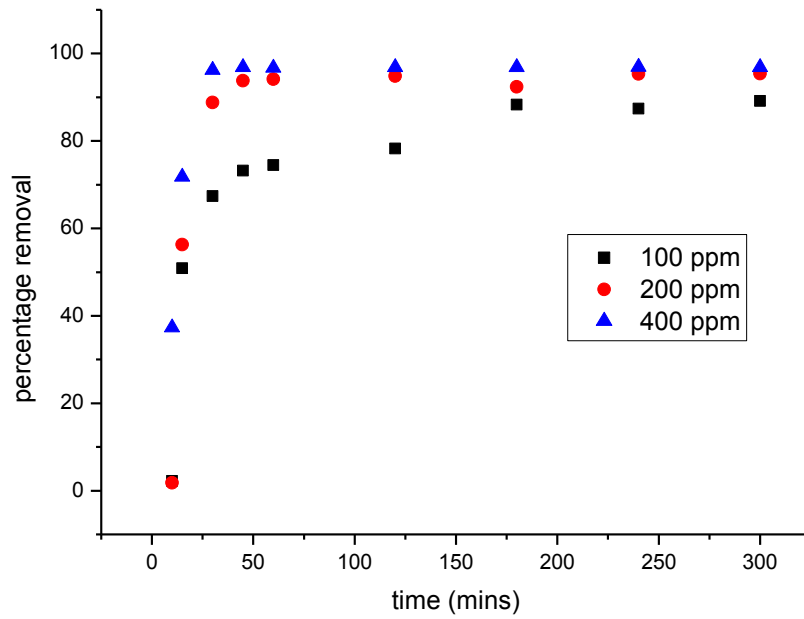


Fig 4.29 Percentage removal of phosphate against time using the magnetic nanocomposite.

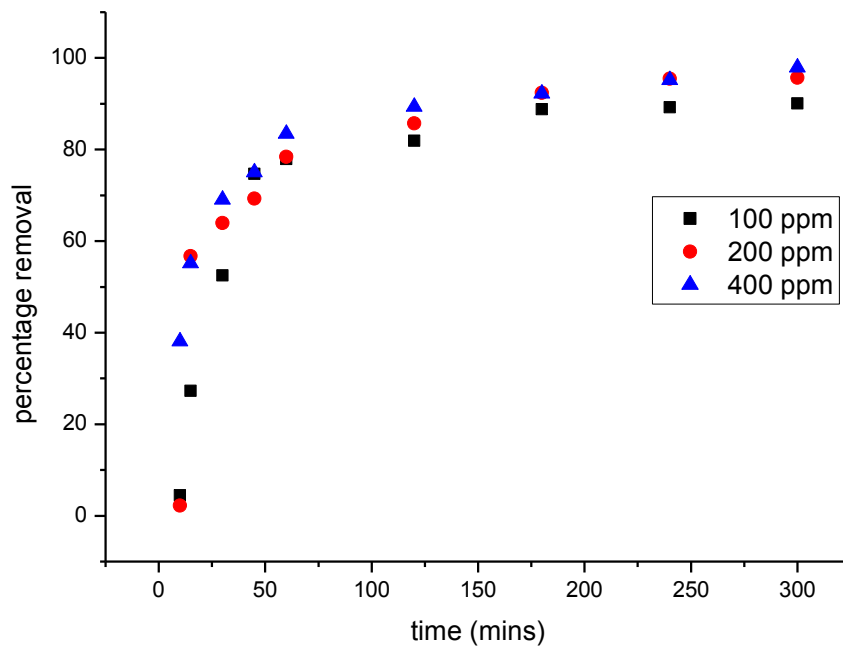


Fig 4.30 Percentage removal of phosphate against time using the magnetic beads.

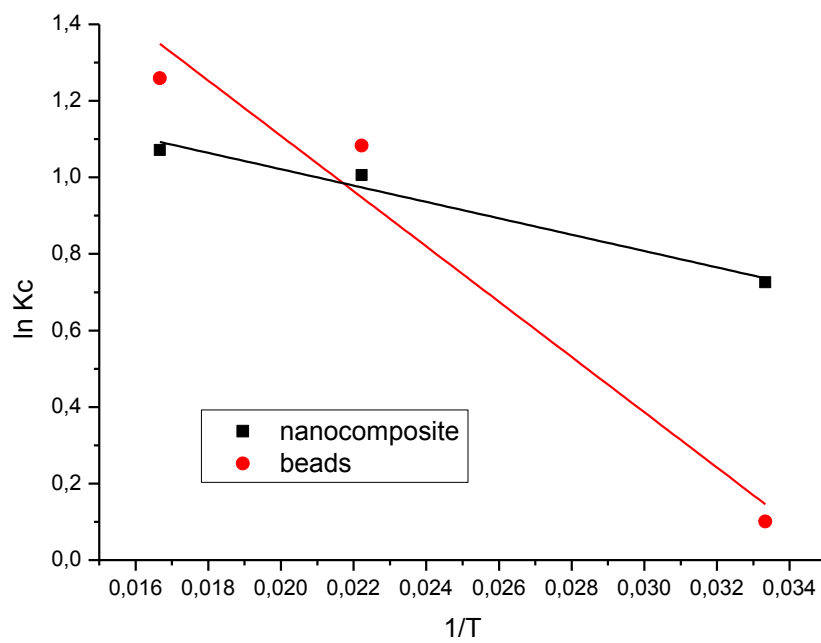


Fig 4.31 Thermodynamics studies of phosphate adsorption

Table 4.9: Thermodynamic parameters for the adsorption of phosphate

temperature (K)	thermodynamics					
	ΔG° (KJmol ⁻¹)		ΔS° (J mol ⁻¹ K ⁻¹)		ΔH° (KJmol ⁻¹)	
	NC	BD	NC	BD	NC	BD
294	-2,619	-3,078				
313	-2,617	-2,818	12,046	21,225	-0,177,7	-0,6004
333	-2,009	-0,278				

4.6 Adsorption studies of chromium

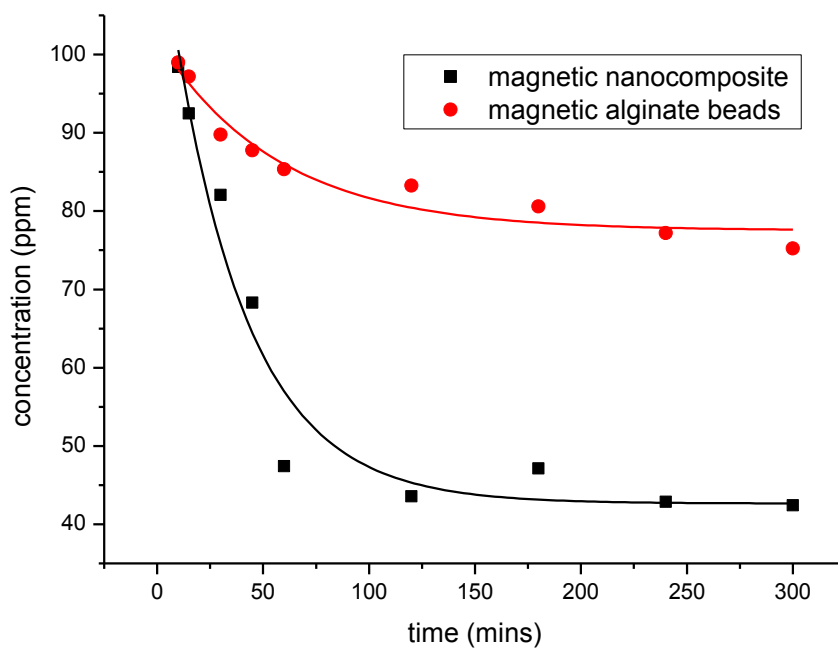


Fig 4.32 Adsorption of 100 ppm solution of chromium

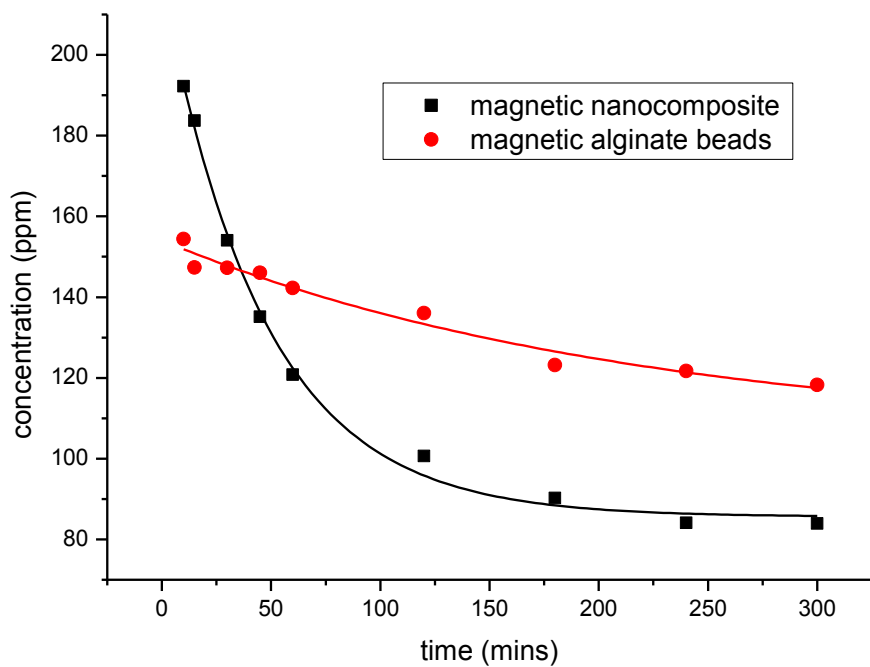


Fig 4.33 Adsorption of 200 ppm solution of chromium

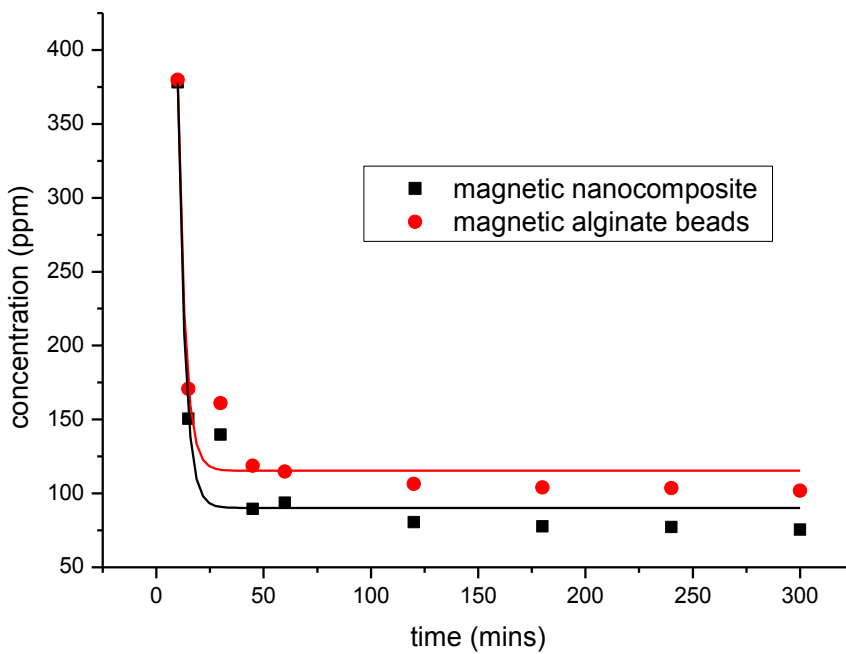


Fig 4.34 Adsorption of 400 ppm solution of chromium

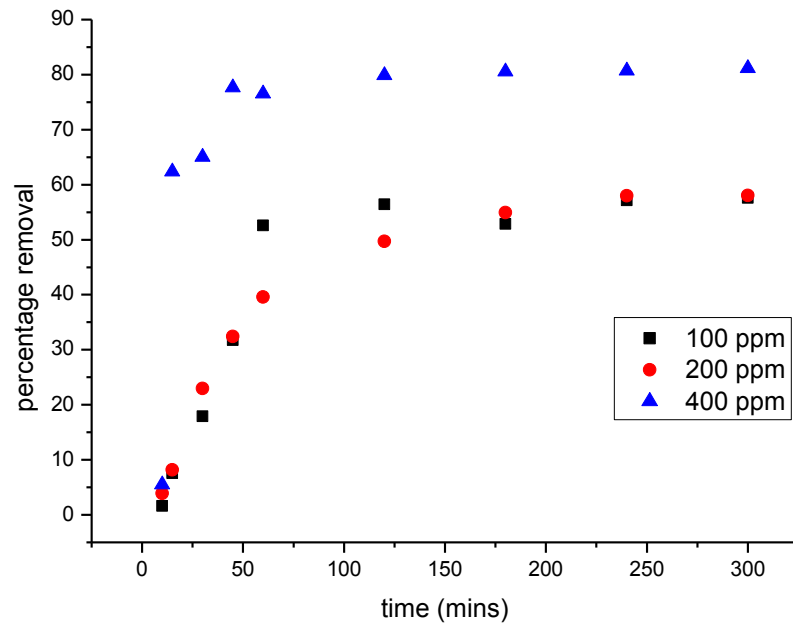


Fig 4.35 Percentage removal of chromium against time using the magnetic nanocomposite.

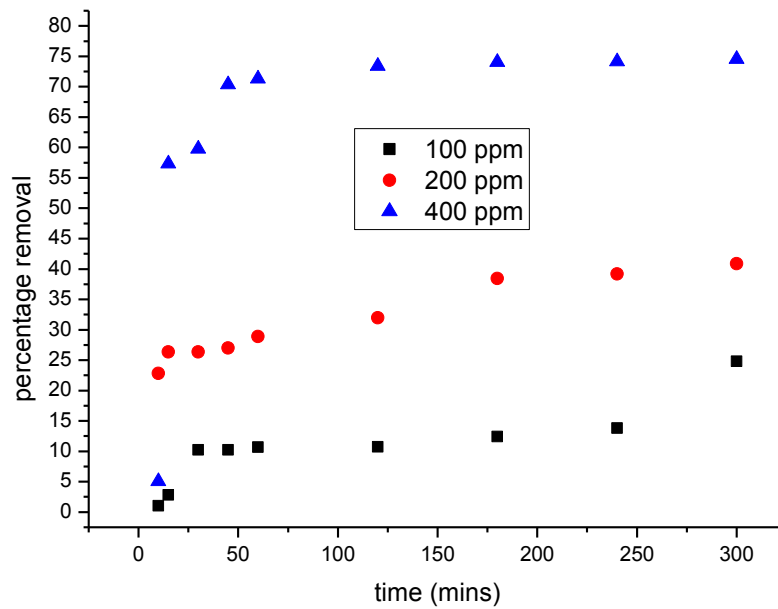


Fig 4.36 Percentage removal of chromium against time using the magnetic alginate beads

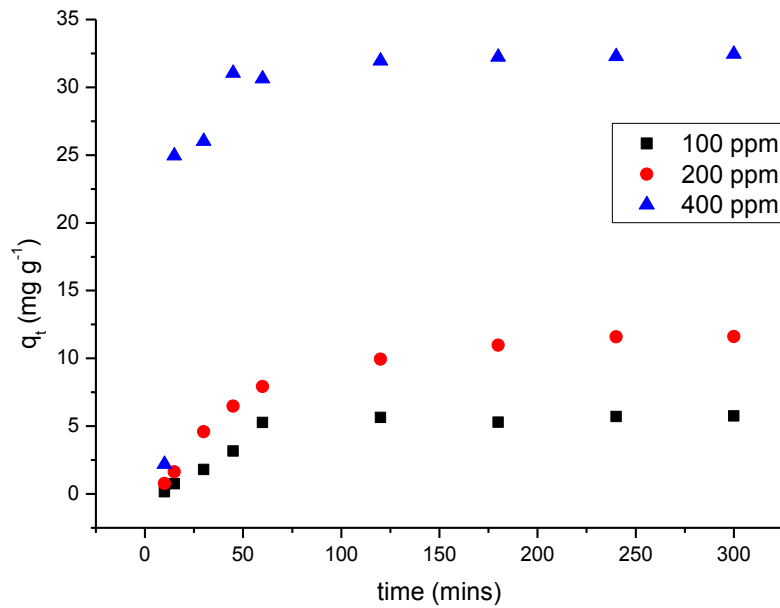


Fig 4.37 Effect of initial chromium concentrations against contact time (Q_t vs time). using the magnetic nanocomposite.

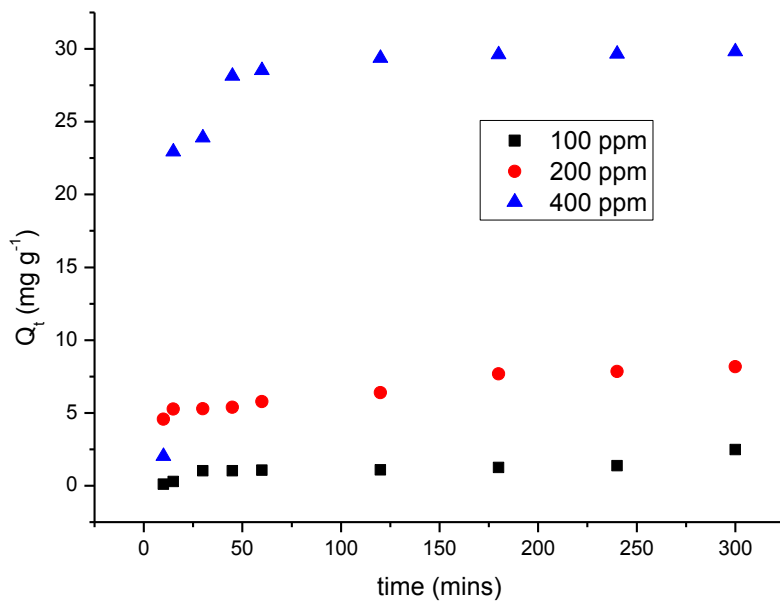


Fig 4.38 Effect of the initial chromium concentrations and contact time (Q_t vs time) using the magnetic alginate beads.

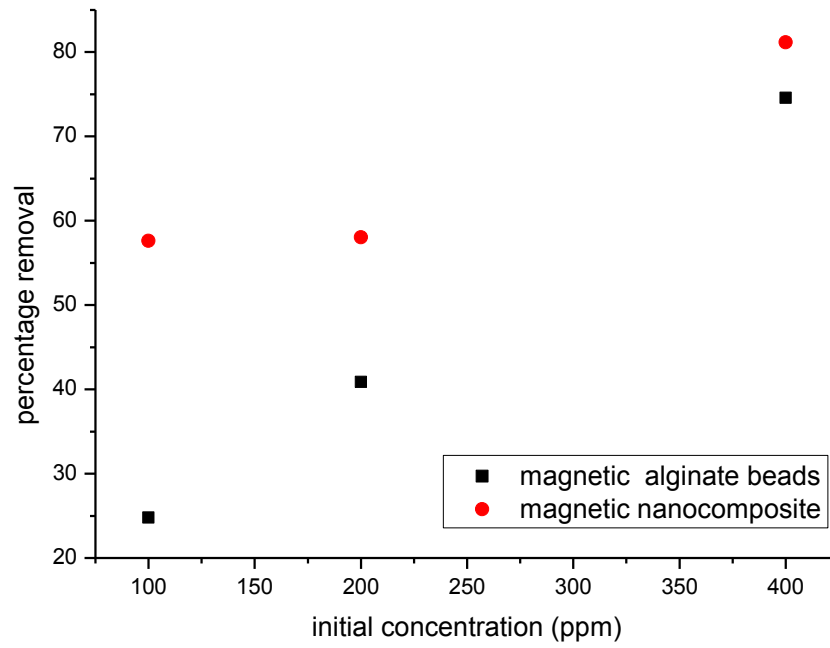


Fig 4.39 Effect of the initial chromium concentrations against contact time (%R vs time) using the magnetic nanocomposite.

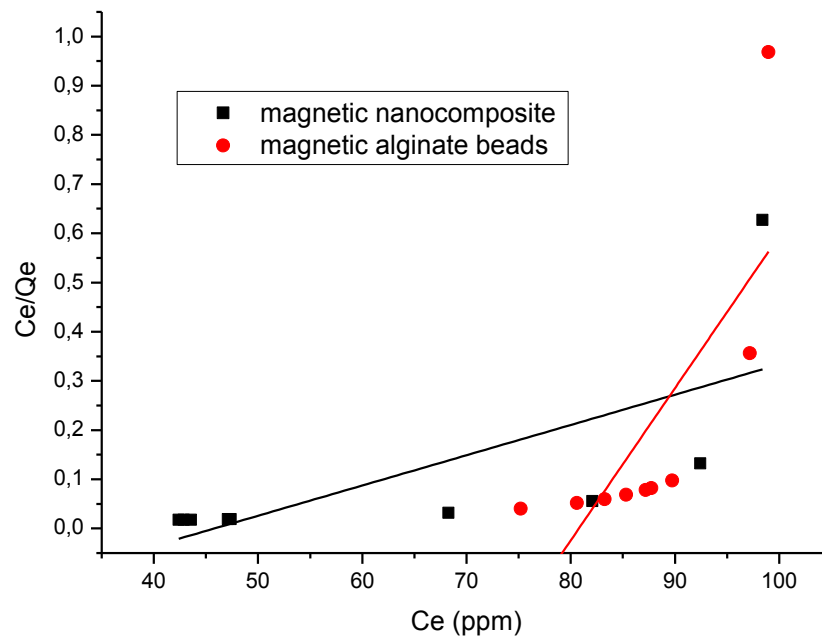


Fig 4.40 Langmuir isotherm for 100 ppm solution of chromium

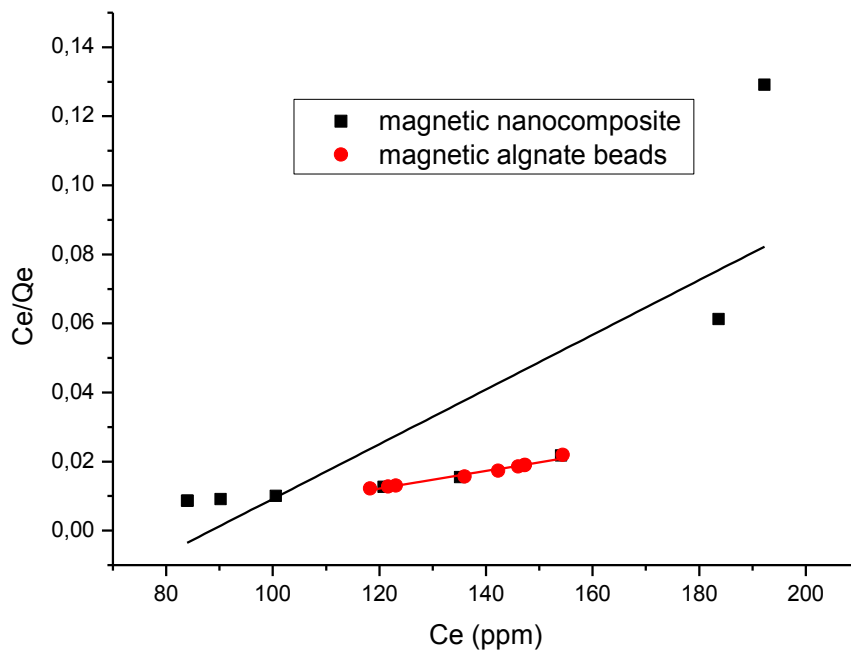


Fig. 4.41 Langmuir isotherm for 200 ppm solution of chromium

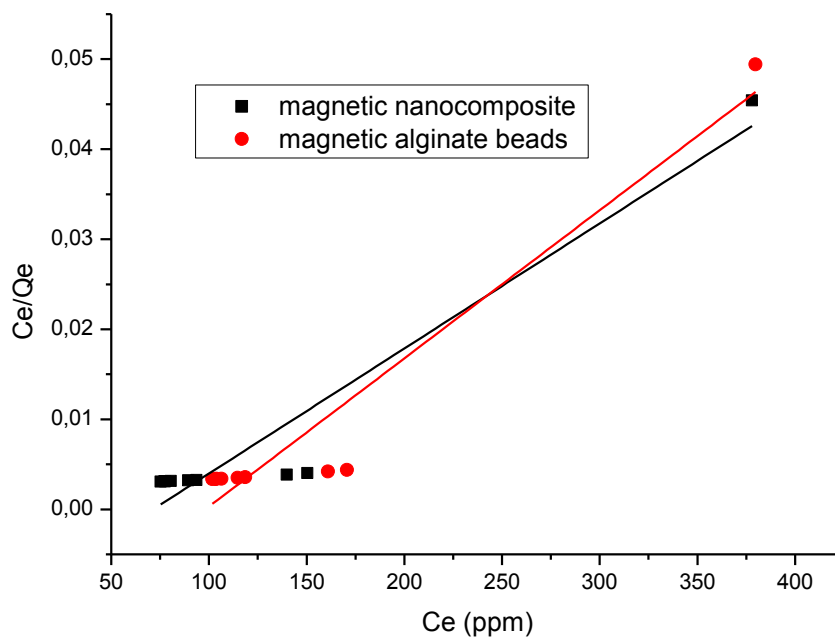


Fig. 4.42 Langmuir isotherm for 400 ppm solution of chromium

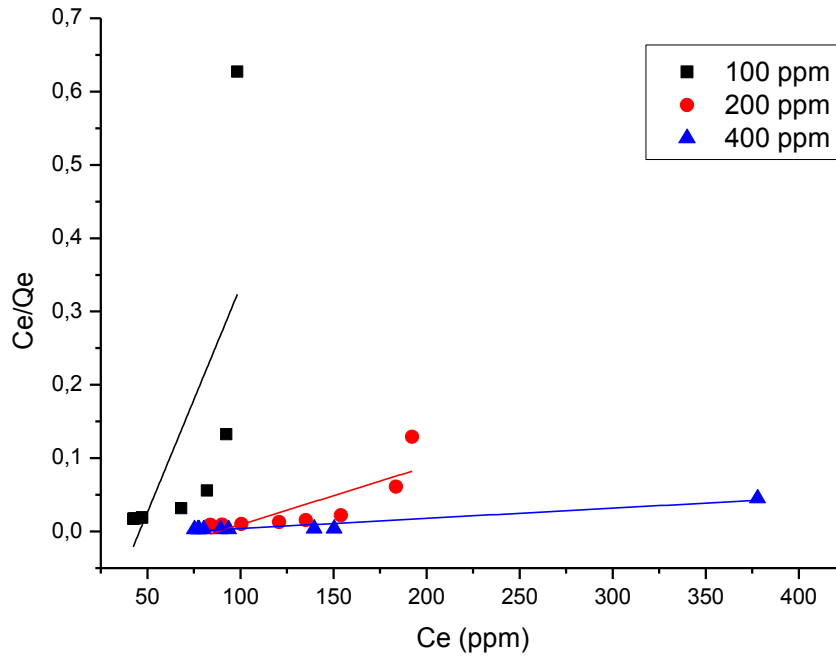


Fig 4.43 Langmuir isotherm comparisons of chromium using the magnetic nanocomposite.

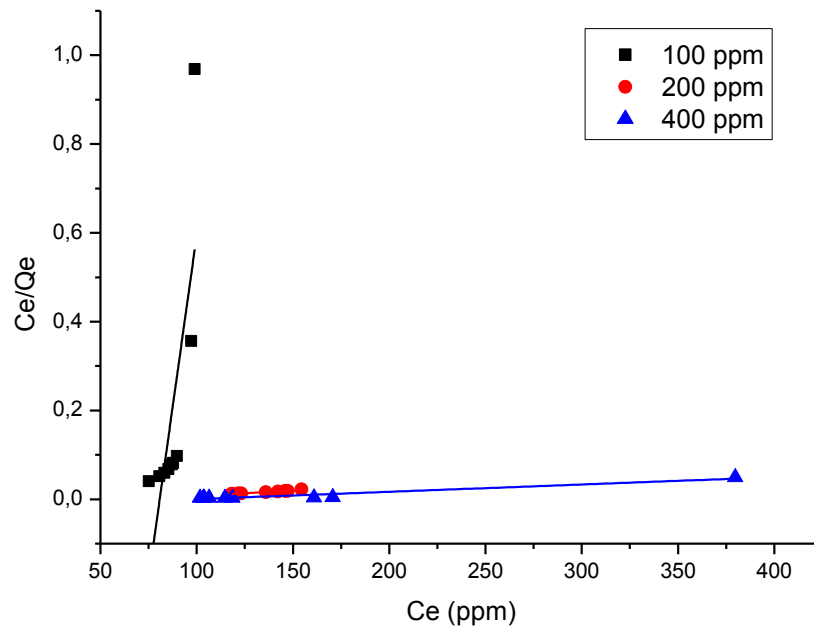


Fig. 4.44 Langmuir isotherm comparisons of chromium using the magnetic beads

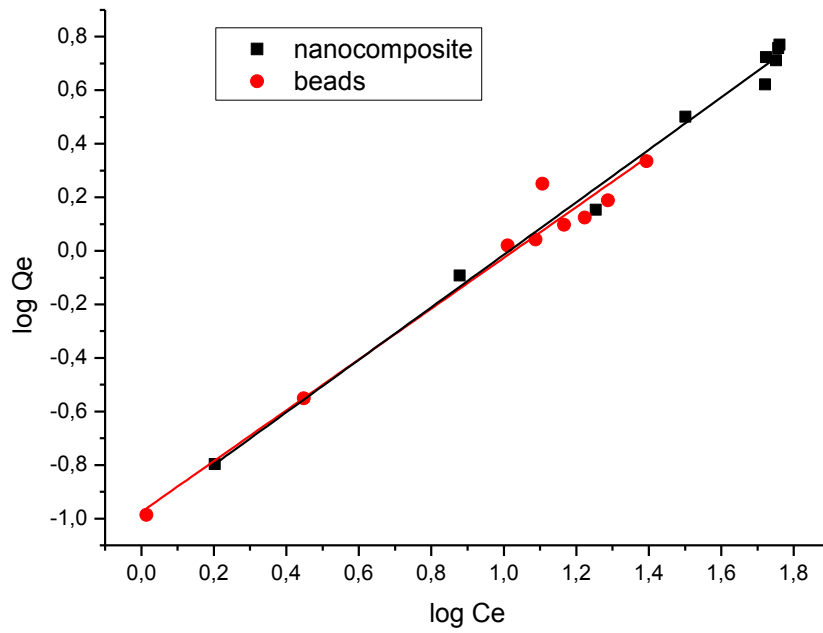


Fig 4.45 Freundlich isotherm for 100 ppm solution of chromium

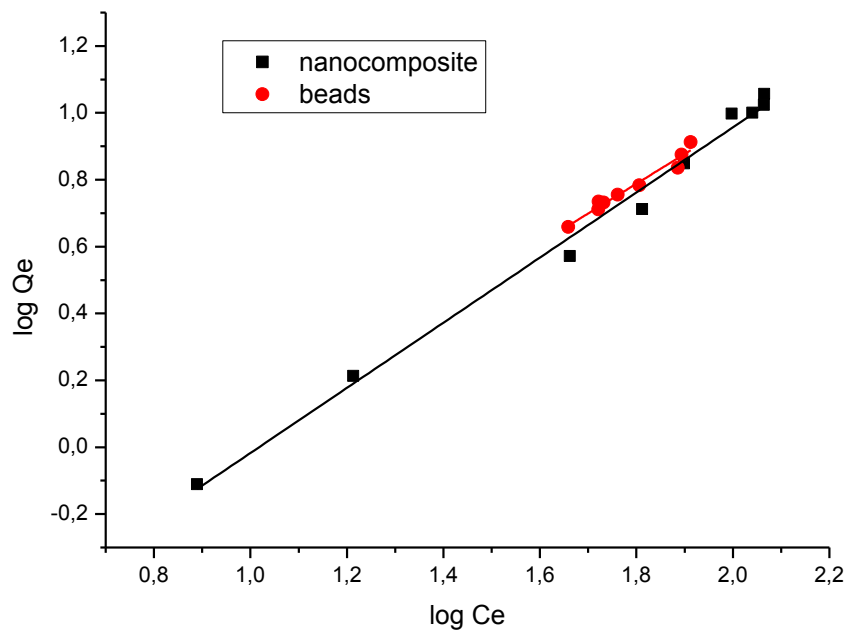


Fig 4.46 Freundlich isotherm for 200 ppm solution of chromium

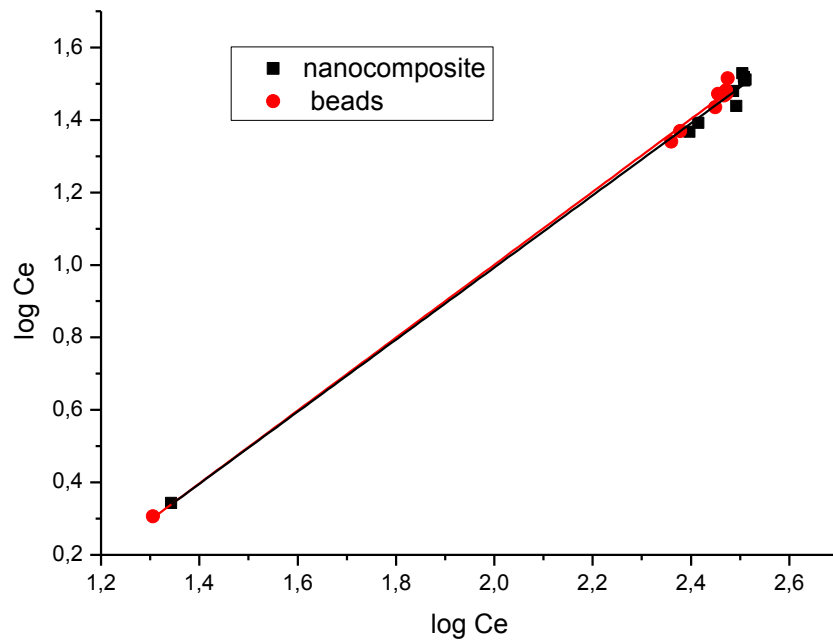


Fig 4.47 Freundlich isotherm for 400 ppm solution of chromium

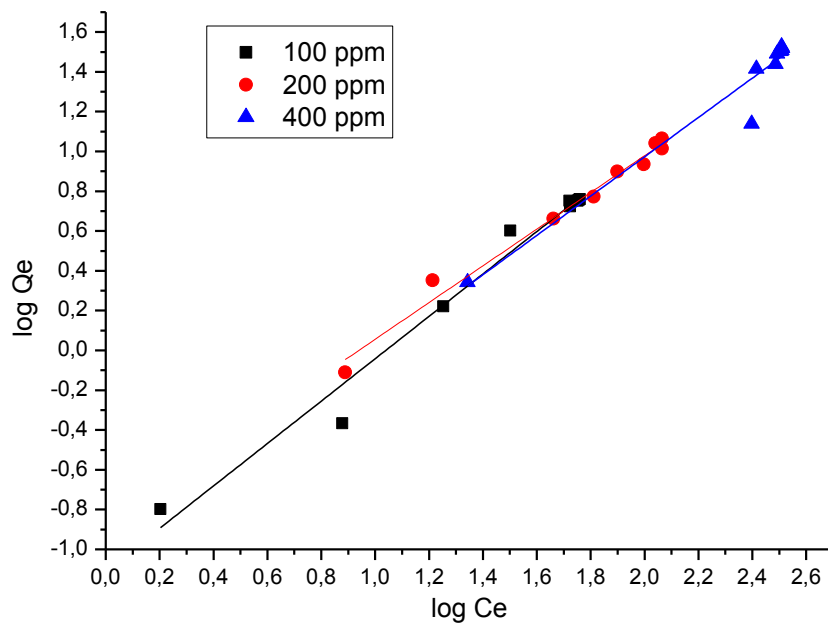


Fig 4.48 Freundlich isotherm comparisons of chromium using the magnetic nanocomposite.

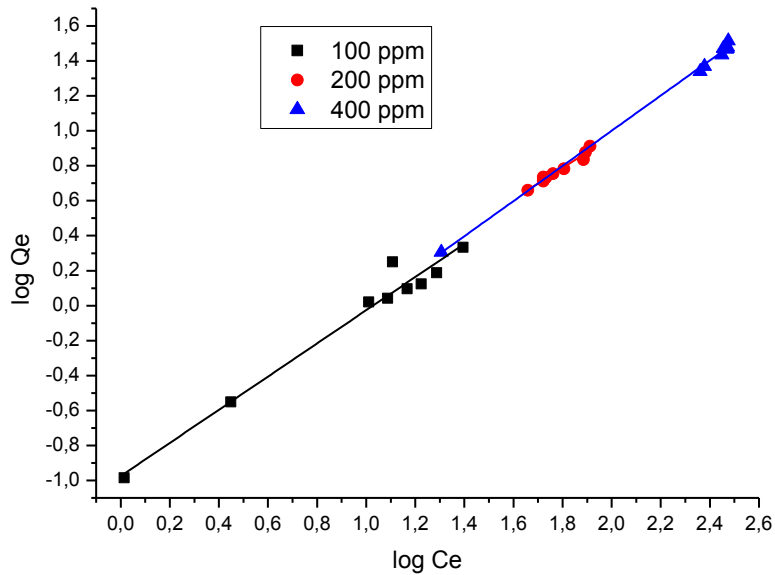


Fig 4.49 Freundlich isotherm comparisons of chromium using the magnetic alginate beads.

Table 4.10: Isotherm parameters for adsorption of chromium

isotherm	parameter	value					
		100		200		400	
		NC	BD	NC	BD	NC	BD
Freundlich	$\frac{1}{n}$	1,06	0,981	0,92	0,991	0,99	0,996
	K_F	0,33	0,36	0,42	0,365	0,37	1,918
	R^2	0,97	0,991	0,98	0,991	0,94	0,996
Langmuir	q_m	100,8	32,3	3,55	55,2	14,3	61,9
	K	71,42	67,517	461,98	65,533	88,38	65,757
	R^2	0,92	0,526	0,429	0,974	0,63	0,920

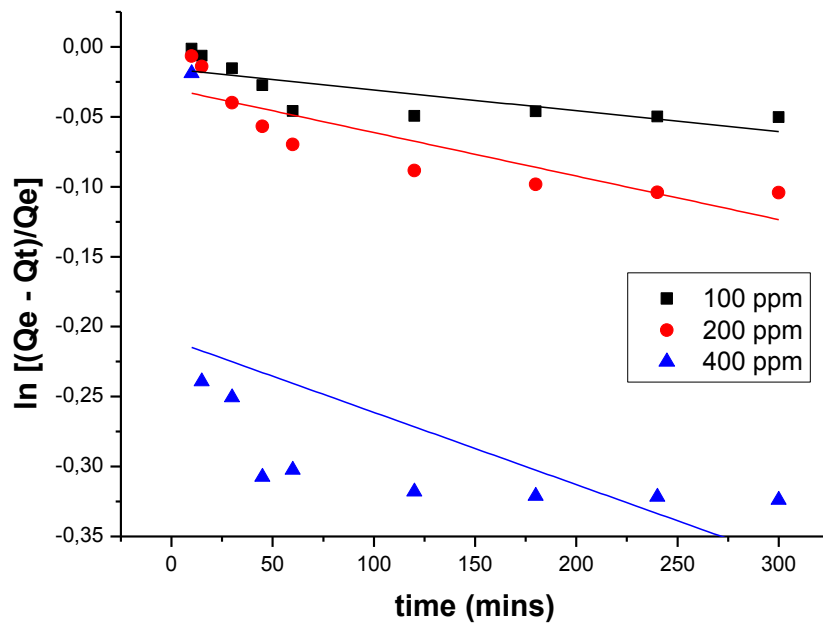


Fig 4.50 Pseudo First Order kinetics of chromium using the magnetic nanocomposite.

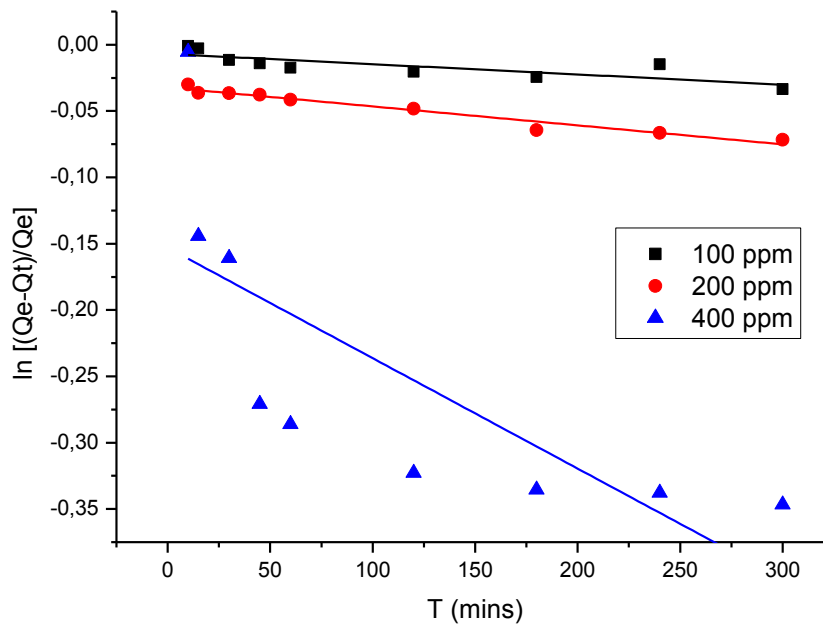


Fig 4.51 Pseudo First Order kinetics of chromium using the magnetic alginate beads

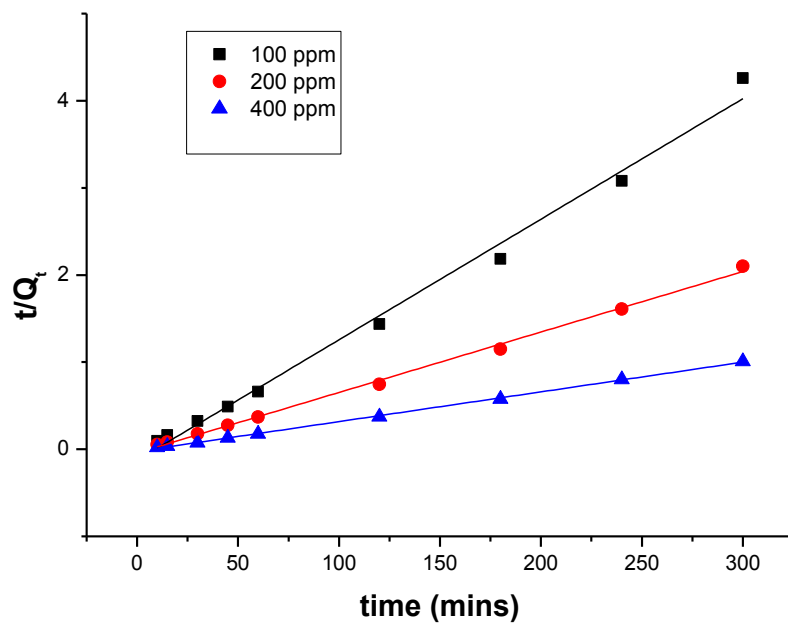


Fig 4.52 Pseudo Second Order kinetics of chromium using the magnetic nanocomposite.

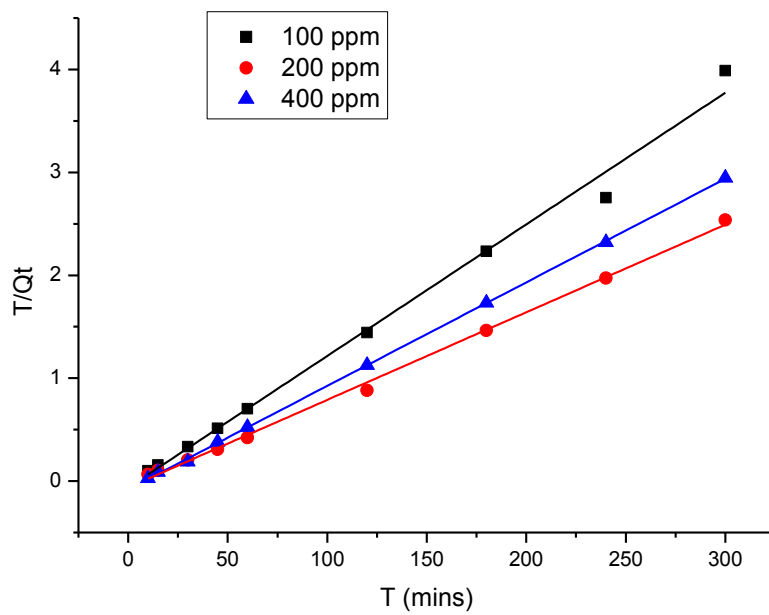


Fig 4.53 Pseudo Second Order kinetics of chromium using the magnetic alginate beads.

Table 4.11: Kinetics parameters for adsorption of chromium

	initial sorbate concentration					
	100		200		400	
	NC	BD	NC	BD	NC	BD
Q_e (exp)(mg /g)	42,402	75,213	83,904	118,24	75,38	101,77
Pseudo-first-order						
Q_e (calc)	0,9842	0,99	0,97	0,97	0,81	0,86
$k_1 \times 10^{-4}$	1,48	7,726	3,11	1,43	5,17	8,325
R^2	0,56	0,61	0,73	0,955	0,21	0,505
Pseudo-second-order						
R^2	0,992	0,991	0,997	1	0,999	0,998
Q_e (calc)	72,254	78,19	144,092	99,4	293,255	117,51
$1/(k^2Q_e^2)$	-0,127	-0,063	-0,04206	-0,0814	-0,0241	-0,062

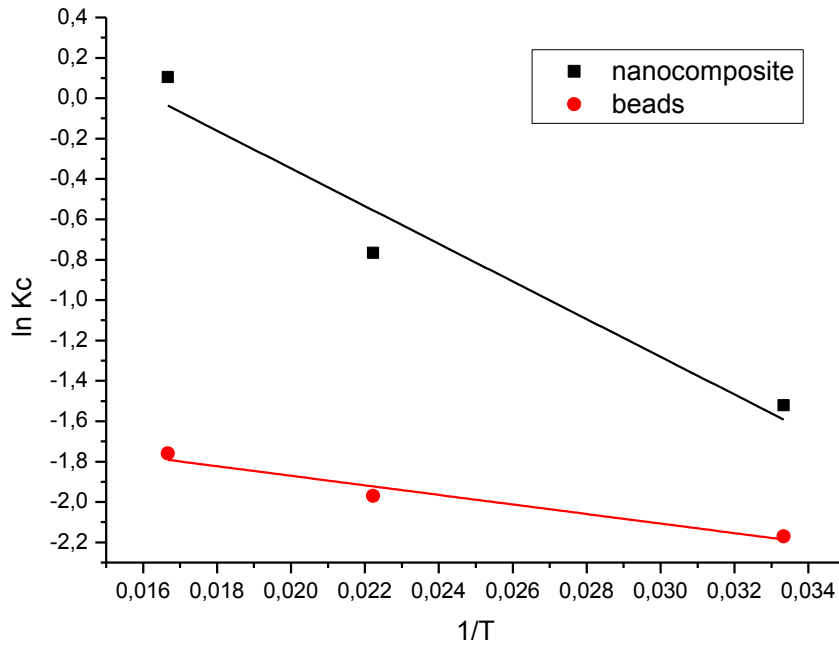


Fig 4.54 Thermodynamics studies of chromium adsorption

Table 4.12: Thermodynamic parameters for the adsorption of chromium

temperature (K)	thermodynamics					
	ΔG° (KJmol ⁻¹)		ΔS° (J mol ⁻¹ K ⁻¹)		ΔH° (KJmol ⁻¹)	
	NC	BD	NC	BD	NC	BD
294	-0,255	0,735				
313	1,995	0,877	12,626	-11,611	-0,0776	-0,197
333	4,212	1,067				

4.7 Adsorption studies of copper

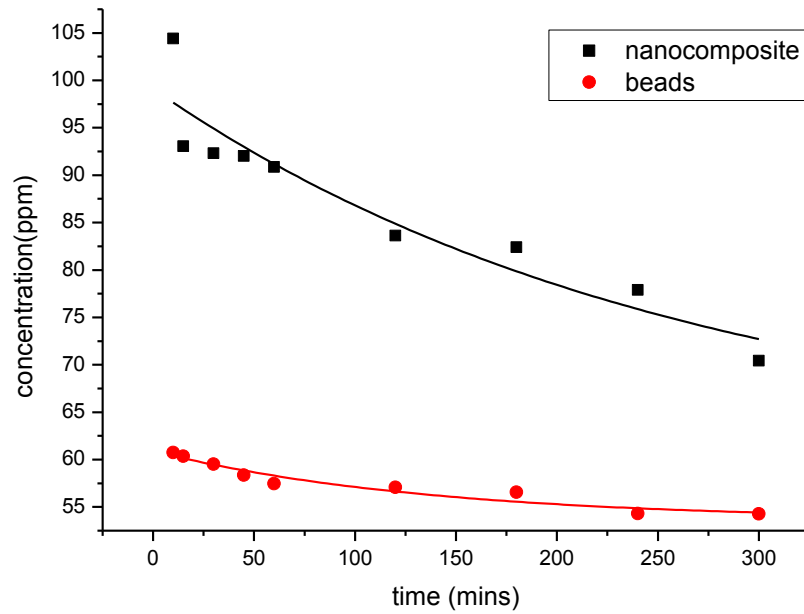


Fig 4.55 Adsorption of 100 ppm Copper solution

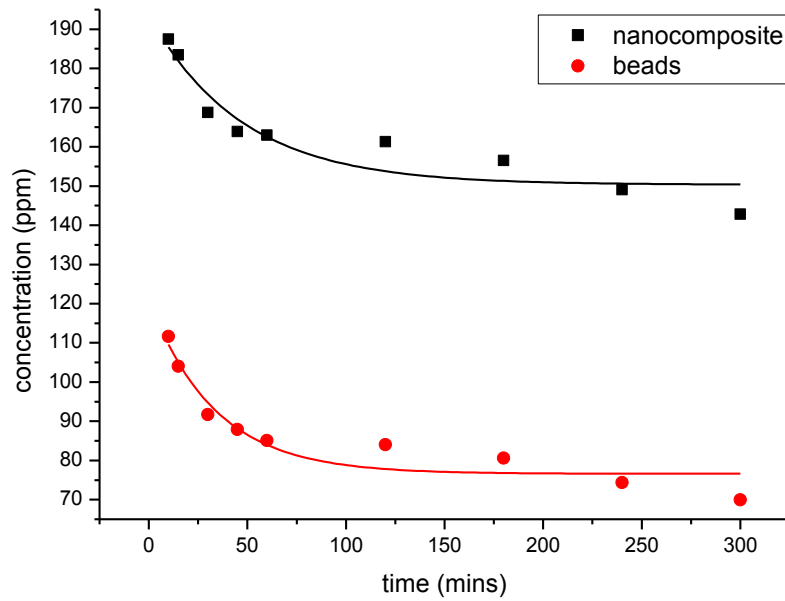


Fig 4.56 Overlay of adsorption graphs of different copper solutions using magnetic nanocomposite.

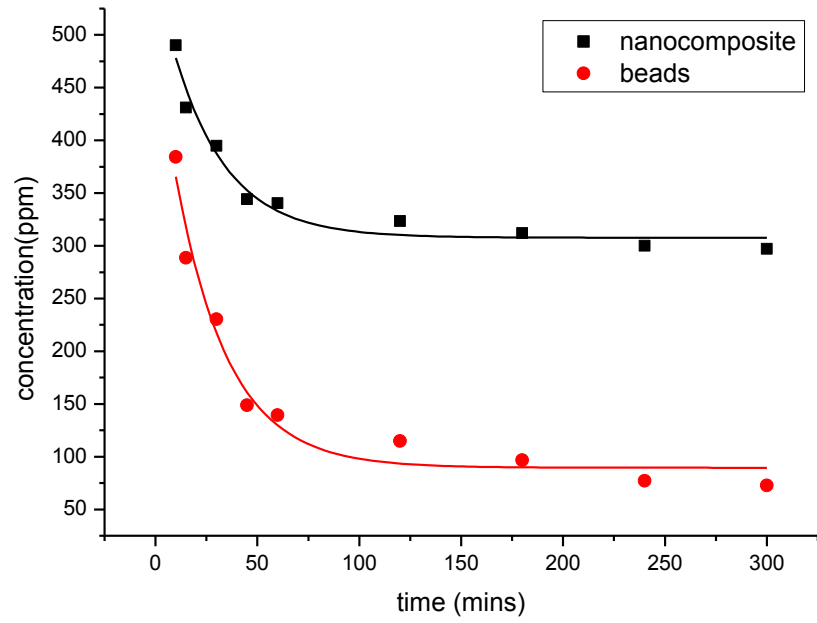


Fig 4.57 Overlay of adsorption graphs of different copper solutions using magnetic beads.

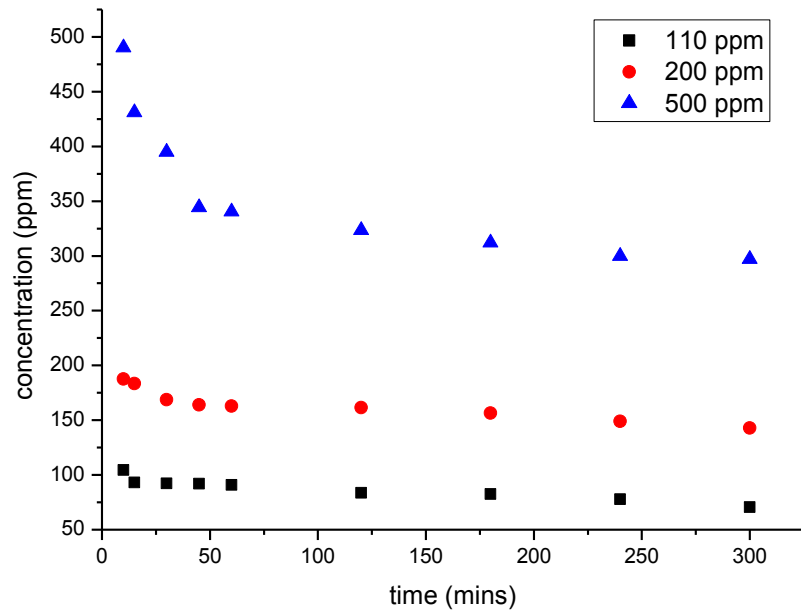


Fig 4.58 Overlay of adsorption graphs of different copper solutions using magnetic nanocomposite

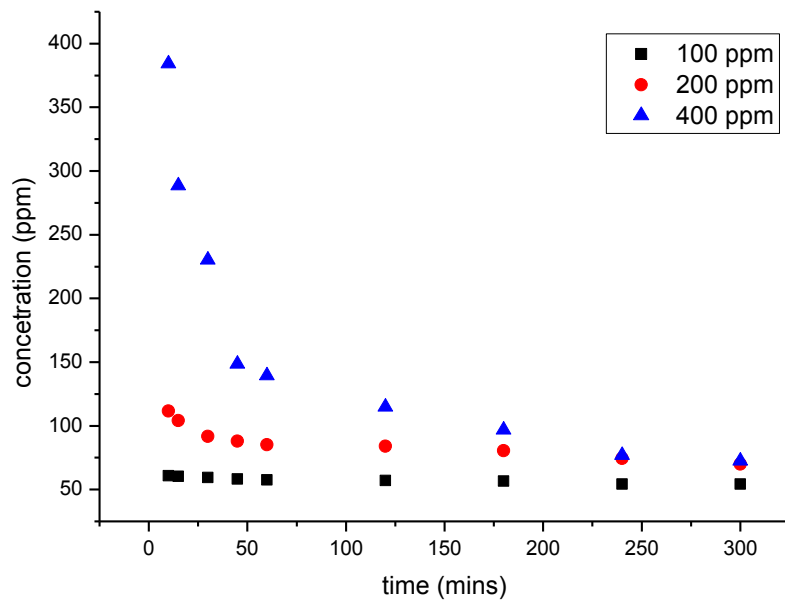


Fig 4.59 Overlay of adsorption graphs of different copper solutions using magnetic beads

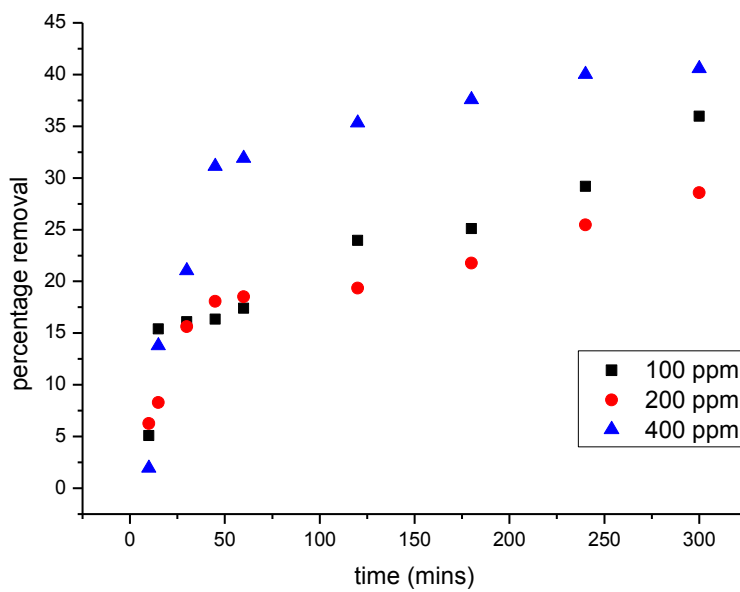


Fig 4.60 Percentage removal of copper by magnetic nanocomposite

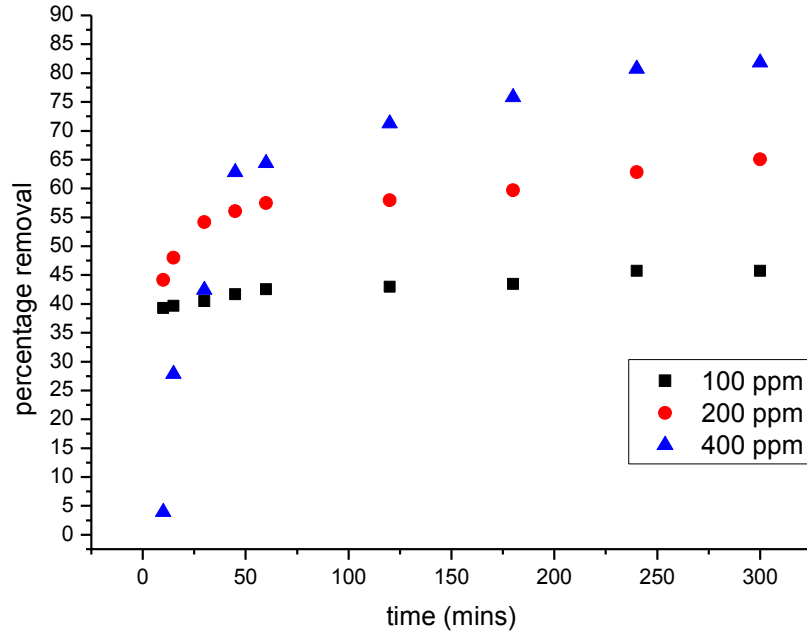


Fig 4.61 Percentage removal of copper by magnetic beads

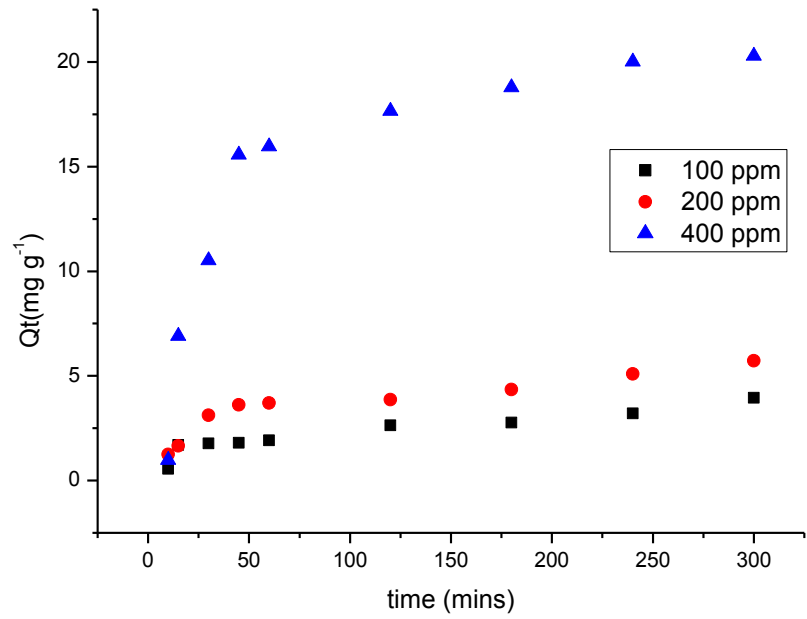


Fig 4.62 Qt against time for magnetic nanocomposite of copper

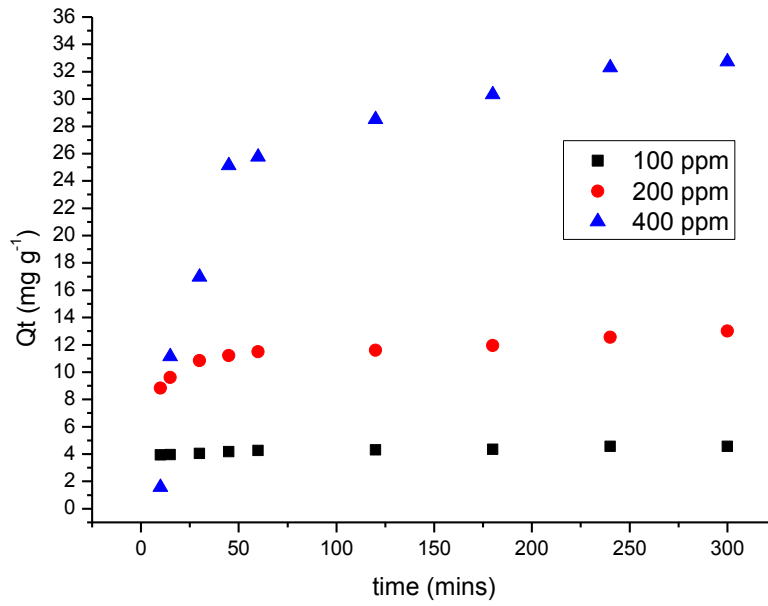


Fig 4.63 Q_t against time for magnetic beads of copper

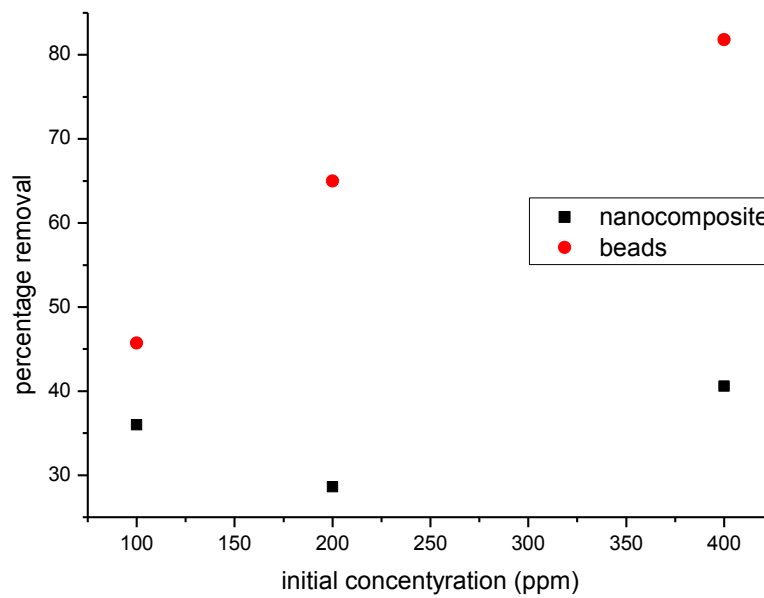


Fig 4.64 Effect of the initial chromium concentrations against contact time (%R vs time) using the magnetic nanocomposite of copper

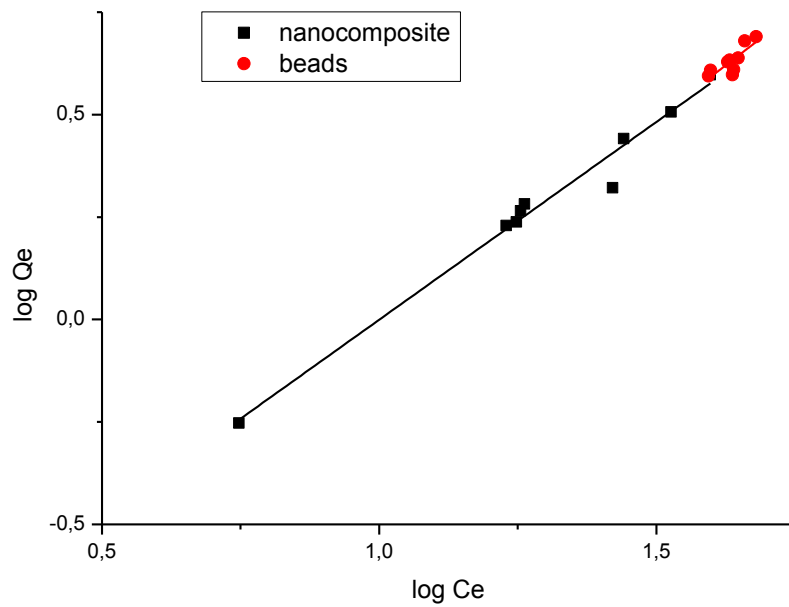


Fig 4.65 Freundlich isotherm for 100 ppm solution of copper

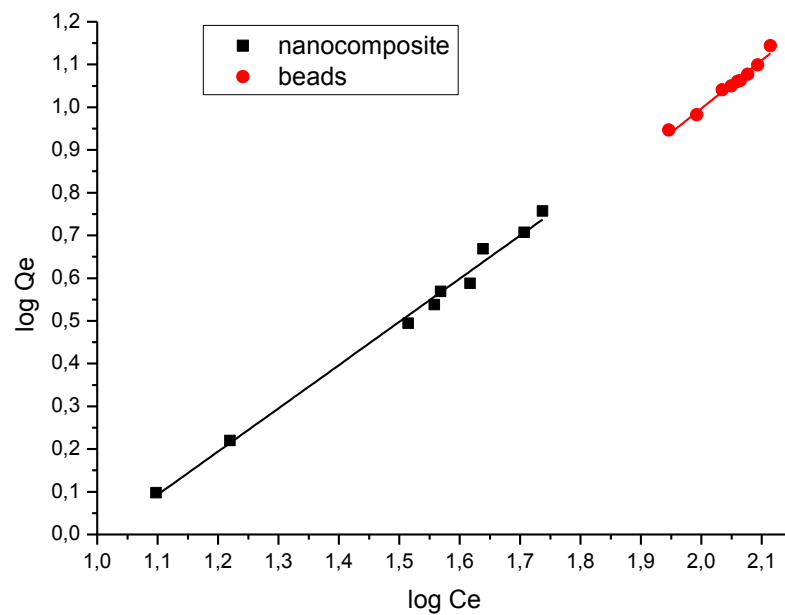


Fig 4.66 Freundlich isotherm for 200 ppm solution of copper

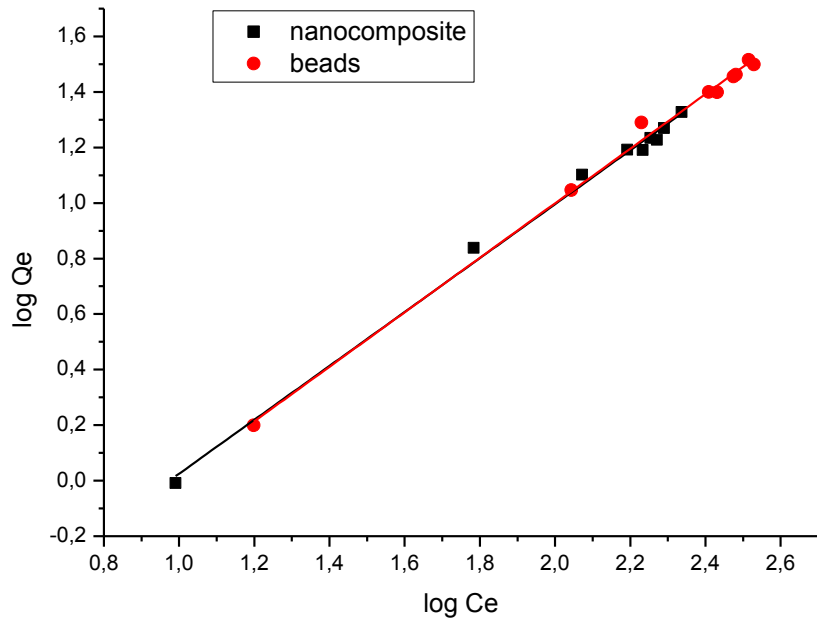


Fig 4.67 Freundlich isotherm for 400 ppm solution of copper

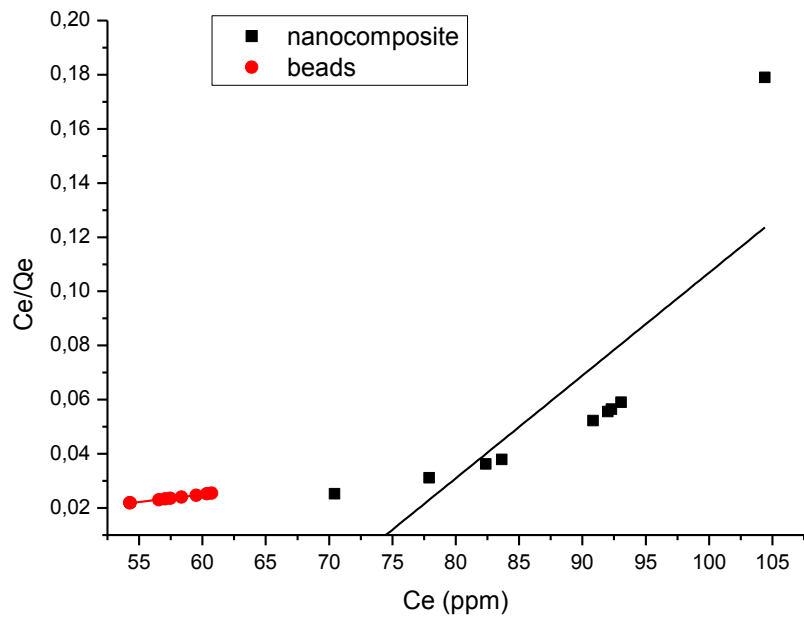


Fig 4.68 Langmuir isotherm for 100 ppm solution of copper

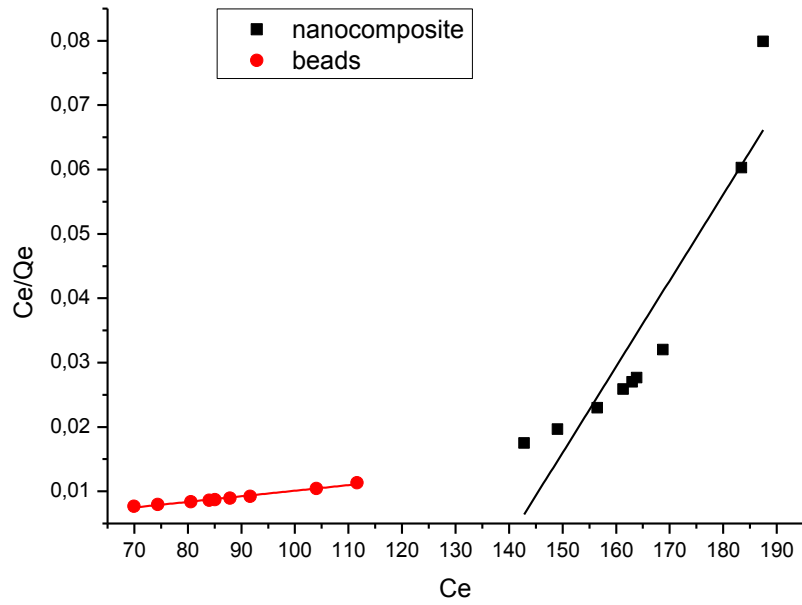


Fig 4.69 Langmuir isotherm for 200 ppm solution of copper

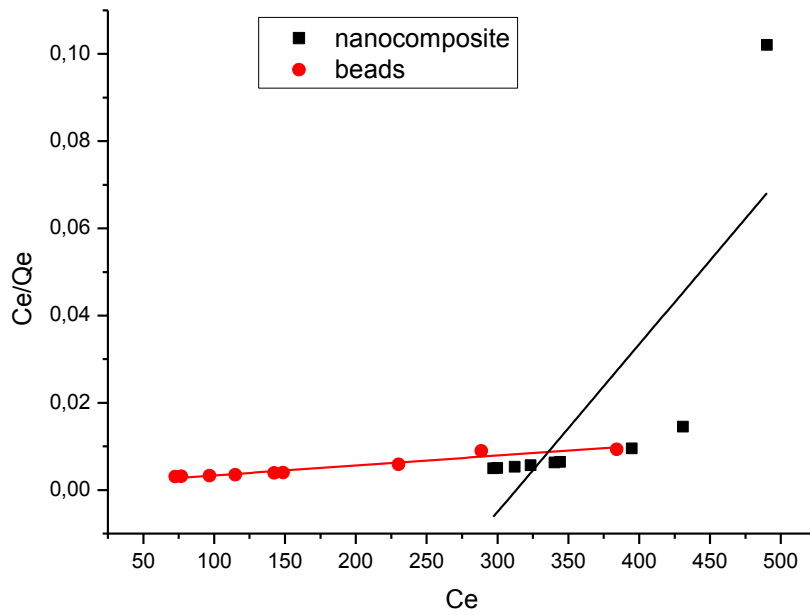


Fig 4.70 Langmuir isotherm for 400 ppm solution of copper

Table 4.13: Isotherm parameters for adsorption of copper

isotherm	parameter	value					
		100		200		400	
		NC	BD	NC	BD	NC	BD
Freundlich	$\frac{1}{n}$	1,06	1,0405	0,92	1,1272	0,99	0,982
	K_F	0,33	0,343	0,42	0,285	0,37	0,381
	R^2	0,97	0,635	0,98	0,974	0,94	0,995
langmuir	Q_m	100,8	120,77	3,55	709,2	14,3	934,58
	K	71,42	15,05	461,98	16,23	88,38	46,99
	R^2	0,92	0,997	0,429	0,984	0,63	0,935

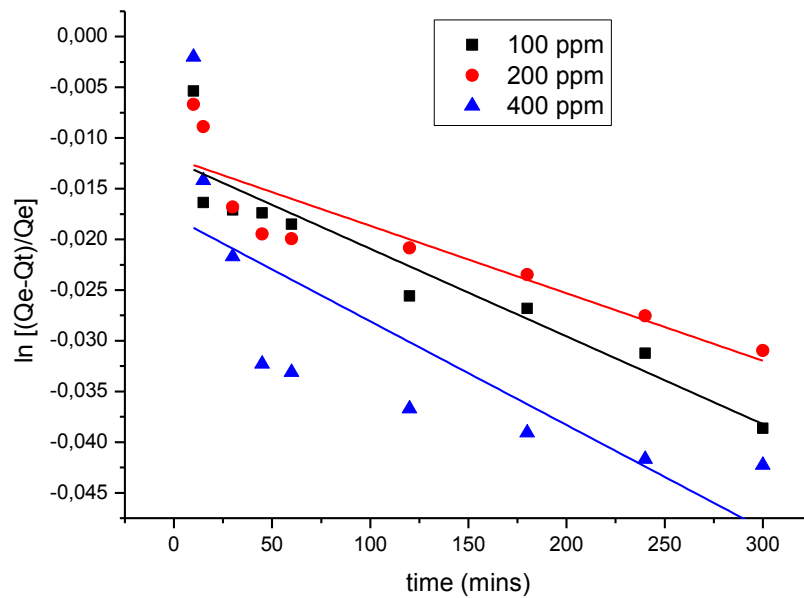


Fig 4.71 Pseudo first order kinetics of copper for magnetic nanocomposite

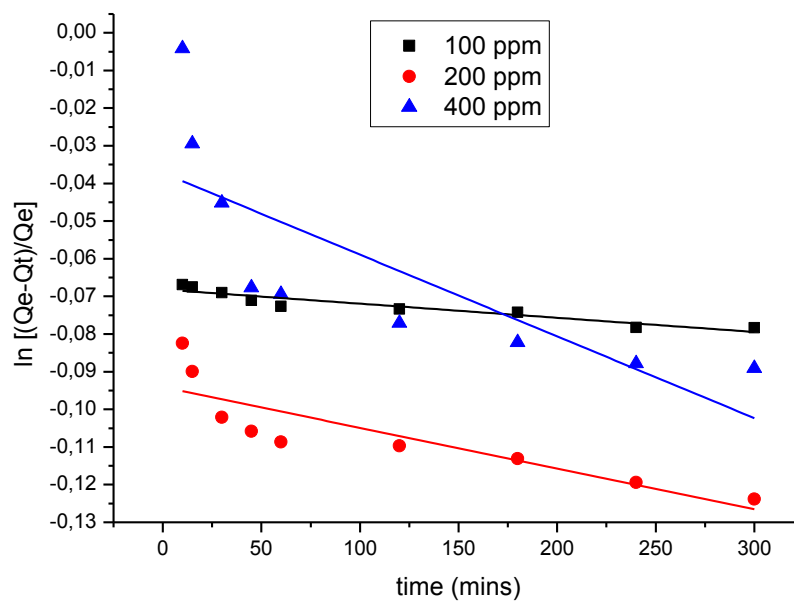


Fig 4.72 Pseudo first order kinetics of copper for magnetic beads

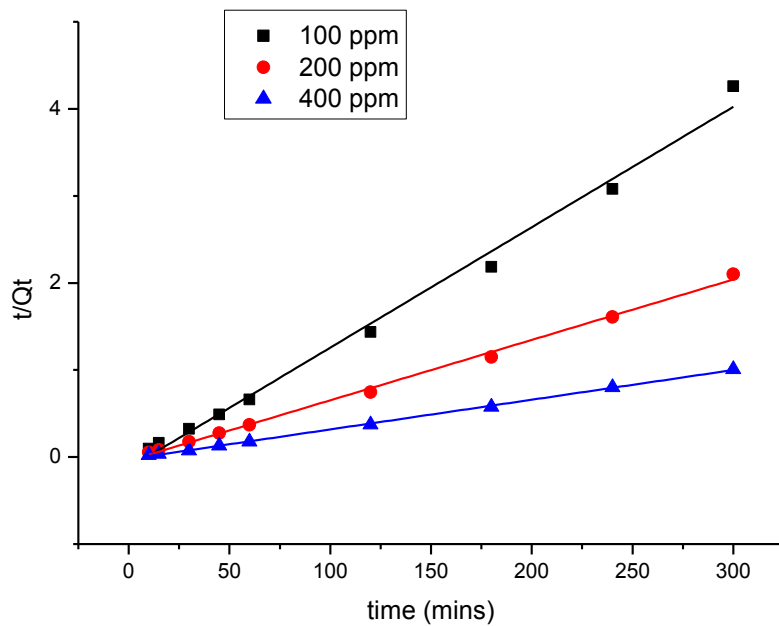


Fig 4.73 Pseudo second order kinetics of copper for magnetic nanocomposites

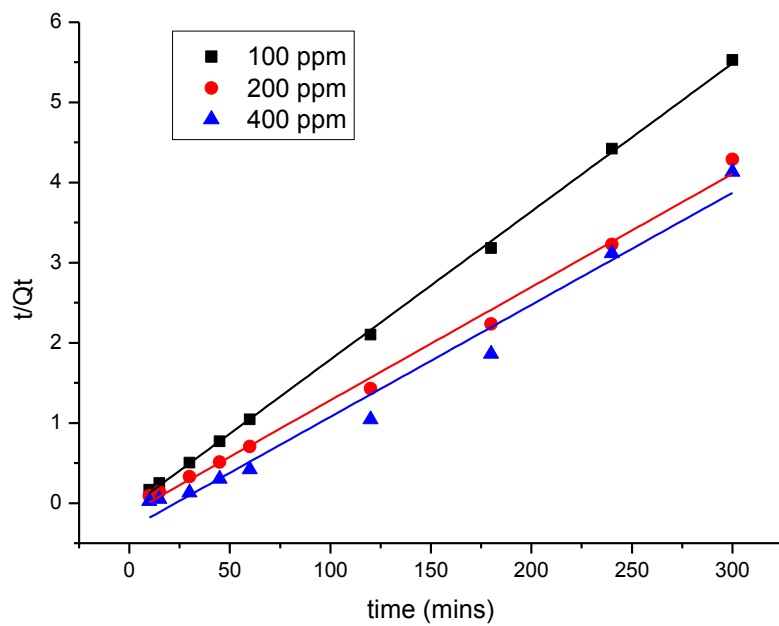


Fig 4.74 Pseudo second order kinetics of copper for magnetic beads

Table 4.14: kinetics parameters for adsorption of copper

	initial sorbate concentration					
	100		200		400	
	NC	BD	NC	BD	NC	BD
Q_e (exp)(mg /g)	70,437	54,263	142,835	69,935	297,155	72,608
Pseudo-first-order						
Q_e (calc)	0,988	0,934	0,988	0,91	0,982	0,963
$k_1 \times 10^{-4}$	8,652	3,757	6,656	1,081	1,023	2,173
R^2	0,867	0,886	0,775	0,718	0,564	0,569
Pseudo-second-order						
R^2	0,992	0,999	0,997	993	0,999	0,976
Q_e (calc)	72,254	54,11	144,092	70,77	293,255	71,53
$1/(k^2Q_e^2)$	-0,127	-0,063	-0,04206	-0,0814	-0,0241	-0,062

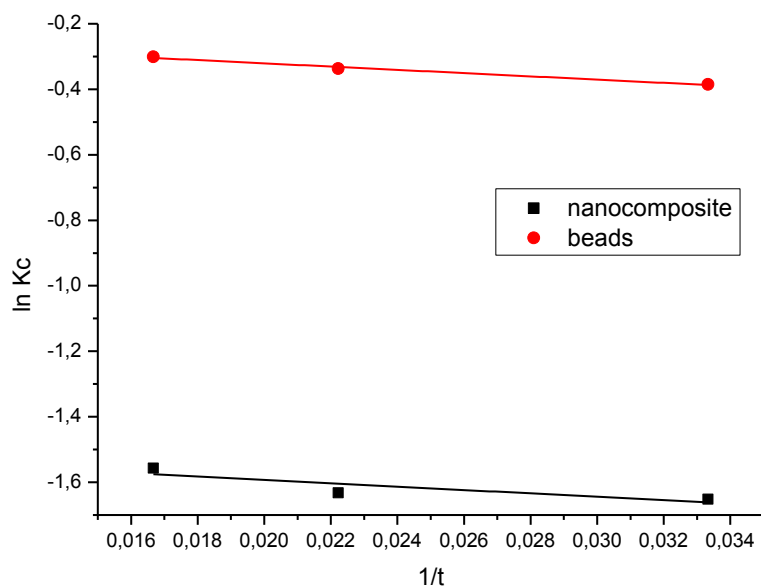


Fig 4.75 Thermodynamics studies of copper adsorption

Table 4.15: Thermodynamics parameters for adsorption of copper

temperature (K)	thermodynamics					
	ΔG° (KJmol ⁻¹)		ΔS° (J mol ⁻¹ K ⁻¹)		ΔH° (KJmol ⁻¹)	
	NC	BD	NC	BD	NC	BD
294	3,806	0,735				
313	4,247	0,877	-1,841	12,388	-0,0413	-0,0427
333	4,573	1,066				

4.8 Adsorption studies of toluene

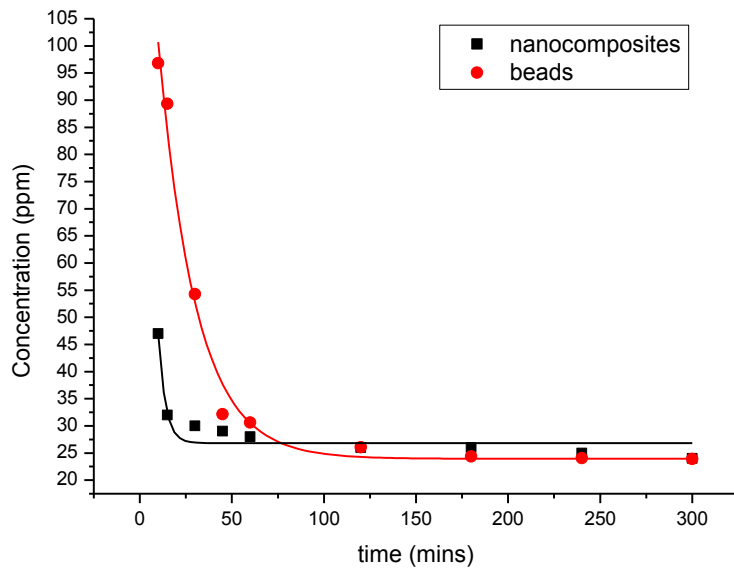


Fig 4.76 Adsorption of 100 ppm solution of toluene

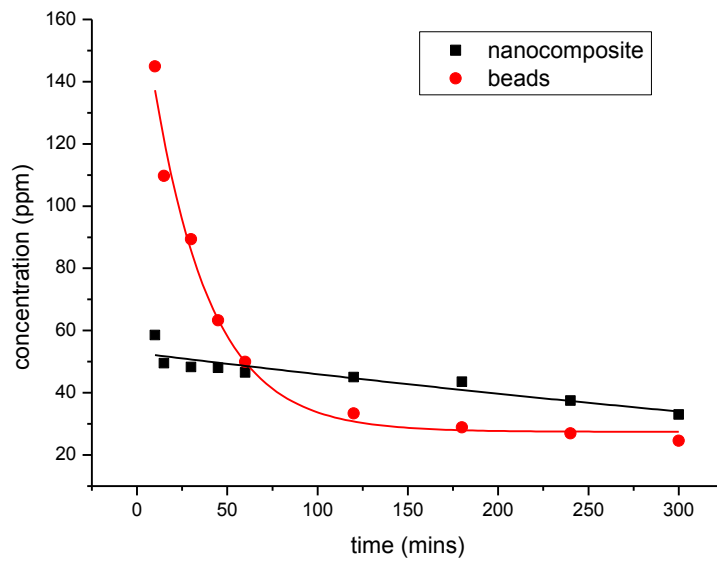


Fig 4.77 Adsorption of 200 ppm solution of toluene

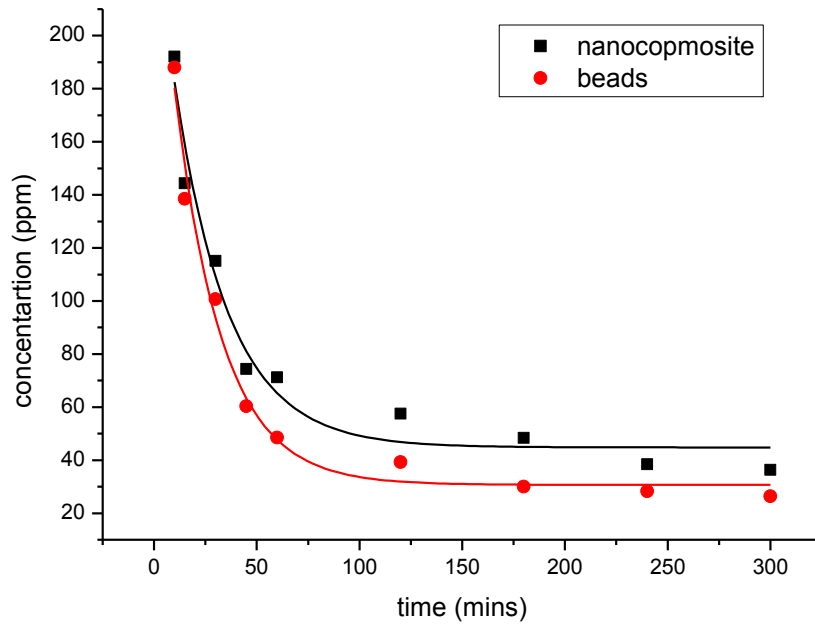


Fig 4.78 Adsorption of 400 ppm solution of toluene

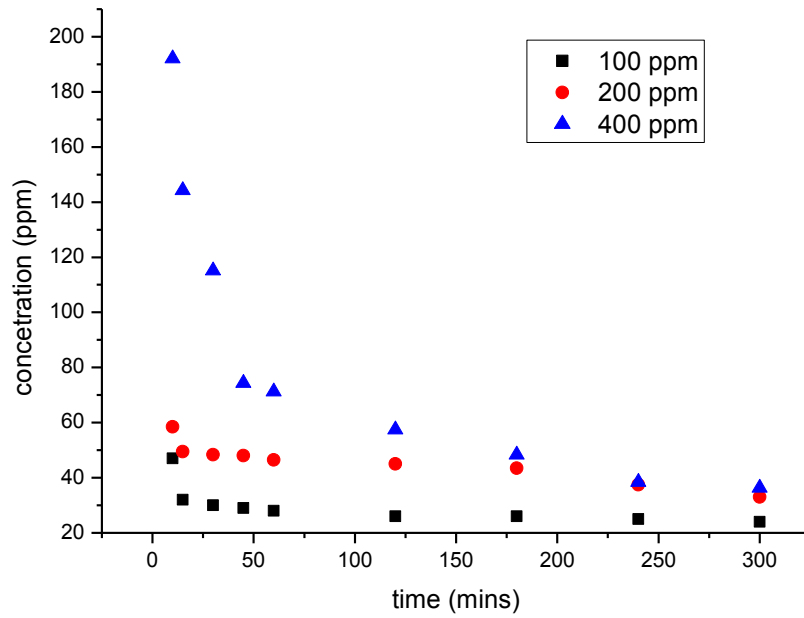


Fig 4.79 Overlay of adsorption graphs of different toluene concentrations using magnetic nanocomposite.

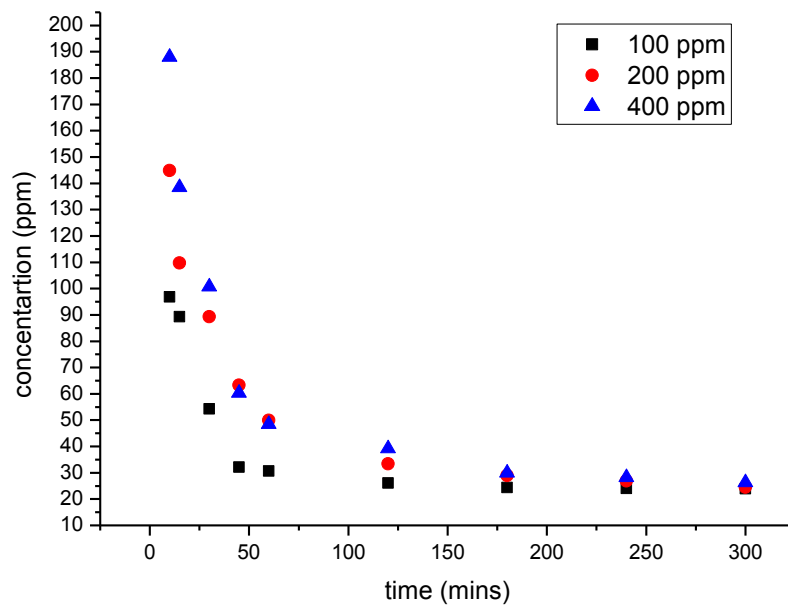


Fig 4.80 Overlay of adsorption graphs of different toluene concentrations using magnetic beads.

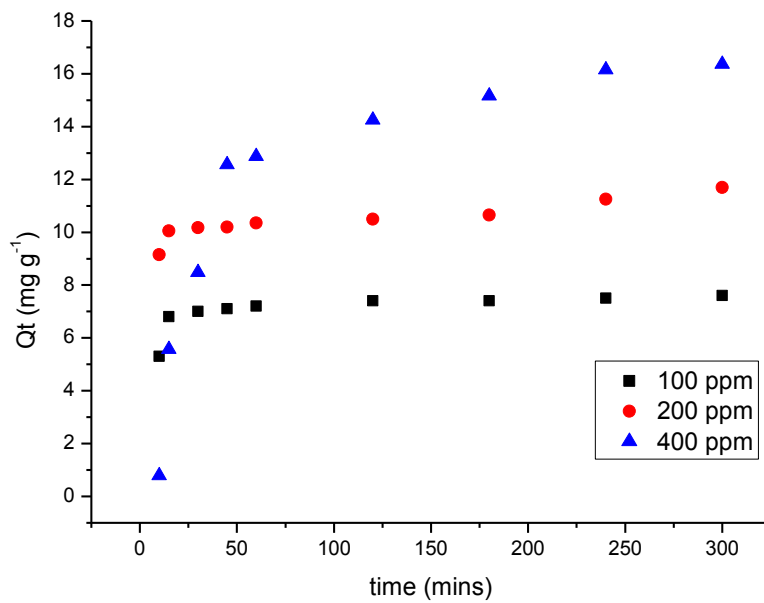


Fig 4.81 Q_t against time for toluene comparisons for magnetic nanocomposites

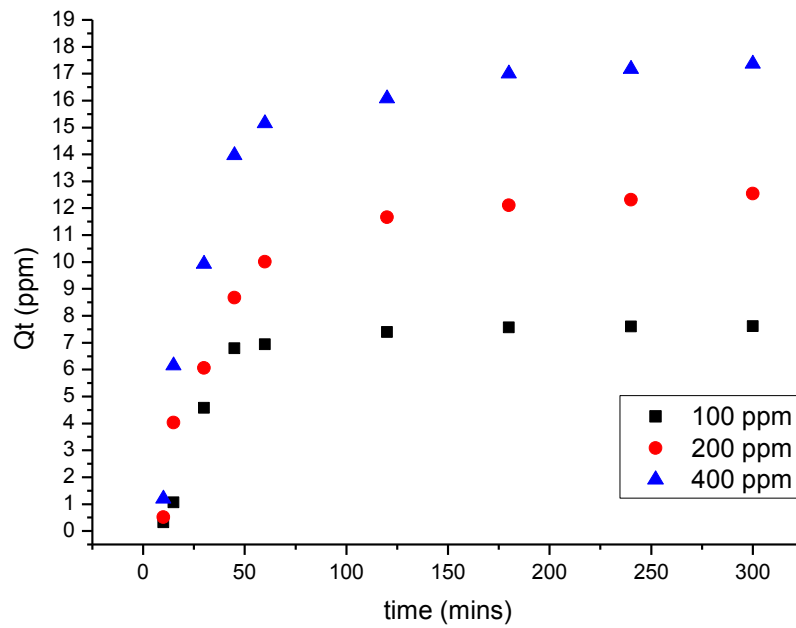


Fig 4.82 Qt against time for toluene comparisons for magnetic beads.

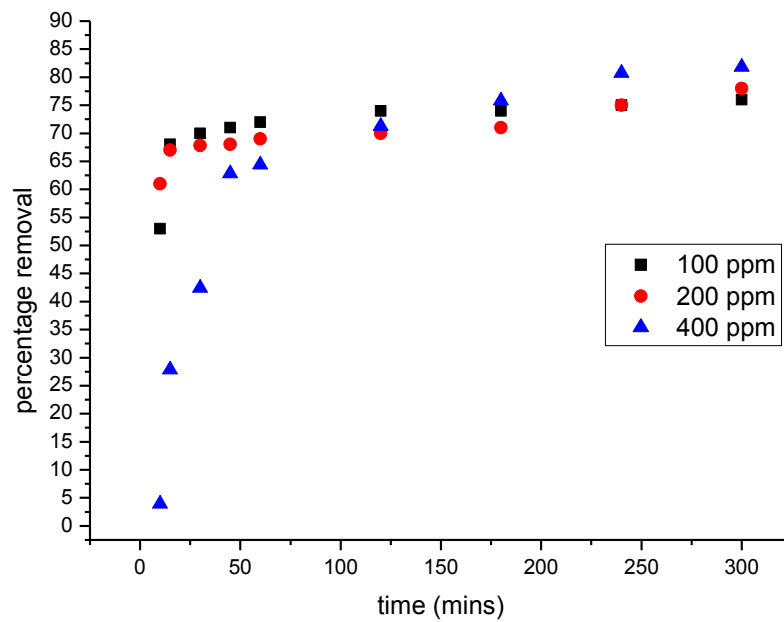


Fig 4.83 Percentage removal against time for different toluene concentrations using magnetic nanocomposites.

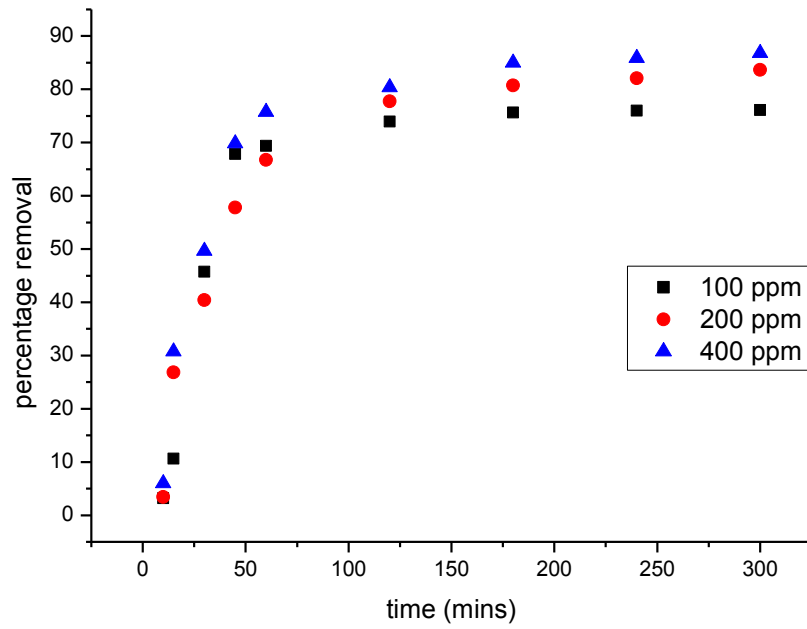


Fig 4.84 Percentage removal against time for toluene comparisons for magnetic beads.

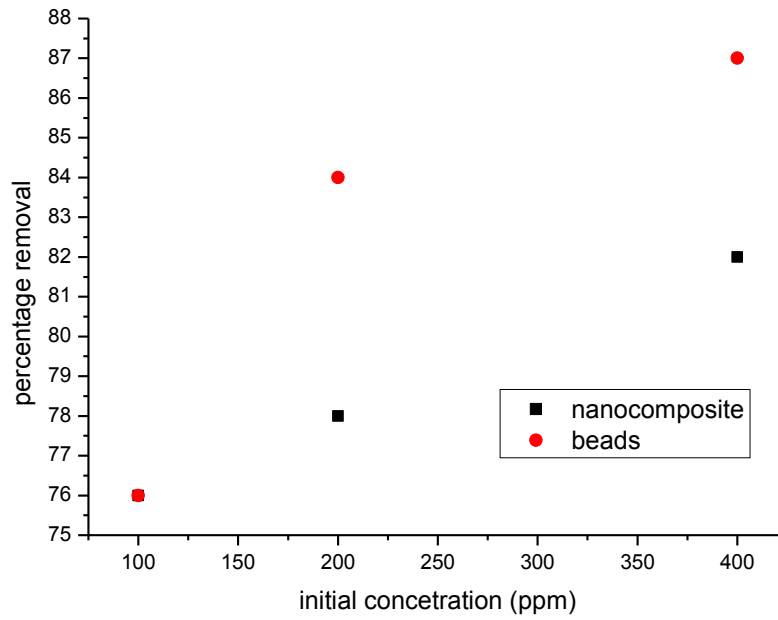


Fig 4.85 Percentage removal for toluene against initial concentration

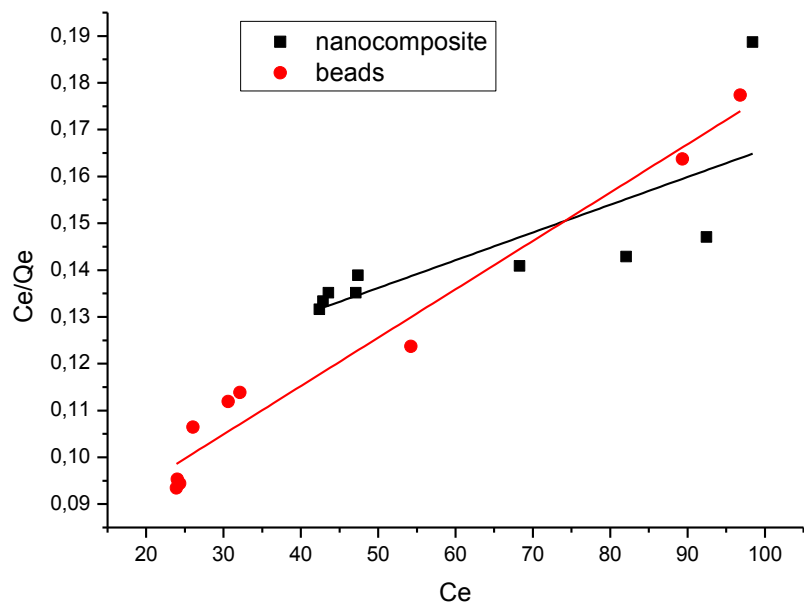


Fig 4.86 Langmuir isotherms for 100 ppm solution of toluene

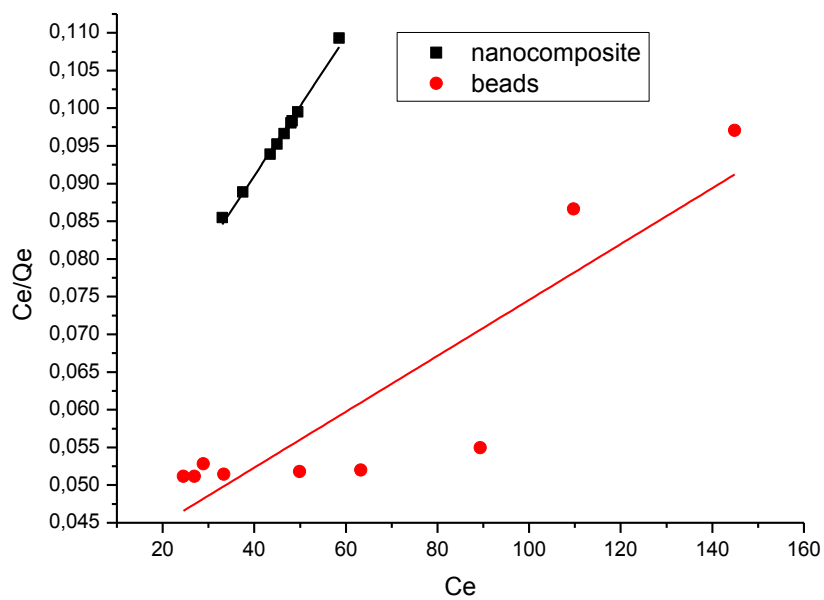


Fig 4.87 Langmuir isotherms for 200 ppm solution of toluene

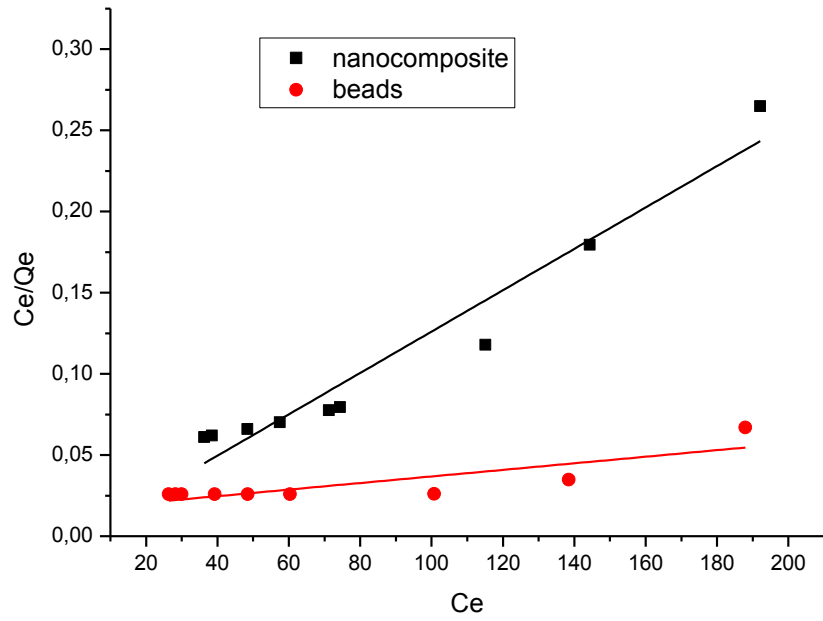


Fig 4.88 Langmuir isotherms for 400 ppm solution of toluene

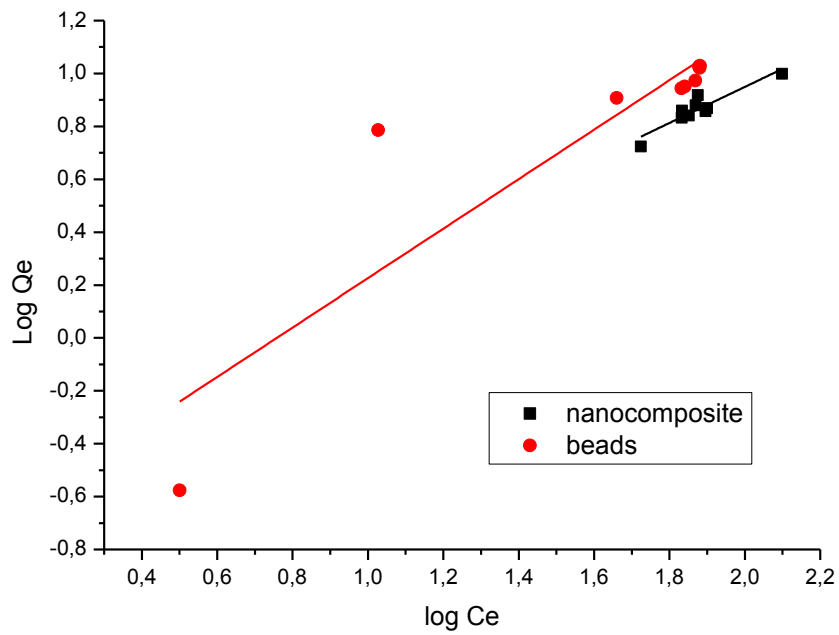


Fig 4.89 Freundlich isotherms for 100 ppm solution of toluene

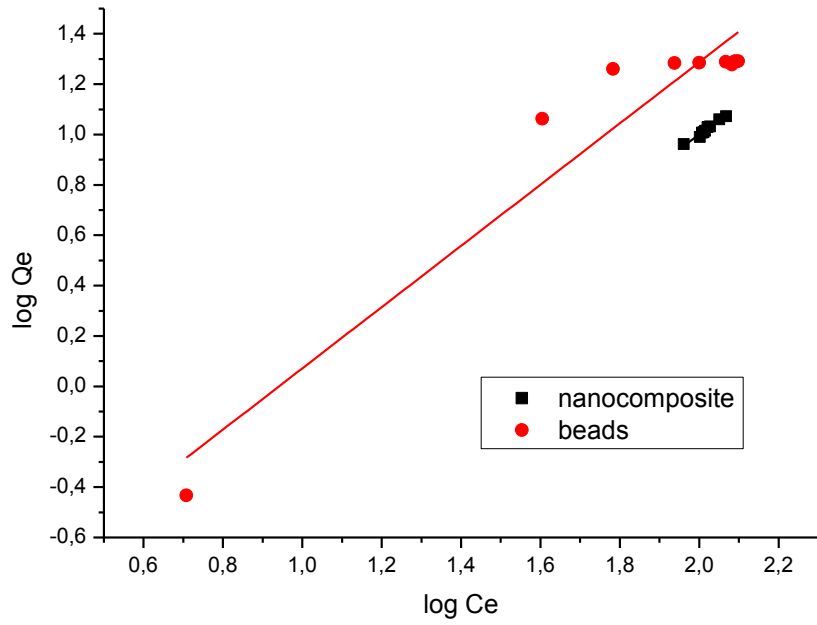


Fig 4.90 Freundlich isotherms for 200 ppm solution of toluene

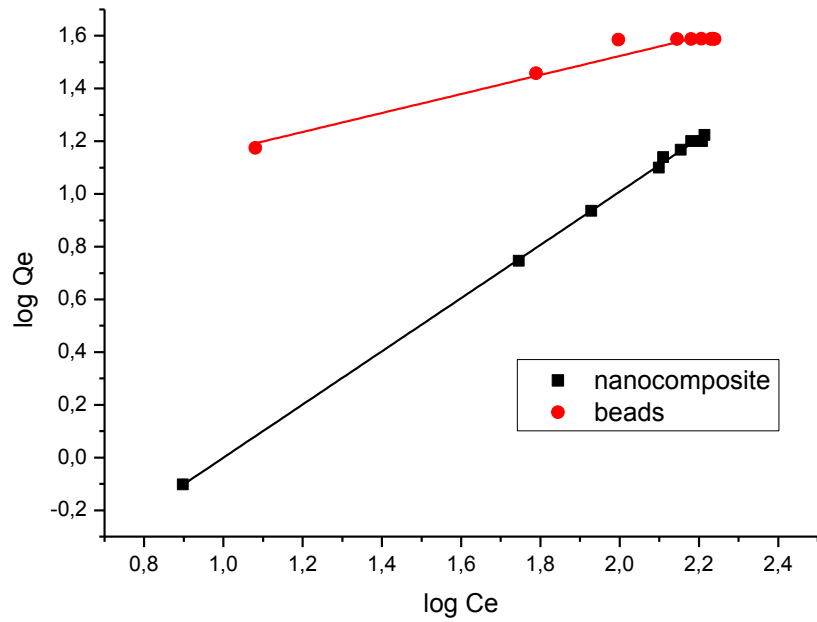


Fig 4.91 Freundlich isotherms for 400 ppm solution of toluene

Table 4.15: Isotherm parameters for adsorption of toluene

isotherm	parameter	value					
		100		200		400	
		NC	BD	NC	BD	NC	BD
Freundlich	$\frac{1}{n}$	0,6823	0,9354	1,1078	1,2158	1,0089	0,3612
	K_F	0,66	0,49	0,296	0,318	0,36	2,23
	R^2	0,836	0,777	0,972	0,915	0,999	0,957
langmuir	Q_m	9,383	13,53	18,49	26,68	724,6	60,24
	K	0,018	71,75	58,58	101,11	1,09	81,73
	R^2	0,542	0,964	0,990	0,769	0,940	0,681

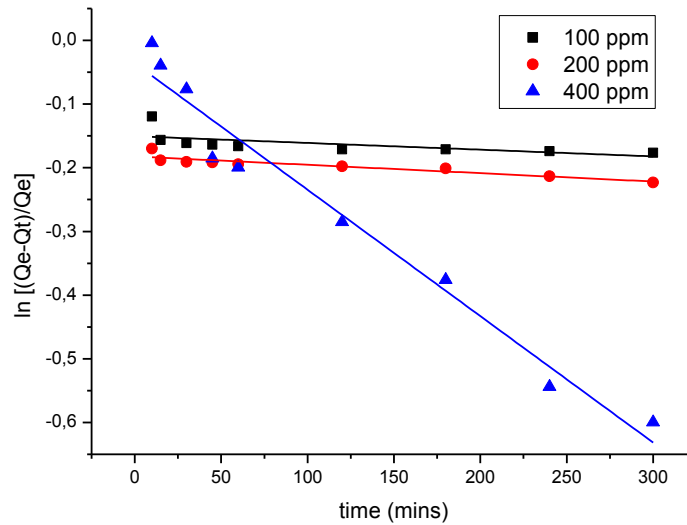


Fig 4.92 Pseudo first order kinetics of toluene for magnetic nanocomposite

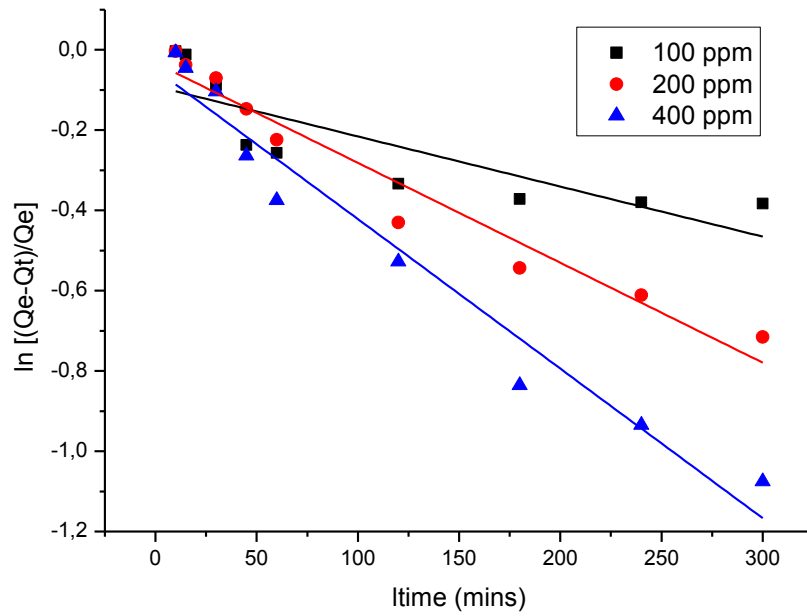


Fig 4.93 Pseudo first order kinetics of toluene for magnetic beads

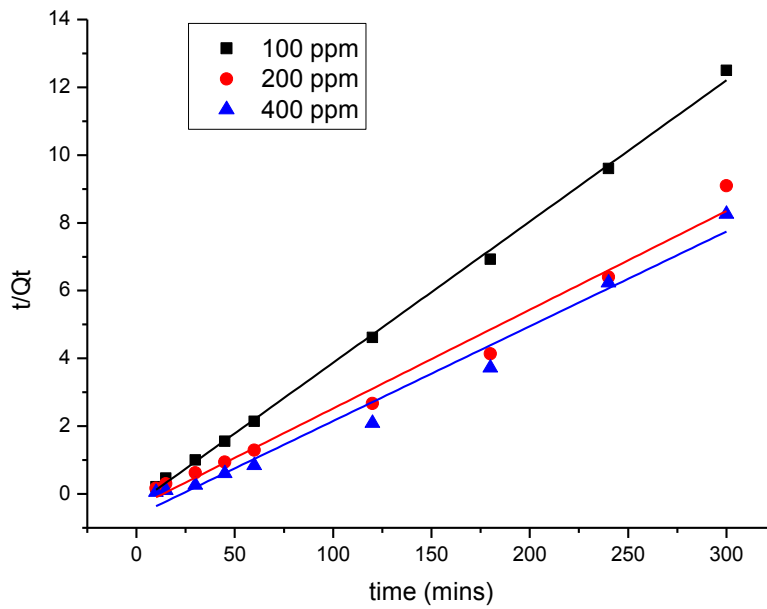


Fig 4.94 Pseudo second order kinetics of toluene for magnetic nanocomposite

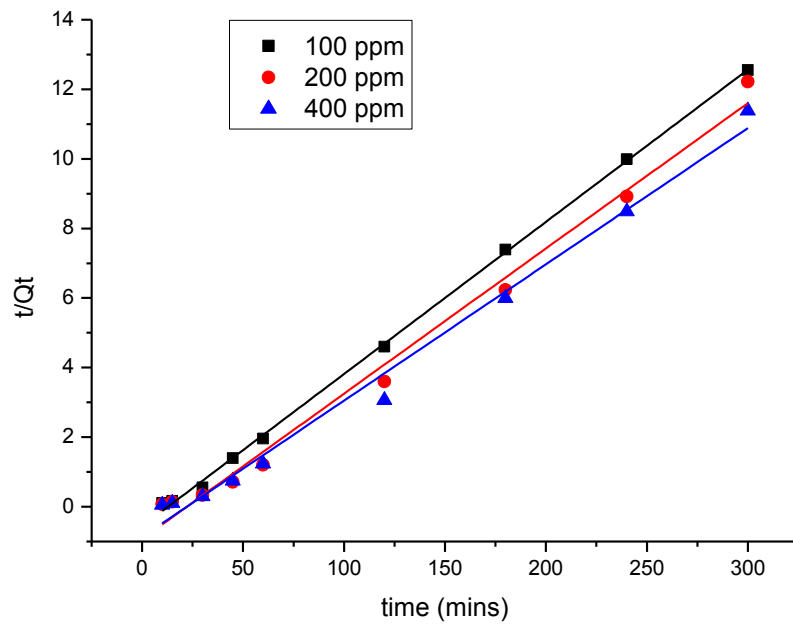


Fig 4.95 Pseudo second order kinetics of toluene for magnetic beads

Table 4.16: Kinetics parameters for adsorption of toluene

	initial sorbate concentration					
	100		200		400	
	NC	BD	NC	BD	NC	BD
Q_e (exp)(mg /g)	24	23,9	33	24,5	36,3	26,4
Pseudo-first-order						
Q_e (calc)	0,86	0,91	0,833	0,356	0,968	0,952
k_1	$1,057 \times 10^{-4}$	0,00125	$1,315 \times 10^{-4}$	0,00249	0,00199	0,00373
R^2	0,343	0,673	0,825	0,951	0,963	0,957
Pseudo-second-order						
R^2	0,998	0,999	0,979	0,989	0,977	0,989
Q_e (calc)	23,99	22,86	34,33	23,95	35,78	25,52
$1/(k^2Q_e^2)$	-0,296	-0,560	-0,391	-0,925	-0,643	-0,868

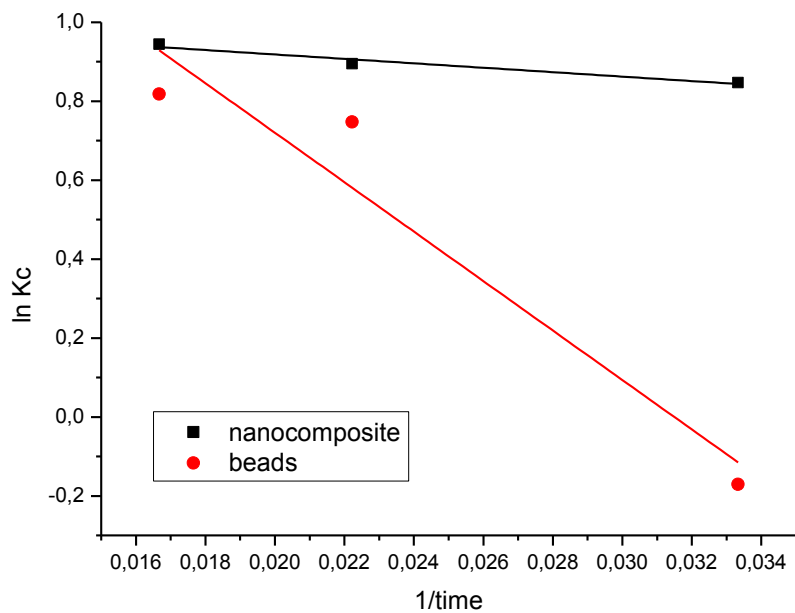


Fig 4.96 Thermodynamic studies for toluene adsorption

Table 4.17: Thermodynamics parameters for adsorption of toluene

temperature (K)	thermodynamics					
	ΔG° (KJmol ⁻¹)		ΔS° (J mol ⁻¹ K ⁻¹)		ΔH° (KJmol ⁻¹)	
	NC	BD	NC	BD	NC	BD
294	-2,309	-1,999				
313	-2,330	-1,945	8,57	16,409	-0,0453	-0,521
333	-2,345	0,0923				

5.0 DISCUSSIONS

5.1 Characterization of zeolites

The FT-IR spectra of zeolites in Figs 4.1 - 4.3 show adsorption bands in the region of 3400 to 3500 cm^{-1} corresponding to terminal silanol groups on the external surface of the zeolite crystals save for the spectra of the zeolite synthesised from the silica and aluminium oxide which is not as defined as the others. The adsorption bands at 823 to 1240 cm^{-1} are resulted from stretching and bending modes of Si-O or Al-O in zeolite framework for example the band at 1110 cm^{-1} is assigned to the asymmetric and symmetric stretching modes of internal tetrahedra, and the band at 950 cm^{-1} is associated with the asymmetric and symmetric stretching modes of external linkages [105]. Zeolites of the same morphology can be seen in Figs 4.3 a1-a3) in the SEM images. The XRD diffraction peaks on Fig. 4.13 c1) - Fig 4.13 c4) show that zeolite structure ($\text{Na}_8[\text{AlSiO}_4]_6(\text{OH})_2 \cdot 2\text{H}_2\text{O}$) is stable with the sum of reflection intensities peaks at 2θ of 14.12°, 20.00°, 24.51°, 31.8°, 35.00°, 37.91°, 38.18°, 45.71°, 43.64°, 47.96°, 56.56°, 57.68°, 58.74°, 60.92°, 64.52°, 68.34°, 70.40°, 72.10°, 73.91° and 79.10° which is in agreeance with that of Treacy and Higgins at Collection of simulated XRD powder patterns for zeolites [113].

5.2 Characterisation of magnetic nanoparticles (Fe_3O_4)

The characteristic adsorption bands were observed in the FT-IR spectrum at 547.89 and 469.34 cm^{-1} in spectrum of Fe_3O_4 MPNs correspond to the Fe-O bonds i.e. $\text{Fe}^{2+}\text{-O-Fe}^{3+}$, $\text{Fe}^{3+}\text{-O}$ and $\text{Fe}^{2+}\text{-O}$ bonds [40, 76,77]. The XRD diffraction peaks on Fig. 4.4 show peaks at 2θ of 36.36°, 44.10°, 54.51°, 57.09°, 62.78° and 74.34° which are related to the 311, 400, 422, 511, 440 and 662 crystallographic planes of face-centered cubic (fcc) iron oxide nanocrystals, respectively [113] (card number 11 - 0614, ICDD Database). The small signal evidenced at $2\theta = 44.6$ could

be due to a small amount of ferrite phase (110 plane, card number 6-0696) whose formation could occur randomly during the synthetic procedure [114].

5.3 Characterisation of Zn/Al layered double hydroxides

Fig 4.5 shows FT-IR spectrum of Aluminium – Zinc layered double hydroxide. The adsorption bands at wavenumber 3404.71 cm^{-1} corresponds to the O-H [106]. The XRD diffraction peaks on Fig. 4.5 c) show basal peaks at $2\theta^\circ$ of 11.84° , 23.40° , 34.71° and 39.24° which form a close-to-integer series making it possible to consider them basic 003, 006, 009, and 00.12 reflections of a hydrotalcite-like structure respectively [115]. The position of the basal peak at 11.84° is attributed to (003) peak, indicating that the distance between the two adjacent metal hydroxide sheets was about 0.76 nm [116].

5.4 Characterization of magnetic nanocomposite

The FT-IR spectrum shows adsorption bands at 3369 cm^{-1} corresponds to the O-H stretch, adsorption bands at 1367 and 1633 corresponding to the C-H and C=C in the activated charcoal, adsorption bands at 823 to 1240 cm^{-1} which correspond to stretching and bending modes of Si-O or Al-O in zeolite framework and peaks at 547.89 and 469.34 cm^{-1} in spectrum of Fe_3O_4 MPNs which correspond to the Fe–O bonds this shows that the composite was successfully synthesised [40,41,76,106]. The XRD spectrum on Fig. 4.6 c) show that the nanocomposite was successfully synthesised with diffraction peaks that correspond to the zeolites, magnetic iron oxide and layered double hydroxides.

5.5 Equilibrium study

Equilibrium batch experiments were performed to investigate the effect of initial concentration and isotherm modelling.

The initial pollutant concentration has a great effect on all of the adsorptive removal processes. Initial concentrations of 100, 200 and 400 ppm of solution were investigated.

Equilibrium batch experiments were performed to investigate the effect of the initial concentration. The sorbent dose was 10 gL⁻¹, pH was 0.98, and the temperature was ambient. The initial concentrations used were 100, 200 and 400 ppm over time intervals of 10, 15, 30, 45, 60, 120, 180, 240 and 300 mins. The volume used was 100 mL. The amount adsorbed was determined using the equation

$$q_t = \frac{(C_o - C_t)}{m} V \quad (1)$$

$$q_e = \frac{(C_o - C_e)}{m} V \quad (2)$$

And the percentage removal by the equation

$$\%R = \frac{(C_o - C_t)}{C_o} \times 100 \quad (3)$$

Where C_o is the initial concentration of sorbate and C_t and C_e are the concentrations of sorbate, at time *t* and at equilibrium, respectively (mg L⁻¹); *m* is the weight of the sorbent (g); and *V* is the volume of the adsorbate solution (L).

The initial concentration of 400 ppm had the highest percentage removal for all the sorbates with phosphate having the highest of 97 % and copper with the lowest of 57 % as shown in Tables 4.1 – 4.12. Greater percentage removal was observed by the nanocomposite beads compared to the un entrapped nanocomposite which suggests that there were more active site added by the introduction of alginate though the chromium uptake was reduced probably due to the fact that alginate exchanges its Ca²⁺ thus it has a better ion exchange capacity for the M²⁺ than M³⁺ aqueous ions. Q_t increases as the initial concentration increases until it becomes

constant. The increase in Q_t with increase in initial concentration can be explained by the existence of a higher concentration gradient of sorbate, which increases the diffusive contribution of the mass transfer process. Q_t increases with increase in contact time until equilibrium is reached due to the prolonged interaction between the sorbate and sorbent thereby increasing the amount adsorbed. Nonetheless removal is faster in the initial minutes where equilibrium is reached at around 45 mins of the process because of availability of more adsorption sites at the start of the sorption process and as the sites become used up, rate of sorption decreases. It is also important to note is that as the initial concentration increases, more time is required for equilibrium to be reached possibly due to the fact that a higher concentration of adsorbate in the solution increases the electrostatic repulsion between molecules present in the medium, increasing the diffusive resistance to mass transfer within the solution which results in a slower process [74].

The equilibrium, C_e amount vs time showed that by increasing the initial concentration, the amount of adsorbed sorbate increased as is clearly and this can be related to the initial concentration ranges and the maximum capacity of the beads. This suggests that the ranges of sorbate initial concentrations which were used were very low respect to maximum capacity of the adsorbent thus sorption increases with the same rate as the initial concentration increases with a greater percentage removal by the beads [2]. Mechanisms of adsorption were identified using two models i.e. pseudo-first and pseudo-second order given by the equations (4) and (5) respectively shown below.

$$\ln\left(\frac{q_e - q_t}{q_e}\right) = -k_1 t \quad (4)$$

$$\frac{1}{q_e} = \frac{1}{k_2 q_e^2} + \frac{1}{q_e} t \quad (5)$$

Where k_1 is the pseudo-first order rate constant (min^{-1}). The k_1 parameter can be determined from the slope of the line of $\ln ((q_e - q_t)/q_e)$ versus t for the pseudo-first order and k_2 is the pseudo-second-order rate constant ($\text{g mg}^{-1} \text{min}^{-1}$). Same applies as in the pseudo-first-order kinetic model, the k_2 and q_e parameters were determined from the slope and intercept of the equations formed by regressing t/q_t versus t , respectively [74,100]. The R^2 values at different initial concentrations are $>0,96$ for the pseudo-second-order and $< 0,70$ for the pseudo-first-order thus which suggests that the pseudo-second-order is the governing kinetic model wherein the rate of chemical interactions between the sorbates and the sites of composite is the step that controls the overall kinetics of the process [74]. Furthermore, the calculated Q_e , (Q_e (calc)) is consistent with the experimental Q_e , (Q_e (exp)) as shown in Table 2.

5.6 Isotherm study

Adsorption isotherm models are used to describe the interactive behaviour between the adsorbate and adsorbent, and also for investigating the mechanisms of adsorption [74]. The Freundlich and Langmuir isotherms were used in this study. The Langmuir model is based on the assumption of monolayer adsorption on a structurally homogeneous adsorbent, where all sorption sites are identical with no interaction between molecules on different sites and that the sorption sites have the same ΔH_{ads} thus energetically equivalent and do not depend on the fraction covered [74]. The linear form of the Langmuir equation can be expressed by the equation

$$\frac{1}{q_e} = \frac{1}{bC_e q_m} + \frac{1}{q_m} \quad (6)$$

Where q_e (mg/g) and C_e (mg/L) signify the adsorption capacity and the equilibrium concentration of the adsorbate in the aqueous solution, respectively; q_m (mg/g) is the maximum adsorption capacity of adsorbents and b (L/mg) is the constant of the Langmuir model related to the affinity of binding sites [100].

The empirical Freundlich equation is applied to adsorption on heterogeneous surfaces, where the interaction between the adsorbed molecules is not limited to the formation of a monolayer. The Freundlich constant, K_F is related to the adsorption capacity of the adsorbent: the higher the value, the greater the affinity for the adsorbate. The empirical parameter $\frac{1}{n}$ is related to the strength of adsorption, which varies with the heterogeneity of the material. When the values of $\frac{1}{n}$ are between 0.1 and 1.0, the adsorption process is considered favourable. The linearized form of the Freundlich equation is expressed by the equation

$$\log q_e = \log K_F + \frac{1}{n} \log C_e \quad (7)$$

Where K_F is the Freundlich constant (Lg^{-1}) and $\frac{1}{n}$ is a dimension-less empirical parameter.

The $\frac{1}{n}$ and K_F values were determined from the linear and angular coefficients of the equation formed by regressing $\log q_e$ as a function of $\log C_e$. The values for the isotherms are shown on table 1. The R^2 values were used to see which model fits best the data and it was shown that the Freundlich and Langmuir isotherms models fits for adsorption since the average R^2 for all the initial concentrations has an average which is > 0.95 . However it should be noted that the

correlation coefficient of the fitting is not the only parameter that should determine the best fitting isotherm model [107].

5.7 Thermodynamics studies

Thermodynamics experiments were performed at 294, 313 and 333 K at an initial phosphate concentration of 100 ppm. Thermodynamic studies of an adsorption process are necessary to deduce the spontaneity of the reaction. Gibb's free energy change, ΔG° , is used to determine the spontaneity. If ΔG° is a negative, then the reaction is spontaneous [108]. The thermodynamic parameters of Gibb's free energy change, ΔG° , enthalpy change, ΔH° , and entropy change, ΔS° , for the adsorption processes were calculated using the following equations:

$$\Delta G^\circ = -RT \ln K_c \quad (8)$$

Where R is the universal gas constant ($8.314 \text{ J mol}^{-1}\text{K}^{-1}$), T is temperature (K) and K_c is the equilibrium stability constant, which was calculated at each temperature by the equation

$$K_c = \frac{C_s}{C_e} \quad (9)$$

Where C_s and C_e are the equilibrium concentrations on the adsorbent and in the solution, respectively. The enthalpy change (ΔH°) and entropy change (ΔS°) were calculated from the slope and intercept of the plot of $\ln K_c$ versus $1/T$, based on the Van't Hoff equation [74]

$$\ln K_c = \left(\frac{\Delta S^\circ}{R} \right) - \left(\frac{\Delta H^\circ}{R} \right) \frac{1}{T} \quad (10)$$

The results of the thermodynamics studies are shown in Table 4.3; 4.6; 4.9; 4.12. The negative values of ΔG° show that the adsorption process was spontaneous for phosphate adsorption but positive ΔG° values for the rest. As the temperature increases, ΔG° increases as well, indicating

less driving force and hence slower adsorption capacity at higher temperatures. The negative value of ΔH° indicates that the adsorption process is exothermic. This magnitude is related to adsorbate interactions with the adsorbent and rearrangement of the surface during the adsorption process. It is also observed experimentally as the fraction of the surface that is covered by adsorbate. Enthalpy change data is used to differentiate physisorption and chemisorption. Generally, the adsorption process is assigned to physisorption in nature when the ΔG° value is in the range of -20 to 0 kJmol^{-1} , and to chemisorption when the ΔG° value ranges from -400 to -80 kJmol^{-1} [74,109,110]. The typical value for physisorption usually lies below -84 kJ mol^{-1} [74,111,112] hence it shows that the adsorption followed the physisorption process. Finally, the results of ΔS° indicate increased randomness at the solid/solute interface during the adsorption of phosphate. This phenomena was also observed by Zeng et al [111] and Bonetto et al [74],

6.1 CONCLUSIONS

The magnetic nanocomposite beads were successfully synthesized for the simultaneous removal of mixtures of inorganic and organic pollutants in water under highly acidic water. The beads showed greater percentage removal than the nanocomposite not entrapped. The beads also showed greater affinity for the anion than the cation and organic pollutants. The adsorption process fits the pseudo second order mechanism and fit also both the Langmuir and Freundlich isotherms with a more perfect fit for the Freundlich isotherm. On average, the adsorption process was spontaneous with an high entropy and the adsorption process showed that it was exothermic. It can therefore be recommended that the adsorbent here synthesized can be used for simultaneous removal of cationic, anionic and organic mixtures under highly acidic solution.

6.2 RECOMMENDATIONS

It is recommended that the study the adsorption processes be done different pH, adsorbent dosage and different aspect ratios of the composite. Furthermore, investigations of more isotherms and kinetic models with more parameters should be done and a computational approach to the adsorption process should be included. The study of the adsorption process using the column process at different flow rates would also be interesting to compare findings from batch and continuous processed.

REFERENCES

¹J.-W. Choi, K.-S. Yang, D.-J. Kim, C.E. Lee, *Adsorption of zinc and toluene by alginate complex impregnated with zeolite and activated carbon*, *Current Applied Physics*. **9** (2009) 694–697.

² A. Esmailiana, , A. Mahdavi Mazdehb, H. Ghaforianc, A.M. Liaghatd, *A novel nanopore biopolymer multi adsorbent for simultaneous removal of anionic and cationic mixtures*, *Desalination and Water Treatment* **53** (2015) 2235–2248

³ Dimple Lakherwal, *Adsorption of Heavy Metals: A Review*, *International Journal of Environmental Research and Development*. Volume **4**, Number 1 (2014), pp. 41-48

⁴ Kwon J.S., Yun S.T., Lee J.H., Kim S.O., Jo H.Y., *Removal of divalent heavy metals (Cd, Cu, Pb, and Zn) and arsenic (III) from aqueous solutions using scoria: kinetics and equilibrium of sorption*, *Journal of Hazardous Materials*, **174**, (2010), 307–313.

⁵ Yadanaparthi S.K.R., Graybill D. and Wandruszka R., , *Adsorbents for the removal of arsenic, cadmium, and lead from contaminated waters*, *Journal of Hazardous Materials*. **171**, (2009), 1-15.

⁶ Zhang,S, Xu Fang, *Silica modified calcium alginate-xanthan gum hybrid bead composites for the removal and recovery of Pb(II) from aqueous solution*. *Chemical Engineering Journal* Vol. **234**, (2013), Pages 33-42.

⁷ Jahangirian et al, *Synthesis And Characterization Of Zeolite/Fe₃O₄Nanocomposite By Green Quick Precipitation Method* Digest Journal of Nanomaterials and Biostructures Vol. **8**, No. **4**, October - December (2013), p. 1405 – 1413

⁸ Song et al, *Adsorption Studies of Coconut Shell Carbons Prepared by KOH Activation for Removal of Lead(II) From Aqueous Solutions*, Sustainability, **6**, (2014), 86-98

⁹ Williams GR, Hare DO'. *Towards understanding, control and application of layered double hydroxide chemistry*. Journal of Materials Chemistry, **16**, (2006):3065–3074

¹⁰ Goh, K.H., Lim, T.T., Dong, Z.L.. *Application of layered double hydroxides for removal of oxyanions: A review*. Water Resources, **42**, (2008):1343-1368.

¹¹ Wang SL, Liu CH, Wang MK, Chuang YH, Chiang PN .*Arsenate adsorption by Mg/Al–NO₃ layered double hydroxides with varying the Mg/Al ratio*. Applied Clay Science,**43**,(2009) (1):79–85

¹² Hirohisa Yamada, Yujiro Watanabe, Kenji Tamura, *Development of environmental purification materials with smart functions*, NUKLEONIKA **51** (Supplement 1) (2006); S61–S67.

¹³ M.E. Molina, A.J. Quiroga, *Alginates: Production, Types and Applications*, Nova Science Publishers , Hauppauge, New York, (2012).

-
- ¹⁴ S.K. Papageorgiou, F.K. Katsaros, E.P. Kouvelos, J.W. Nolan, H. Le Deit, N.K. Kanellopoulos, *Heavy metals sorption by calcium alginate beads from Laminaria digitata*, Journal of Hazardous Materials. **137** (2006) 1765–1772.
- ¹⁵ S.K. Papageorgiou, E.P. Kouvelos, E.P. Favvas, A.A. Sapalidis, G.E. Romanos, F.K. Katsaros, *Metal–carboxylate interactions in metal–alginate complexes studied with FTIR spectroscopy*, Carbon Resources. **345** (2010) 469.
- ¹⁶ S.K. Papageorgiou, E.P. Kouvelos, F.K. Katsaros, *Calcium alginate beads from Laminaria digitata for the removal of Cu^{+2} and Cd^{+2} from dilute aqueous metal solutions*, Desalination **224** (1–3) (2008) 293–306.
- ¹⁷ S.K. Papageorgiou, F.K. Katsaros, E.P. Kouvelos, N.K. Kanellopoulos, *Prediction of binary adsorption isotherms of Cu^{2+} , Cd^{2+} and Pb^{2+} on calcium alginate beads from single adsorption data*, Journal of Hazardous Materials. **162** (2–3) (2009) 1347–1354
- ¹⁸ C.P. Athanasekou, S.K. Papageorgiou, V. Kaselouri, F.K. Katsaros, N.K. Kakizis, A.A. Sapalidis, N.K. Kanellopoulos, *Development of hybrid alginate/ceramic membranes for Cd^{2+} removal*, Microporous and Mesoporous Materials. **120** (1–2) (2009) 154–164.

-
- ¹⁹ S.K. Papageorgiou, F.K. Katsaros, E.P. Favvas, G.E. Romanos, C.P. Athanasekou, K.G. Beltsios, Tziaila, P. Falaras, *Alginate fibers as photocatalyst immobilizing agents applied in hybrid photocatalytic/ultrafiltration water treatment processes*, *Water Resources*. **46** (6) (2012) 1858–1872.
- ²⁰ R. Lagoa, J.R. Rodrigues, *Kinetic analysis of metal uptake by dry and gel alginate particles*, *Biochemical Engineering Journal*, **46**, (2009) 320–326.
- ²¹ Zhou Qiusheng, Lin Xiaoyan, Qian Jin, Wang Jinga and Luo Xuegangb, *Porous zirconium alginate beads adsorbent for fluoride adsorption from aqueous solutions*, *Royal Society of Chemistry Advances*, **5**, (2015), 2100–2112
- ²² Ghorai S, Sinhamahapatra A, Sarkar A, Panda AB, Pal S: *Novel biodegradable nanocomposite based on XG-g-PAM/SiO₂: application of an efficient adsorbent for Pb²⁺ ions from aqueous solution*. *Bioresources Technology*. (2012) Sep; 119:181-90
- ²³ Park, H. G., Kim, T. W., Chae, M. Y., Yoo, I. K., *Activated carbon-containing alginate adsorbent for the simultaneous removal of heavy metals and toxic organics*. *Process Biochemistry*, **42**, (2007) 1371-1377.
- ²⁴ Vijaya, Y., Srinivasa R. P., Boddu V. M., Krishnaiah A., *Modified chitosan and Calcium alginate biopolymer sorbents for removal of nickel (II) through adsorption*. *Carbohydrate Polymers*, **72**, (2008) 261-271.

²⁵ Min, J. H., Hering, J. G., *Arsenate sorption by Fe (III)-doped alginate gels*. Water Research **32** (1988), 1544-1552.

²⁶ E. Chmielewski^I, L. Sabová^{IV}, H. Peterlik^{II}; A. Wu^{III}, *Batch-wise adsorption, saxs and microscopic studies of zeolite pelletized with biopolymeric alginate*, Brazil Journal of Chemistry. Eng. São Paulo vol.**28** no.1 Jan./Mar. (2011)

²⁷ Mohamad Anuar Kamaruddin, Mohd Suffian Yusoff, Hamidi Abdul Aziz, Rasyidah Alrozi: *Preparation and Characterization of Activated Carbon Embedded Clinoptilolite Adsorbent for Colour Removal from Textile Effluent*: Journal of Materials and Chemical Engineering, Vol. **2** Issue. 1:Jan. (2014), , PP. 1-10

²⁸ Wan Ngah W. S. ; Fatinathan S. *Adsorption of Cu (II) ions in aqueous solution using chitosan beads, chitosan-GLA beads and chitosan-alginate beads*, Chemical Engineering Journal **143**, (2008), 62.

²⁹ Chen, J. P.; Tendeyong, F.; Yiacoumi, S. *Equilibrium and kinetic studies of copper ion uptake by calcium alginate* Environmental Science and technology **21** (1997), , 1433

³⁰ Sonyeo Jeon, Jumi Yun, Young-Seak Lee and Hyung-II Kim: *Removal of Cu (II) ions by Alginate/Carbon Nanotube/Maghemite Composite Magnetic Beads*: Carbon Letters Vol. **11**, No. 2 (2010) 117-121

-
- ³¹ Lim, S. F.; Chen, J. P. *Synthesis of an innovative calcium-alginate magnetic sorbent for removal of multiple contaminants*, Applied Surface Science. **253** (2007), , 5772.
- ³² Rocher, V.; Siaugue, J. M.; Cabuil, V.; Bée, A. *Removal of organic dyes by magnetic alginate beads*. Water Research. **42** (2008), , 1290.
- ³³ Huidong, L.; Zhao, L.; Ting, L.; Xiao, X.; Zhihui, P.; Le, D. *A novel technology for bio-sorption and recovery hexavalent chromium in water* Bioresources Technology **99** (2008), , 6271.
- ³⁴ Babak Kakavandi, Roshanak Rezaei Kalantary, Mahdi Farzadkia, Amir Hossein Mahvi, Ali Esrafil, Ali Azari, Ahmad Reza Yari and Allah Bakhsh Javid *Enhanced chromium (VI) removal using activated carbon modified by zero valent iron and silver bimetallic nanoparticles*, Journal of Environmental Health Science & Engineering, **12**: (2014), 115
- ³⁵ V. Chandra and K. S. Kim. *Highly selective adsorption of Hg²⁺ by a polypyrrole-reduced graphene oxide composite*. Chemistry Communications, **47** (2011), , 3942-3942
- ³⁶ V. Chandra, J. Park, Y. Chun, J. W. Lee, I.-C. Hwang and K. S. Kim, *Water-dispersible magnetite-reduced graphene oxide composites for arsenic removal*. American Chemistry Society . Nanomaterials, **4** (2010) , 3979.

³⁷ Ling Sun, Fugetsu Bunshi: *Effect of encapsulated graphene oxide on alginate-based bead adsorption to remove acridine orange from aqueous solutions*. Cornell University Library (2013) arXiv:1307.0223

³⁸ S. Vadahanambi , S. Lee , W. Kim , I. Oh: *Arsenic Removal from Contaminated Water Using Three-Dimensional Graphene-Carbon Nanotube-Iron Oxide Nanostructures*. Environ. Sci. Technol. **47 (18)**, (2013), , pp 10510–10517

³⁹ A. Santhana Krishna Kumar, Shruti Singh Kakan , N. Rajesh. *A novel amine impregnated graphene oxide adsorbent for the removal of hexavalent chromium*. Chemical Engineering Journal **230** (2013) 328–337

⁴⁰ Ning Gan , Jiabing Zhang, Shaichai Lin, Nengbing Long, Tianhua Li and Yuting Cao ,*A Novel Magnetic Graphene Oxide Composite Absorbent for Removing Trace Residues of Polybrominated Diphenyl Ethers in Water*. Materials ,**7**, (2014), 6028-6044;

⁴¹ A. Muthukrishnaraj, J. Manokaran, M. Vanitha, K.V. Thiruvengadaravi, P. Baskaralingam & N. Balasubramanian: *Equilibrium, kinetic and thermodynamic studies for the removal of Zn(II) and Ni(II) ions using magnetically recoverable graphene/Fe₃O₄ composite*, Desalination and Water Treatment, Volume **56**, Issue 9 (2015)

⁴² Mohamed A. Farghali, Taher A. Salah El-Din, Abdullah M. Al-Enizi, Ramadan M. El Bahnasawy. *Graphene/ Magnetite Nanocomposite for Potential Environmental Application*. International Journal of Electrochemical Science, **10** (2015) 529 – 537

⁴³ Debabrata Nandi , Kaushik Gupta, Arup Kumar Ghosh, Amitabha De, Sangam Banerjee and Uday Chand Ghosh, *Manganese - incorporated iron (III) oxide–graphene magnetic nanocomposite: synthesis, characterization, and application for the arsenic(III) - sorption from aqueous solution*, Journal of Nanoparticles Research ,**14**, (2012) :1272

⁴⁴ Tahereh Poursaberi, Z. Falsafi, M. Hassanisadi and A. Jabbari, *Simultaneous adsorption and dechlorination of carbon tetrachloride using copper nanoparticles@graphene oxide composites*, Journal of Iran Chemical Society ,**12**, (2015):67–74

⁴⁵ Dichiara A.B, Sherwood T.J, Benton-Smith J, Wilson J.C, Weinstein S.J and Rogers R.E: *Free-standing carbon nanotube/graphene hybrid papers as next generation adsorbents*: **6(12)** (2014):6322-7

⁴⁶ Jodra Y, Mijangos F. *Phenol adsorption in immobilized activated carbon with alginate gels*. Sep. Sci. Technol.**38**,(2003):1851-1867,

⁴⁷ Zhou Qiusheng, Lin Xiaoyan, Qian Jin, Wang Jing and Luo Xuegang. *Porous zirconium alginate beads adsorbent for fluoride adsorption from aqueous solutions*. Royal Society of Chemistry Advances **5**, (2015), 2100

⁴⁸ Mahmood Zahid, Saqid Nasir, Nadia Jamil, Asma Sheikh and Adnan Akram. *Adsorption studies on phosphate ions on alginate calcium carbonate composite beads*. AJEST. Vol. **9(3)** (2015), pp.274-281

⁴⁹ Shihong Lin, Rixiang Huang , Yingwen Cheng, Jie Liu, Boris L.T. Lau and Mark R. Wiesner. *Silver nanoparticle-alginate composite beads for point-of-use drinking water disinfection*. Water Research. Vol. **47** (2013) 3959-3965

⁵⁰ Ye Kuang, Jianhua Dub, Rongbing Zhou, Zuliang Chen, Mallavarapu Megharaj and Ravendra Naidu. *Calcium alginate encapsulated Ni/Fe nanoparticles beads for simultaneous removal of Cu (II) and monochlorobenzene*. Journal of Colloid and Interface Science **447** (2015) 85–91

⁵¹ Huayue Zhu, Yongqian Fu, Ru Jiang, Jun Yao, Ling Xiao, Guangming Zeng. *Optimization of copper (II) adsorption onto novel magnetic calcium alginate/ maghemite hydrogel beads using response surface methodology*. Laboratory of Environmental Biology and Pollution Control, Hunan University, Ministry of Education, Changsha, Hunan 410082, China

⁵² Xu, Z.P., Jin, Y.G., Liu, S.M., Hao, Z.P. and Lu, G.Q. *Surface charging of layered double hydroxides during dynamic interactions of anions at the interfaces*. Journal of Colloid Interface Science. **326**, (2008), 522-529.

⁵³ Guoqing Zhang, Chong Liu, Jun Zhao, Ji Zhi Zhou, Guangren Qian, Jianyong Liu, Yueying Wu, *Effective Removal of Anionic Dye by Ni-Zn-Cr-Ldhs Prepared from Electroplating Wastewater via Accelerated Carbonation*, Journal of Water Sustainability, Volume **2**, Issue 1, March (2012), 25–34

⁵⁴ Cavani, F., Trifirò, F. and Vaccari, A.. *Hydrotalcite-type anionic clays: Preparation, properties and applications*. Catalysis. Today, **11**,(1991): 173-301.

⁵⁵ Chao Gao, Xin-Yao Yu, Tao Luo, Yong Jia, Bai Sun, Jin-Huai Liu and Xing-Jiu Huang. *Millimeter-sized Mg–Al-LDH nanoflake impregnated magnetic alginate beads (LDH-n-MABs): a novel bio-based sorbent for the removal of fluoride in water*. Journal of Materials Chemistry, **2**, (2014), 2119

⁵⁶ Yong-Un Han, Won-Suk Lee, Chang-Gu Lee, Seong-Jik Park, Ki-Woo Kim and Song-Bae Kim. *Entrapment of Mg-Al layered double hydroxide in calcium alginate beads for phosphate removal from aqueous solution*. Desalination and Water Treatment **36** (2011) 178–186

⁵⁷ Yong-Un Han, Chang-Gu Lee, Jeong-Ann Park, Jin-Kyu Kang, In Lee and Song-Bae Kim. *Immobilization of Layered Double Hydroxide into Polyvinyl Alcohol/Alginate Hydrogel Beads for Phosphate Removal*. Environmental and Engineering Resources. **3**, (2012): 133-138

⁵⁸ Phuong N.T.K. *Entrapment of Mg–Al layered double hydroxide into alginate/polyvinyl alcohol beads for water remediation*. *Journal of Environmental Chemical Engineering* **06**; **2** (2014):1082–1087.

⁵⁹ Dong-Wan Cho , Woosik Jung , Abinashi Sigdel , Oh-Hun Kwon , Sang-Hun Lee , Akhil N. Kabra & Byong-Hun Jeon. *Adsorption of Pb(II) and Ni(II) from aqueous solution by nanosized graphite carbon-impregnated calcium alginate bead*, *Geosystem Engineering*, **16**:**3** (2013), 200-208

⁶⁰ A.N. Bezbaruah, S. Krajangpan, B.J. Chisholm, E. Khan ,J.J.E. Bermudez, *Entrapment of Iron Nanoparticles in Calcium Alginate Beads for Groundwater Remediation Applications*, *Journal of Hazardous Materials* **166** (2009) 1339–1343

⁶¹ Jae-Hwan Kim, Ji-Hun Kim, Varima Bokare, Eun-Ju Kim, Yoon-Young Chang and Yoon-Seok Chang, *Enhanced removal of chromate from aqueous solution by sequential adsorption–reduction on mesoporous iron–iron oxide nanocomposites*. *Journal of Nanoparticles Research*, **14**, (2012) : 1010

⁶² E. Chmielewská, L. Sabová, H. Peterlik and A. Wu, *Batch-wise adsorption, saxs and Microscopic studies of zeolite Pelletized with biopolymeric alginate*. *Bjchemistry* Vol. **28**, No. 01, January - March, (2011) pp. 63 - 71

-
- ⁶³ Evangelia G. Deze, Sergios K. Papageorgiou, Evangelos P. Favvas and Fotis K. Katsaros. *Porous alginate aerogel beads for effective and rapid heavy metal sorption from aqueous solutions: Effect of porosity in Cu^{2+} and Cd^{2+} ion sorption*. Chemical Engineering Journal **209** (2012) 537–546.
- ⁶⁴ Dongbei Wu, Jing Zhao, Ling Zhang, Qingsheng Wu and Yuhui Yang. *Lanthanum adsorption using iron oxide loaded calcium alginate beads*. Hydrometallurgy **101** (2010) 76–83
- ⁶⁵ S.B. Hammouda, Nafaâ Adhoum and Lotfi Monser. *Synthesis of magnetic alginate beads based on Fe_3O_4 nanoparticles for the removal of 3-methylindole from aqueous solution using Fenton process*. Journal of Hazardous Materials **294** (2015) 128–136
- ⁶⁶ Salvatore Cataldo, Giuseppe Cavallaro, Antonio Gianguzza, Giuseppe Lazzara, Alberto Pettignano, Daniela Piazzese and Isabel Villaescusa. *Kinetic and equilibrium study for cadmium and copper removal from aqueous solutions by sorption onto mixed alginate/pectin gel beads*. Journal of Environmental Chemical Engineering **10** (2013): 1016
- ⁶⁷ T.J. Sudha Vani, N. Sivagangi Reddy, P. Ramasubba Reddy, K.S.V. Krishna Rao, Jayshree Ramkumar & A.V.R. Reddy, *Desalination and Water Treatment: Synthesis, characterization, and metal uptake capacity of a new polyaniline and poly(acrylic acid) grafted sodium alginate/gelatin adsorbent*, Desalination and Water Treatment, Vol. **52** Issue 1-3 (2014), p526
- ⁶⁸ Lee C.G, Kim S.B. *Magnetic alginate-layered double hydroxide composites for phosphate removal*. Environmental Technology (Impact Factor: 1.2). **10** (2013) ; 34(17-20):2749-56.

-
- ⁶⁹ Ghorai S, Sinhamahpatra A, Sarkar A, Panda AB, Pal S. *Novel biodegradable nanocomposite based on XG-g-PAM/SiO₂: application of an efficient adsorbent for Pb²⁺ ions from aqueous solution*. *Bioresources Technology*. **119** (2012) 181-90
- ⁷⁰ Ghorai S, Sinhamahpatra A, Sarkar A, Panda AB, Pal S. *Effective removal of Congo red dye from aqueous solution using modified xanthan gum/silica hybrid nanocomposite as adsorbent*. *Bioresources Technology*. **144** (2013) :485-91
- ⁷¹ Ali Pourjavadi, Malihe Doulabi, Mohadese Doroudian. *Adsorption characteristics of malachite green dye onto novel kappa-carrageenan-g-polyacrylic acid/TiO₂-NH₂ hydrogel nanocomposite*. *Journal of Iran Chemical Society*, **11**, (2014):1057–1065
- ⁷² X. Zhang et al. *Adsorption of methylene blue onto humic acid-coated Fe₃O₄ nanoparticles*. *Colloids and Surfaces A: Physicochemistry Engineering Aspects* **435** (2013) 85– 90
- ⁷³ Roshanak Rezaei Kalantry, Ahmad Jonidi Jafari, Ali Esrafil, Babak Kakavandi, Abdolmajid Gholizadeh & Ali Azari: *Optimization and evaluation of reactive dye adsorption on magnetic composite of activated carbon and iron oxide*, *Desalination and Water Treatment*, **10** (2015) 1080
- ⁷⁴ L.R. Bonetto, F. Ferrarini, C. De Marco, J.S. Crespo, R. Guégan and A.M. Giovanela, *Removal of methyl violet 2B dye from aqueous solution using a magnetic composite as an adsorbent*. *Journal of Water Process Engineering* **6** (2015) 11–20

⁷⁵ Hemant Mittal, Arjun Maity and Suprakas Sinha Ray. *Synthesis of co-polymer-grafted gum karaya and silica hybrid organic–inorganic hydrogel nanocomposite for the highly effective removal of methylene blue*. Chemical Engineering Journal **279** (2015) 166–179

⁷⁶ H. Mittal, V. Parashar, S.B. Mishra and A.K. Mishra. *Fe₃O₄ MNPs and gum xanthan based hydrogels nanocomposites for the efficient capture of malachite green from aqueous solution* Chemical Engineering Journal **255** (2014) 471–482

⁷⁷ Giuliana Magnacca, Alex Allera, Enzo Montoneri, Luisella Celi, Damian E Benito, Leonardo G. Gagliardi, Daniel Osvaldo Mártire, Mónica C Gonzalez and Luciano Carlos. *Novel magnetite nanoparticles coated with waste sourced bio-based substances as sustainable and renewable adsorbing materials*. American Chemical Society Sustainable Chemistry & Engineering. **2** (6), (2014). pp 1518–1524

⁷⁸ Lofgreen, J.E., Moudrakovski, I.L. and Ozin, G.A., *Molecularly Imprinted Mesoporous Organosilica*, American Chemical Society Nanomaterials, **5**, (2011) pp. 2277-2287.

⁷⁹ Mosha, D.M.S. and Mkayula L.L. *Metal ion sequestration: An exciting dimension for molecularly imprinted polymer technique*, Tanzania Journal of Science, **31**, (2005), pp. 91-98.

⁸⁰ Esfandyari-Manesh, M., Javanbakht, M., Atyabi, F., Badiei, A. and Dinarvand, R., *Effect of porogenic solvent on the morphology, recognition and release properties of carbamazepine-molecularly imprinted polymer nanospheres*, Journal of Applied Polymer Science, **121**, (2011) pp. 1118-1126

⁸¹ Karim, K., Breton, F., Rouillon, R., Piletska, E.V., Guerreiro, A., Chianella, I. and Piletsky, S.A., *How to find effective functional monomers for effective molecularly imprinted polymers?* Advanced Drug Delivery Reviews, **57**, (2005). 1795-1808

⁸² Park, J.K. and Seo J, *Characteristics of Phenylalanine Imprinted Membrane Prepared by the Wet Phase Inversion Method*, Korean Journal of Chemical Engineering, **19**, (2002) pp. 940-948

⁸³ Yu, J.C.C. and Lai, E.P.C., *Molecularly Imprinted Polymers for Ochratoxin A Extraction and Analysis*, Toxins, **2**, (2010) pp. 1536-1553

⁸⁴ Pichon, V. and Chapuis-Hugon, F. *Role of molecularly imprinted polymers for selective determination of environmental pollutants*, Analytica Chimica Acta, **622**, (2008) pp. 48-61.

⁸⁵ Turiel, E. and Martín-Esteban A, *Molecularly imprinted polymers for sample preparation: A review*, Analytica Chimica Acta, **668**, (2010) pp. 8799

⁸⁶ Daniel, S., Babu, P.E.J. and Rao, T.P. *Pre concentrative separation of palladium(II) using palladium(II) ion-imprinted polymer particles formed with different quinoline derivatives and evaluation of binding parameters based on adsorption isotherm models*, Atlanta, **65**, (2005), pp. 441-452.

⁸⁷ Rao, T.P., Daniel, S. and Gladis, J.M., *Tailored materials for pre concentration or separation of metals by ion-imprinted polymers for solid-phase extraction (IIP-SPE)* Trends in Analytical Chemistry, **23**, (2004) pp. 28-35

⁸⁸ Rao, T.P., Kala, R. and Daniel, S., *Review: Metal ion-imprinted polymers-Novel materials for selective recognition of inorganics*, Analytica Chimica Acta,**578**, (2006) pp. 105-116

⁸⁹ Nishide, H., Deguchi, J. and Tsuchida, E., *Selective adsorption of metal ions on cross-linked poly(vinylpyridine) resin prepared with a metal ion as a template*, Chemistry Letters, **5**, (1976) pp. 169-174

⁹⁰ Metilda, P., Gladis, J.M. and Rao, T.P., *Influence of binary/ternary complex of imprint ion on the pre concentration of uranium(VI) using ion imprinted polymer materials*, Analytica Chimica Acta, **512**, (2004) pp. 63-73

⁹¹ Scorrano, S., Mergola, L., Sole, R.D. and Vasapollo, G., *Synthesis of Molecularly Imprinted Polymers for Amino Acid Derivates by Using Different Functional Monomers*, International Journal of Molecular Sciences, **12**, (2011) pp.1735-1743

⁹² Zhan, Y., Luo, X., Nie, S., Huang, Y., Tu, X. and Luo, S., *Selective Separation of Cu (II) from Aqueous Solution with a Novel Cu (II) Surface Magnetic Ion-Imprinted Polymers*, Industrial and Engineering Chemistry Research, **50**, (2011) pp. 6355-6361

⁹³ Philippova, O., Barabanova, A., Molchanov, V. and Khokhlov, A., *Magnetic polymer beads: Recent trends and developments in synthetic design and applications*, European Polymer Journal, **47**, (2011) pp. 542-559

⁹⁴ Ansell, R.J., Wang, D.Y. and Kuah, J.K.L, *Imprinted polymers for chiral resolution of (\pm)-ephedrine. Part 2: probing pre-polymerization equilibria indifferent solvents by NMR*, Analyst, **133**, (2008) pp. 1673-1683

⁹⁵ Pan, J., Yao, H., Xu, L., Ou, H., Huo, P., Li, X. and Yan, Y., *Selective Recognition of 2,4,6-Trichlorophenol by Molecularly Imprinted Polymers Based on Magnetic Halloysite Nanotubes Composites*, Journal of Physical Chemistry, **115**, (2011) pp. 5440-5449

⁹⁶ N. T. Tavengwa. *Preparation of magnetic nano-composite-beads and their application to remediation of Cr(VI) and U(VI) from acid mine drainage*. MSc thesis. WITS University, Johannesburg, (2013)

⁹⁷ Nikita Tawanda Tavengwa, Ewa Cukrowska, Luke Chimuka. *Synthesis of bulk ion-imprinted polymers (IIPs) embedded with oleic acid coated Fe₃O₄ for selective extraction of hexavalent uranium*. Water SA Vol. No. **4**, October (2014) 40

⁹⁸ Hemant Mittal, Arjun Maity, and Suprakas Sinha Ray. *The Adsorption of Pb²⁺ and Cu²⁺ onto Gum Ghatti-Grafted Poly (acrylamide-co-acrylonitrile) Biodegradable Hydrogel: Isotherms and Kinetic Models*. Journal of Physical Chemistry **10** (2014) 1021

⁹⁹ Claudia-Mihaela Hristodor, Narcisa Vrinceanu, Rodica Pode, Violeta Elena Copcia, Elena Botezatu and Eveline Popovici. *Preparation and thermal stability of Al₂O₃ - clay and Fe₂O₃ - clay nanocomposites, with potential application as remediation of radioactive effluents*. Journal Thermal Analytical Calorimetry **10** (2013) 1007

¹⁰⁰ KatayoonKalantari, Mansor B. Ahmad, Hamid Reza Fard Masoumi, Kamyar Shameli, Mahiran Basri and Roshanak Khandanlou, *Rapid and high capacity adsorption of heavy metals by Fe₃O₄ / montmorillonite nanocomposite using response surface methodology: Preparation, characterization, optimization, equilibrium isotherms, and adsorption kinetics study*, Journal of the Taiwan Institute of Chemical Engineers **10** (2014) 1016

¹⁰¹ Abbas Afkhamia, Mohammad Saber-Tehranib, Hasan Bagherib. *Simultaneous removal of heavy-metal ions in wastewater samples using nano-alumina modified with 2,4-dinitrophenylhydrazine*. Journal of Hazardous Materials **181** (2010) 836–844

¹⁰² A. Bhatnagara and M. Sillanpää, *A review of emerging adsorbents for nitrate removal from water*, Chemical Engineering Journal **168** (2011) 493–504.

¹⁰³ Y. Li, B. Xia, Q. Zhao, F. Liu, P. Zhang, Q. Du, D. Wang, D. Li, Z. Wang, Y. Xia, *Removal of copper ions from aqueous solution by calcium alginate immobilized kaolin*, J. Environ. Sci. **23** (2011) 404–411.

¹⁰⁴ Abdul-Halim A. Mohammed and Zeinab K. Nassrullah: *Preparation and Formation of Zeolite 5A from Local Kaolin Clay for Drying and Desuphurization of Liquefied Petroleum Gas*. IJCPE Vol.14 No.1 (March 2013)

¹⁰⁵ Hossein Jahangiriana B, Mohd Halim Shah Ismaila, Md Jelas Haronc, Roshanak Rafiee-Moghaddamb D, Kamyar Shamelie, Soraya Hosseinia, Katayoon Kalantarie, Roshanak Khandanloue, Elham Gharibshahif and Sepideh Soltaninejad. *Synthesis and characterization of zeolite/Fe₃O₄ nanocomposite by green quick precipitation method*. Digest Journal of Nanomaterials and Biostructures Vol. 8, No. 4, (2013) p. 1405 - 1413

¹⁰⁶ Junyan Hu, Gang Lei, Zhouguang Lu, Kaiyu Liu, Shangbin Sang and Hongtao Liu *Alternating Assembly of Ni-Al Layered Double Hydroxide and Graphene for High-Rate Alkaline Battery Cathode*, The Royal Society of Chemistry **51** (2015) 9983-9986

¹⁰⁷ Lima E.C, Royer B, Vaghetti J.C, Brasil J.L, Simon N.M, Dos Santos A.A Jr, Pavan F.A, Dias S.L, Benvenuto E.V and Silva EA. *Adsorption of Cu(II) on Araucaria angustifolia wastes: Determination of the optimal conditions by statistic design of experiments*. Journal of Hazardous Materials **140** (2007) 211–220

-
- ¹⁰⁸ Jing He, Song Hong, Liang Zhang, Fuxing Gan and Yuh-Shan Ho: *Equilibrium and thermodynamic parameters of adsorption of methylene blue onto rectorite*. *Fresenius Environmental Bulletin*, PSP Volume **19** – No 11a, (2010)
- ¹⁰⁹ Suyuan Zeng, Shengxia Duan, Rongfeng Tang, Lei Li, Caihua Liu and Dezhi Sun. *Magnetically separable Ni_{0.6}Fe_{2.4}O₄ nanoparticles as an effective adsorbent for dye removal: Synthesis and study on the kinetic and thermodynamic behaviours for dye adsorption*. *Chemical Engineering Journal* **258** (2014) 218–228
- ¹¹⁰ Andreia Neves Fernandes, Carlos Alberto Policiano Almeida, Nito Angelo Debacher and Maria Marta de Souza Sierra. *Isotherm and thermodynamic data of adsorption of methylene blue from aqueous solution onto peat*. *Journal of Molecular Structure* **982** (2010) 62–65
- ¹¹¹ Suyuan Zeng, Shengxia Duan, Rongfeng Tang, Lei Li, Caihua Liu and Dezhi Sun. *Magnetically separable Ni_{0.6}Fe_{2.4}O₄ nanoparticles as an effective adsorbent for dye removal: Synthesis and study on the kinetic and thermodynamic behaviours for dye adsorption*. *Chemical Engineering Journal* **258** (2014) 218–228
- ¹¹² Andreia Neves Fernandes, Carlos Alberto Policiano Almeida, Nito Angelo Debacher and Maria Marta de Souza Sierra. *Isotherm and thermodynamic data of adsorption of methylene blue from aqueous solution onto peat*. *Journal of Molecular Structure* **982** (2010) 62–65
- ¹¹³ M. M. J. Treacy, J. B. Higgins, Access Online via Elsevier: (2001).

¹¹⁴ Giuliana Magnacca, Alex Allera, Enzo Montoneri, Luisella Celi, Damian E Benito, Leonardo G. Gagliardi, Daniel Osvaldo Mártire, Mónica C Gonzalez, and Luciano Carlos. *Novel magnetite nanoparticles coated with waste sourced biobased substances as sustainable and renewable adsorbing materials*. ACS Sustainable Chemical Engineering, **2** (6), (2014), pp 1518–1524

¹¹⁵ G. N. Pshinko. *Layered Double Hydroxides as Effective Adsorbents for U(VI) and Toxic Heavy Metals Removal from Aqueous Media*. Hindawi Publishing Corporation, Journal of Chemistry Volume (2013), Article ID 347178

¹¹⁶ Huang NH, Wang JQ. *A new route to prepare nanocomposites based on polyvinyl chloride and Mg/Al layered double hydroxide intercalated with lauryl ether phosphate*. Express Polymer Letters. **3**, (2009); 595–604.